# Development of an Itaconic Acid Production Process on Alternative Feedstocks

## Entwicklung eines Verfahrens zur Herstellung von Itaconsäure aus alternativen Rohstoffen

Von der Fakultät für Maschinenwesen der Rheinisch-Westfälischen Technischen Hochschule Aachen zur Erlangung des akademischen Grades eines Doktors der Naturwissenschaften genehmigte Dissertation

vorgelegt von

**Paul-Joachim Niehoff**

Berichter: Universitätsprofessor Dr.-Ing. Dr. h. c. (Osaka) Jochen Büchs

Universitätsprofessor Dr. Nick Wierckx

Tag der mündlichen Prüfung: 01. März 2024

—— Für Paul Norbert Niehoff ——

Du Fehlst

# Danksagung

Die vorliegende Arbeit wurde während meiner Tätigkeit als wissenschaftlicher Mitarbeiter am Lehrstuhl für Bioverfahrenstechnik der RWTH Aachen im Rahmen des BioökonomierREVIER_INNO (Teilprojekt UpRePP) Projekts, mit Projektnummer 031B0918E angefertigt.

Mein besonderer Dank gilt Prof. Dr.-Ing. Jochen Büchs für die Möglichkeit am Lehrstuhl für Bioverfahrenstechnik zu promovieren. Ihre Betreuung und Unterstützung haben den Grundstein dieser Arbeit gelegt. Ihre unglaubliche wissenschaftliche Neugier waren immer wieder eine große Inspiration und damit ein wesentlicher Beitrag zum Gelingen der Promotion. Vielen Dank, dass Sie mich auf meiner wissenschaftlichen Laufbahn unterstützt und gefördert haben.

Weiterhin möchte ich mich bei Prof. Dr. Nick Wierckx für die Übernahme des Koreferats und bei Univ. Prof. Dr.-Ing Klaus Radermacher für die Übernahme des Prüfungsvorsitzes bedanken.

Meine Arbeit lebte von der Kooperation und dem Austausch mit den Projektpartnern. Hier gilt mein Dank besonders Katharina Saur und Robert Kiefel (Aachener Verfahrenstechnik, Fluidverfahrenstechnik), sowie Philipp Ernst, Prof. Nick Wierckx und Dr. Stephan Noack (IBG-1: Biotechnology, Forschungszentrum Jülich). Ebenfalls möchte ich mich bei Jordy Hofstede und Dr. Jörn Viell (Aachener Verfahrenstechnik, Systemverfahrenstechnik) für die gute Zusammenarbeit bedanken.

Tatkräftige Studierende haben als HiWis oder im Rahmen von Abschlussarbeiten zum Gelingen dieser Arbeit beigetragen. Durch die gemeinsame Arbeit habe ich persönlich viel lernen können und bedanke mich daher herzlich bei: Waldemar Müller, Anna Ida Luca Hampe, David Kisser, Simon Bussmann und Anna Müller.

Ich möchte mich auch bei allen Mitarbeitenden des Lehrstuhls bedanken, die im Sekretariat, in der IT, im Labor und in der Buchhaltung für einen reibungslosen Ablauf gesorgt haben. Ohne euch, wäre diese Dissertation nicht möglich gewesen.

Meinen lieben Kolleg:innen und Freund:innen am Lehrstuhl danke für die gute Arbeitsatmosphäre, die ständige Hilfsbereitschaft und die schöne gemeinsame Zeit. Besonders danken möchte ich Marcel Mann und Katharina Miebach (sowie den jeweiligen Kleingruppen) für die Diskussionen und Hilfe bei der Erarbeitung möglicher Publikationen, sowie Sarah

Straaten für die Arbeit an Cell free Pro$^2$. Außerdem sind besonders hervorzuheben Maurice Finger, Carl Dinter und Johannes Pastoors. Neben der wissenschaftlichen Zusammenarbeit sind hier auch Freundschaften entstanden, für die ich sehr dankbar bin.

Von Herzen bedanken möchte ich mich bei meiner Familie. Ihr habt mir nicht nur während des Studiums, sondern auch während der Promotion Rückhalt gegeben und mich immer bedingungslos unterstützt. Ohne euch, wäre ich heute nicht da, wo ich bin.

Zu guter Letzt möchte ich Dir, meine liebe Jenny, danken. Während der Promotion hast du entschieden dein Leben mit mir als Ehemann zu teilen und bist nun die Mutter unseres ersten Kindes. Vielen Dank für alles!

# Zusammenfassung

Die wirtschaftlichen Nachteile von Bioraffineriekonzepten, im Vergleich zu konventionellen petrochemischen Produktionswegen, behindern deren Etablierung in einer zirkulären Bioökonomie. Bei der mikrobiellen Herstellung von Plattformchemikalien ist die Substratwahl wesentlich für die Gesamtkosten. Die Verwendung von alternativen Rohstoffen aus lokaler Produktion ist daher von zentraler Bedeutung für den Übergang zu einer dezentralen und nachhaltigen Bioökonomie.

In der vorliegenden Arbeit wurde ein Produktionsprozess für Itaconsäure entwickelt, in dem alternative Rohstoffe als einzige Kohlenstoffquelle genutzt werden. Hierfür wurden fünf verschiedene *Ustilago*-Stämme auf Wachstum und Produktion von Itaconsäure in Minimalmedium in Kleinkultursystemen untersucht. *U. cynodontis* ITA Max pH, ein hochentwickelter Produktionsstamm, wurde im Folgenden verwendet um ein geeignetes alternatives Substrat zu finden. Dabei wurde die biologisch verfügbare Stickstoffkonzentration in Dicksaft und Melasse bestimmt. Auf Grundlage dieser Ergebnisse wurde Dicksaft als Substrat für das folgende Scale-up gewählt. Weiterhin wurde der Produktionsstamm im Hinblick auf Osmotoleranz und Produktinhibition charakterisiert. Ein erfolgreiches Scale-up vom Schüttelkolben in einen 2-Liter-Rührkesselreaktor wurde ohne Einbußen bezüglich Titer oder Ausbeute im Vergleich zu reinen Glukosefermentationen erreicht. Der Prozess wurde hinsichtlich pH-Wert, Stickstoffkonzentration und pH-Stellmittel weiter optimiert, bevor ein weiteres Scale-up in den 150-Liter-Bioreaktor erfolgte. Die Fermentation stellt die Umsetzbarkeit der Itaconsäureproduktion mit alternativem Substrat als einziger Kohlenstoffquelle dar.

Insbesondere in der frühen Phase der Bioprozessentwicklung sind Schüttelkolben unverzichtbar. Um die Eignung der verschiedenen Kolbengrößen zu bewerten, wurde eine verfahrenstechnische Analyse der handelsüblichen Schüttelkolben von 50 – 5000 mL durchgeführt. Dabei zeigte sich, dass keine allgemeingültige Empfehlung für Schüttelparameter gegeben werden kann. Vielmehr hängen diese vom gewählten Produktionsstamm und -verfahren ab.

Diese Arbeit beschreibt einen Ansatz zur schnellen und zuverlässigen Prozessentwicklung für Bioraffineriekonzepte und verdeutlicht die Bedeutung der technischen Parameter für die erfolgreiche Implementierung von Schüttelkolben.

# Abstract

The establishment of biorefinery concepts is hindered by their economic disadvantages compared to conventional petrochemical production routes. For the production of bulk chemicals via microbial cultivation, substrate costs are a major contributor to the overall costs. Therefore, the use of locally sourced alternative feedstocks is of key importance for the transition towards a decentralized and sustainable bioeconomy.

In this thesis, a production process for itaconic acid was developed using alternative feedstocks as sole carbon source. Early-stage process development was conducted in small-scale shaken bioreactors like microtiter plates and shake flasks. In the first part of this work, five different *Ustilago* strains were screened for their growth and production of itaconic acid on defined media. *U. cynodontis* ITA Max pH, a highly engineered production strain, was selected to determine the biologically available nitrogen concentration in thick juice and molasses. Based on these findings, thick juice was chosen as feedstock to ensure the necessary nitrogen limitation for itaconic acid production. *U. cynodontis* ITA Max pH was further characterized regarding osmotolerance and product inhibition.

A successful scale-up to a 2-liter stirred tank reactor was accomplished without drawbacks in either titer or yield compared to pure glucose fermentations. The process was then further optimized regarding pH, nitrogen concentration, and pH adjusting agent before being scaled to a 150 L bioreactor. The fermentation shows the proof-of-concept for the scale-up of itaconic acid production with an alternative feedstock as the sole carbon source.

Especially early-stage bioprocess development is impossible without shake flasks. To evaluate the suitability of different shake flask sizes, a procedural analysis of the commercially available shake flasks from 50 – 5000 mL was conducted. This analysis showed that no general recommendation for a specific parameter set can be made, which is valid for all cultivations. These rather depend on the chosen production strain and process.

This study describes an approach for fast and reliable process development for biorefinery concepts and highlights the importance of engineering parameters for the successful implementation of shake flasks within the process development of these concepts.

# Funding and Publications

This work was funded by the Federal Ministry of Education and Research through grants within the BioökonomieREVIER_INNO (Teilprojekt UpRePP) project, with project no. 031B0918E. Funding is gratefully acknowledged.

Parts of this thesis have been published previously:

- Sauer, K. M.*, Kiefel, R.*, Niehoff, P.-J.*, Hofstede, J., Ernst, P., Brockkötter, J., Gätgens, J., Viell, J., Noack, S., Wierckx, N., Büchs, J., Jupke, A. Holistic Approach to Process Design and Scale-Up for Itaconic Acid Production from Crude Substrates. *Bioengineering* 2023, 10(6), 723.[1]
- Niehoff, P.-J., Müller, W., Pastoors, J., Miebach, K., Ernst, P., Hemmerich, J., Noack, S., Wierckx, N., Büchs, J. Development of an Itaconic Acid Production Process With Ustilaginaceae on Alternative Feedstocks. *BMC Biotechnology* 23, 34 (2023).

Contributions to further publications during the preparation of this thesis:

- Li, W.-J., Narancic, T., Kenny, S. T., Niehoff, P.-J., O'Conner, K., Blank, L. M., Wierckx, N. Unraveling 1,4-Butanediol Metabolism in *Pseudomonas putida* KT2440. *Frontiers in Microbiology* 2020, 11:15.
- Ackermann, Y. S., Li, W.-J., Op de Hipt, L., Niehoff, P.-J., Casey, W., Polen, T., Köbbing, S., Ballerstedt, H., Wynands, H., O'Connor, K., Blank, L. M., Wierckx, N. Engineering adipic acid metabolism in *Pseudomonas putida*. *Metabolic Engineering* 2021, 67:29-40.
- Battling, S., Engel, D., Herweg, E., Niehoff, P.-J., Pesch, M., Scholand, T., Schöpping, M., Sonntag, N., Büchs, J. Highly efficient fermentation of 5-keto-d-fructose with *Gluconobacter oxydans* at different scales. *Microbial Cell Factories* 2022, 21(1):21

* Authors contributed equally to the respective work

[1] Reprinted (adapted) with permission, Open Access https://www.mdpi.com/openaccess

- Helm, T. Niehoff, P.-J., Gätgens, J., Stausberg, T., Pichler, B., Häßler, T., Wiechert, W., Büchs, J., Wierckx, N., Noack, S. Introducing molasses as an alternative feedstock into itaconate production using *Ustilago sp*. *New Biotechnology* 2023, 77:30-39
- Dinter, C., Gumprecht, A., Menze, M. A., Azizan, A., Niehoff, P.-J., Hansen, S., Büchs, J. Validation of computational fluid dynamics of shake flask experiments at moderate viscosity by liquid distributions and volumetric power inputs. *Scientific Reports* 14, 3658 (2024).

Manuscripts submitted or in preparation for submission at the time of submission of this thesis:

- Niehoff, P.-J.*, Straaten, S. L.*, Hampe, A. L. I., Flaskamp, Y., Hemmerich, J., Juergens, H., Roentgen, R., Finnern, R., Büchs, J. Online Monitoring of the Mitochondrial Respiration Activity and Protein Formation in the Almost Living Cell-free Expression (ALiCE) System
- Niehoff, P.-J.*, Straaten, S. L.*, Hampe, A. L. I., Kisser, D., Büchs, J. Investigation of the Influence of Volume Specific Power Input and Bubble Aeration on the Almost Living Cell-free Expression (ALiCE) System
- Niehoff, P.-J.*, Straaten, S. L.*, Büchs, J. Increasing the Proess Window of the Almost Living Cell-free Expression (ALiCE) System
- Ernst, P., Niehoff, P.-J., Saur, K., Kiefel, R., Jupke, A., Büchs, J., Wierckx, N. Balancing pH and Yield: Exploring Itaconic Acid Production in *Ustilago cynodontis* from an Economic Perspective.

Contributions to conferences during the preparation of this thesis:

- Niehoff, P.-J., Brockkötter, J., Ernst, P., Kiefel, R., Saur, K. M., Wierckx, N., Jupke, A., Büchs, J., 2022. Optimization and scale-up of itaconic acid production on complex substrates. Oral presentation. 7th BioProscale Symposium, Berlin, Germany.
- Niehoff, P.-J., Brockkötter, J., Ernst, P., Hemmerich, J., Kiefel, R., Saur, K. M. Noack, S., Wierckx, N., Jupke, A., Büchs, J., 2023. Alternative Feedstocks for the Itaconic Acid Production with *Ustilago cynodontis*. Oral presentation. 19th

* Authors contributed equally to the respective work

International Conference on Renewable Resources & Biorefineries (RRB 2023), Riga, Latvia.

* Authors contributed equally to the respective work

# Contents

**1. Introduction ..... 1**

1.1 Aim of this thesis ..... 3

**2. Development of an Itaconic Acid Production Process with Alternative Feedstocks in Shaken Bioreactors ..... 7**

2.1 Background ..... 7
2.2 Material and Methods ..... 8
2.2.1 Microbial strains and media composition ..... 8
2.2.2 Cultivation in shaken systems ..... 9
2.2.3 Offline analytics ..... 9
2.2.4 Calculations ..... 10
2.3 Results ..... 12
2.3.1 Screening for a suitable production organism and feedstock ..... 12
2.3.2 Determination of biologically available nitrogen in molasses and thick juice ..... 16
2.3.3 Influence of osmolality, pH and ITA concentrations on *U. cynodontis* cultivations ..... 18
2.4 Discussion ..... 20
2.4.1 Screening for a suitable production organism and feedstock ..... 20
2.4.2 Determination of biologically available nitrogen in molasses and thick juice ..... 23
2.4.3 Influence of osmolality, pH and ITA concentrations on *U. cynodontis* cultivations ..... 24
2.5 Conclusion ..... 26

**3. Optimization and Scale-Up of the Itaconic Acid Production Process in Stirred Tank Reactors ..... 29**

3.1 Background ..... 29
3.2 Material and Methods ..... 30
3.2.1 Microbial strain and media composition ..... 30
3.2.2. Cultivation Conditions ..... 30
3.2.3. Offline Analytics ..... 32
3.2.4 Calculations ..... 32
3.3 Results and Discussion ..... 34

3.3.1 Extended batch stirred tank reactor cultivation of *U. cynodontis* ITA Max pH with thick juice as carbon source ..... 34
3.3.2 Introduction of a pH shift and reduction of added nitrogen ..... 37
3.3.3 Evaluation of using $Mg(OH)_2$ for pH control ..... 39
3.3.4 Scale-Up to 150 L Bioreactor ..... 42
3.4 Conclusion ..... 45

**4. Procedural Analysis of Commercially Available Shake Flasks from 50 – 5000 mL ..... 47**

4.1 Background ..... 47
4.2 Material and Methods ..... 49
4.2.1 Determination of the shaking diameter, the shaking frequency, and the filling volume ..... 49
4.2.2 Volume specific power input and energy dissipation rate ..... 53
4.2.3 Heat transfer coefficients and temperature change ..... 54
4.3 Results and Discussion ..... 59
4.3.1 Determination of shaking frequency, shaking diameter and filling volume ..... 59
4.3.2 Volume specific power input and energy dissipation rate ..... 61
4.3.3 Maximum oxygen transfer capacity ($OTR_{max,plug}$) and oxygen availability ..... 64
4.3.4 Overall heat transfer and temperature change inside liquid volume ..... 65
4.4 Conclusion ..... 71

**5. Summary and Outlook ..... 73**

**6. Bibliography ..... 77**

**7. Appendix ..... 89**

Appendices for Chapter 2 ..... 89
Appendices for Chapter 3 ..... 94
Appendices for Chapter 4 ..... 99

# Nomenclature

## List of Abbreviations

| Abbreviation | Description |
|---|---|
| µTOM | micro(µ)-scale transfer rate online measurement |
| CDW | cell dry weight |
| CFA | confirmatory factor analysis |
| CTR | carbon dioxide transfer rate |
| dgat | diacylglycerol acyltransferase |
| DOT | dissolved oxygen tension |
| GC-ToF-MS | gas chromatography time-of-flight mass spectrometry |
| HPLC | high-performance liquid chromatography |
| IC | ion exchange chromatography |
| ICP-OES | inductively coupled plasma optical emission spectroscopy |
| ITA | itaconic acid |
| KPI | key performance indicator |
| MEL | mannosyl erythritol lipid |
| MES | 2-(N-morpholino)ethane sulfonic acid |
| MTP | microtiter plate |
| OD | optical density |
| OTR | oxygen transfer rate |
| $OTR_{max}$ | maximum oxygen transfer capacity |
| $OTR_{N,max}$ | maximal obtained oxygen transfer rate |
| RAMOS | respiratory activity monitoring system |
| rpm | revolutions per minute |
| RQ | respiratory quotient |
| STR | stirred tank reactor |
| STY | space-time-yield |
| UA | ustilagic acid |

## List of Symbols

| Abbreviation | Description | Unit |
|---|---|---|
| A | heat transfer area | $m^2$ |
| $A_{pl}$ | base area of the sterile barrier (cotton plug) | $m^2$ |
| $c_{ITA}(t)$ | concentration of itaconic acid at time point t | g/L |
| $c_p$ | specific heat capacity of fluid | J/kg/K |
| $c_x(t)$ | concentration of substrate x at time point t | g/L |
| $c_x(t_0)$ | concentration of substrate x at the beginning of the experiment | g/L |
| $c_{x,feed}$ | concentration of substrate x in the feed | g/L |
| d | flask diameter | m |
| D | diameter of cylinder | m |
| $d_0$ | shaking diameter | m |
| $d_N$ | flask neck diameter | m |
| $D_{O2,eff}$ | effective oxygen diffusion coefficient (~1.256 · 10-5 $m^2/s$) | $m^2/s$ |
| $Fr_a$ | axial Froude number | - |
| g | gravitational acceleration (9.81 $m/s^2$) | $m/s^2$ |
| h | vertical length scale for the friction area between liquid and flask wall | m |
| $h_l$ | characteristic length of the turbulence generating element (here: liquid height of the bulk liquid) | m |
| $h_g$ | gas side heat transfer coefficient | $W/m^2/K$ |
| $h_L$ | liquid side heat transfer coefficient | $W/m^2/K$ |
| $H_{pl}$ | height of the sterile barrier (cotton plug) | m |
| k | thermal conductivity of flask material | W/m/K |
| $k_La$ | volumetric gas transfer coefficient | 1/s |
| $k_{pl}$ | mass transfer coefficient of sterile barrier (cotton plug) | mol/s |
| L | shortest distance of the air nozzle to the cylinder | m |
| l | thickness of flask wall | m |

| | | |
|---|---|---|
| $L_{O2}$ | solubility of oxygen in the liquid (0.001 mol/L/bar) | mol/L/bar |
| m | superposition factor for $Nu_{rj}$ | - |
| $m_{ITA}(t)$ | calculated mass of itaconic acid at time point t | g |
| $m_x(t)$ | calculated mass of substrate x at time point t | g |
| n | shaking frequency | rpm or 1/s |
| Ne | Newton number | - |
| Ne' | modified Newton number | - |
| Nu | Nusselt number | - |
| $Nu_j$ | Nusselt number for a cylinder with lateral air flow | - |
| $Nu_r$ | Nusselt number for a rotating cylinder | - |
| $Nu_{rj}$ | Nusselt number for a rotating cylinder with lateral air flow | - |
| Osmol | osmolality | osmol/kg |
| OTR | oxygen transfer rate | mmol/L/h |
| P | power | W |
| $P_V$ | volume specific power input | $W/m^3$ |
| $P_{bio}$ | biological heat production | W |
| Ph | Phase number | - |
| $p_R$ | ambient pressure (1.013 bar) | bar |
| $P_S$ | mechanical heat generation | W |
| $P_{total}$ | total power per flask | W |
| $q_{in}$ | gas flow rate into the reactor | L/h |
| Re | Reynolds number | - |
| $Re_f$ | liquid film Reynolds number | - |
| $Re_j$ | Reynolds number for a cylinder with lateral air flow | - |
| $Re_r$ | Reynolds number for a rotating cylinder | - |
| STY (t) | space-time-yield at time point t | g/L/h |
| t | time | h |
| u | velocity of the turbulence generating element relative to the liquid volume | m/s |
| U | overall heat transfer coefficient | $W/m^2/K$ |

| | | |
|---|---|---|
| UA | heat transfer coefficient | W/K |
| $v_{air}$ | velocity of the lateral air flow | m/s |
| $V_F$ | nominal flask volume | mL |
| $v_F$ | velocity of flask | m/s |
| $V_{feed}(t)$ | added feed volume at time point t | L |
| $V_L$ | filling volume | mL or L |
| $V_L(t)$ | filling volume at time point t | L |
| $V_L(t_0)$ | initial filling volume | L |
| $V_M$ | molar volume of ideal gas at 25 °C | L/mmol |
| $V_{mo}$ | molar gas volume (22.414 L/mol) | L/mol |
| $V_{sample}(t)$ | sample volume at time point t | L |
| $V_{sample,total}(t)$ | total sample volume until time point t | L |
| w | width of the nozzle creating lateral air flow | m |
| $W_F$ | weight of the shake flask | g |
| Y(t) | itaconic acid yield at time point t | g/g |
| $y_{CO2,in}$ | $CO_2$ fraction in the inlet gas | mol/mol |
| $y_{CO2,out}$ | $CO_2$ fraction in the outlet gas | mol/mol |
| $y_{O2}^*$ | oxygen mole fraction in the gas phase | mol/mol |
| $y_{O2,in}$ | $O_2$ fraction in the inlet gas | mol/mol |
| $y_{O2,inside}^*$ | oxygen mole fraction of gas inside the flask | mol/mol |
| $y_{O2,L}$ | oxygen mole fraction inside the liquid | mol/mol |
| $y_{O2,out}$ | $O_2$ fraction in the outlet gas | mol/mol |
| $y_{O2,outside}^*$ | oxygen mole fraction of gas outside the flask | mol/mol |
| $\Delta H_{ox}$ | oxycaloric equivalent | kJ/mol |
| $\Delta T$ | temperature change inside the flask | K |

## List of Greek Symbols

| Abbreviation | Description | Unit |
|---|---|---|
| $\alpha$ | heat transfer coefficient between wall and fluid | W/m$^2$/K |
| $\varepsilon_{max}$ | maximum energy dissipation rate | W/kg |
| $\varepsilon_{\varnothing}$ | average energy dissipation rate | W/kg |
| $\eta$ | dynamic viscosity of the liquid | Pa s |
| $\eta_{air}$ | dynamic viscosity of air | Pa s |
| $\lambda$ | thermal conductivity of the fluid | W/m/K |
| $\rho$ | liquid density | kg/m3 |
| $\rho_{air}$ | density of air | kg/m3 |

# List of Tables

**Table 3.1:** Comparison of fermentation KPI in laboratory and 150 L scale. ..... **44**

**Table 4.1:** Calculated filling volumes for each flask sizes depending on the observed case. ..... **52**

**Table 4.2:** Total ($P_{total}$), biological ($P_{bio}$) and mechanical power through shaking ($P_S$) per flask for each flask volume and observed case. ..... **58**

**Table 4.3:** Calculated shaking diameter ($d_0$) and shaking frequency (n) for the different flask sizes. ..... **59**

# List of Figures

**Figure 2.1:** Growth and production of different Ustilaginaceae strains grown on glucose with limiting ammonium chloride concentration (1 g/L $NH_4Cl$).....**12**

**Figure 2.2:** Cultivation of *U. cynodontis* ITA Max pH on different carbon sources with limiting ammonium chloride concentration (1 g/L $NH_4Cl$).....**14**

**Figure 2.3:** Cultivation of *U. cynodontis* ITA Max pH on different carbon sources available in complex substrates without nitrogen limitation.....**15**

**Figure 2.4:** Determination of a correlation between the maximum obtained oxygen transfer rate ($OTR_{N,max}$) and ammonium ion ($NH_4^+$) concentration using *U. cynodontis* ITA Max pH.....**17**

**Figure 2.5:** Estimation of the biologically available ammonium ion concentration equivalents in thick juice (A) and molasses (C) using *U. cynodontis* ITA Max pH. .....**18**

**Figure 2.6:** Influence of osmolality on growth and productivity of *U. cynodontis* ITA Max pH with limiting ammonium chloride concentration (1 g/L $NH_4Cl$).....**19**

**Figure 2.7:** Influence of itaconic acid concentrations on growth and productivity of on *U. cynodontis* ITA Max pH with limiting ammonium chloride concentration (1 g/L $NH_4Cl$).....**20**

**Figure 3.1:** Extended-batch fermentation of *U. cynodontis* ITA Max pH grown with thick juice as sole carbon source with limiting ammonium chloride concentration (4 g/L $NH_4Cl$).....**35**

**Figure 3.2:** Extended-batch fermentation of *U. cynodontis* ITA Max pH with pH shift and thick juice as sole carbon source.....**38**

**Figure 3.3:** Extended-batch fermentation of *U. cynodontis* ITA Max pH with magnesium hydroxide as pH adjusting agent and thick juice as sole carbon source. .....**40**

**Figure 3.4:** 100 L batch fermentation of *U. cynodontis* ITA Max pH with pH shift and thick juice as sole carbon source.....**43**

**Figure 4.1:** Relative filling volume ($V_L/V_F$) and the fluid volume per tray for the three different cases in dependance of the flask volume ($V_F$). .....**60**

**Figure 4.2:** Phase numbers for the three different cases in dependance of the flask volume ($V_F$).....**61**

**Figure 4.3:** Volume specific power input ($P_V$) and Reynolds number (Re) for the three different cases in dependance of the flask volume ($V_F$). .....**62**

**Figure 4.4:** Average ($\varepsilon_{Ø}$) and maximum energy dissipation rate ($\varepsilon_{max}$) for the three different cases in dependance of the flask volume ($V_F$). .....**63**

**Figure 4.5:** Maximum oxygen transfer capacity ($OTR_{max,plug}$) and the fraction of oxygen inside the flask ($y_{O2,F}$) for the three different cases in dependance of the flask volume ($V_F$).....**64**

**Figure 4.6:** Comparison of the overall heat transfer coefficient (UA) [A] and the heat transfer coefficient (U) [B] calculated after Sumino and Akiyama, Jeng et al., Raval et al. and Dinger et al. for the three different cases in dependance of the flask volume ($V_F$).....**67**

**Figure 4.7:** Temperature difference between flask and surrounding air ($\Delta T_{F/S}$) calculated with UA after Sumino and Akiyama, Jeng et al., Raval et al. and Dinger et al. for the three different cases in dependance of the flask volume ($V_F$).....**69**

Parts of the introduction have been previously published in Sauer, K. M., Kiefel, R., Niehoff, P.-J., Hofstede, J., Ernst, P., Brockkötter, J., Gätgens, J., Viell, J., Noack, S., Wierckx, N., Büchs, J., Jupke, A. Holistic Approach to Process Design and Scale-Up for Itaconic Acid Production from Crude Substrates. *Bioengineering* 2023, 10(6), 723. Sauer, Kiefel, and Niehoff contributed equally to this work.

Additional parts have been published Niehoff, P.-J., Müller, W., Pastoors, J., Miebach, K., Ernst, P., Hemmerich, J., Noack, S., Wierckx, N., Büchs, J. Development of an Itaconic Acid Production Process With Ustilaginaceae on Alternative Feedstocks. *BMC Biotechnology* 23, 34 (2023).

# Chapter 1

## 1. Introduction

Bio-based production of bulk chemicals plays a significant role in the transition towards a circular bioeconomy [40]. Carboxylic acids, amines, and alcohols are already being produced via fermentation and can potentially replace fossil-based chemicals in the packaging, food, and pharmaceutical industries or build new functional materials [9, 82]. However, their market share was only 1 - 2 % in 2019 [115]. One reason is the high production cost of bio-based chemicals, to which the feedstock is an essential factor [3, 145]. While pure substrates are easy to process, they are predominantly destined for the food and feed industry and are typically only used for small-scale, high-value biotechnological processes [115]. Using crude substrates from the food and agricultural sector provides a promising alternative [35, 36, 73, 122]. Especially waste and side streams from local industries present a high potential for economically competitive biorefinery concepts [9, 35, 40].

Different carboxylic acids, like citric, succinic, or lactic acid, have already been produced using alternative feedstocks [2, 13, 94, 142, 153]. Itaconic acid (ITA) is another carboxylic acid of interest, due to its two functional groups. Esterification of the carboxyl groups and polymerization of the methyl group allows for a broad range of applications, such as hydrogel, superabsorber, or additive in industrial adhesives [15, 31, 78, 101, 112, 134]. Considerable potential also lies in replacing malic acid anhydride in polyester resin production [110, 116, 128]. In addition, 3-methyl tetrahydrofuran – a potential biofuel – can be produced from ITA [47]. Interestingly, ITA has been identified within the human immune response, leading to applications as therapeutic agent [7, 26]. Due to the vast application range and expected market size of US$ 117.1 M in 2026 [143], ITA is the perfect bulk chemical for sustainable production on alternative feedstocks.

Until now, industrial production of ITA has been exclusively realized using *Aspergillus terreus* due to its tolerance to low pH, high titers, and yields [76, 83, 86, 88]. Industrially relevant titers of up to 160 g/L in pulsed batch fermentations and yields of up to 0.58 $g_{ITA}/g_{glucose}$ are reported in the literature [86]. However, there are several disadvantages to using this strain. The filamentous morphology poses challenges with respect to oxygenation, shear stress during fermentation, and risk of failed batches [77]. In addition, the pretreatment of complex substrates is necessary for high productivity with this strain [44, 86, 131]. For example, even trace amounts of manganese are highly detrimental to ITA formation [71, 83]. Finally, the pathogenic classification of *A. terreus* limits its applicability even further [56, 133].

To evade these challenges, alternative organisms for ITA production have become the focus of research. These include genetically engineered organisms like *Corynebacterium glutamicum* [113] or *Escherichia coli* [41] and natural ITA producers like *Ustilago sp*. [48] or *Candida sp*. [140]. Of the latter, especially *Ustilago sp*. have found increasing attention in recent years [12, 48, 50, 63, 87, 133, 149, 152]. Two representatives, *U. maydis* and the pH-tolerant *U. cynodontis*, have great potential for tackling the challenges presented for ITA production with *A. terreus*. As plant pathogens infecting corn plants, these strains do not affect animal health [56]. Furthermore, through genetic engineering, yeast-like morphology can be sustained throughout the entire fermentation, allowing for better oxygenation and lower susceptibility to hydromechanical stress than *A. terreus* [61, 63]. Moreover, unwanted side-product formation was deleted [11]. By introducing additional feed pulses, titers of up to 220 g/L (pulsed-batch fermentation with *in-situ* crystallization) and 83 g/L (pulsed-batch fermentation) with yields of up to 0.61 $g_{ITA}/g_{glucose}$ and 0.39 $g_{ITA}/g_{glucose}$ were reached for *U. maydis* and *U. cynodontis*, respectively [61, 62]. Deep metabolic and morphological engineering further enabled itaconic acid production at the maximum theoretical yield in a fermentation with constant glucose feed [12]. However, these key performance indicators (KPI) were reached in defined media. While some years ago, *U. maydis* was shown to produce ITA from alternative feedstocks, like beech wood or brewers' spent grain, only recently such research was published for *U. cynodontis* [57, 111, 127, 132, 148].

In contrast to defined carbon sources, crude substrates differ enormously in composition and seasonal availability [84, 114]. They also vary regarding their regional availability [115]. As a result, transportation costs can be a deciding factor for the economic feasibility

of biorefineries [39], supporting the idea of a local circular bioeconomy. Alternative feedstocks are inherently complex and contain a plethora of compounds besides the carbon source. These include, for example, additional nitrogen sources, pigments, or salts. Different salts have been shown to be detrimental to ITA production [44, 77, 86]. In addition, organic acids, often produced by microbial activity during feedstock storage, can negatively influence growth and product formation in the production process [137]. Furthermore, using complex feedstocks poses additional challenges, as potential impurities can also affect downstream processing [30, 60, 89]. Therefore, the choice of substrate is crucial for the feasibility of the production process.

Early-stage bioprocess development is normally performed in shaken bioreactors, such as microtiter plates (MTP) or shake flasks [80]. Later on in the development, stirred tank reactors (STR) are often employed. Scale-up from shaken bioreactors to STR can present challenges, requiring careful consideration of the hydrodynamic conditions and mixing characteristics [105]. The transition to larger volumes can lead to changes in the oxygen transfer rate (OTR), shear stress, and nutrient distribution within the bioreactor, potentially affecting cell growth and product formation [45, 52]. To avoid these negative impacts, a suitable scale-up criterion must be chosen [100].

## 1.1 Aim of this thesis

This thesis aims to develop an ITA production process using *Ustilago sp*. with alternative feedstocks and the procedural analysis of commercially available, unbaffled shake flasks.

In Chapter 2, shaken bioreactors are applied for early-stage bioprocess development. A suitable production strain is chosen based on growth and product formation in defined media. Subsequently, an investigation of different side and waste streams from local industry is conducted. As a nitrogen limitation is necessary for ITA production with the used *Ustilago sp*., the nitrogen content of the alternative feedstock is of key importance. Hence, a simple method was developed to determine the biologically available nitrogen based on the online monitored OTR. Regarding the feedstocks, this work focuses on substrates for a decentralized biorefinery in the German Rhineland. The region has a large agricultural sector and faces structural and economic changes due to the phasing out of lignite mining. Therefore, feedstocks from the local food industry in the Aachen (Germany) region are used. Replacing pure sugars with crude feedstocks inevitably increases the

osmolality, which can significantly influence the production process [150]. Hence, the influence of the osmolality was analyzed in shake flasks. Finally, because ITA is a carboxylic acid and exhibits weak acid stress [62, 77], the influence of the pH on the process was studied.

Chapter 3 showcases the scale-up of the developed production process to STR. Further optimization was performed regarding substrate availability, pH, initially added nitrogen concentration, and pH adjusting agent. While this thesis focuses on the upstream process, a holistic approach, including the downstream processing, was applied, as seen in Saur et al. (2023) [132]. The feasibility of ITA production on thick juice in larger scale was proven in a 150 L STR.

Lastly, a procedural analysis of commercially available shake flasks from 50 – 5000 mL was performed to investigate whether they can be used reliably over the whole range of flask sizes (Chapter 4). For this purpose, two key assumptions were developed to determine comparable shaking conditions in all flask sizes. Based on these assumptions, classical engineering parameters like volumetric power input, maximum oxygen capacity, and heat transfer were analyzed.

Parts of the following chapter have been published in Niehoff, P.-J., Müller, W., Pastoors, J., Miebach, K., Ernst, P., Hemmerich, J., Noack, S., Wierckx, N., Büchs, J. Development of an Itaconic Acid Production Process With Ustilaginaceae on Alternative Feedstocks. *BMC Biotechnology* 23, 34 (2023). Figure 2.3 and Figure 2.7 are based on the work of Waldemar Müller [109]. His valuable work is greatly appreciated as it supports the research presented in this dissertation.

# Chapter 2

## 2. Development of an Itaconic Acid Production Process with Alternative Feedstocks in Shaken Bioreactors

### 2.1 Background

The first step in the development of an itaconic acid production process is the screening for a production strain and, afterward, for a suitable feedstock. Because both *Ustilago* strains (*U. maydis* and *U. cynodontis*) used in this study require a nitrogen limitation to initiate ITA production [151], the biologically available nitrogen content of the alternative feedstock is of utmost importance and needs to be evaluated. In addition, the use of complex substrates increases the osmolality of the medium, which might lead to a prolonged lag phase or even prevent growth [150]. In addition, the influence of pH on production is of key interest, as the product is a carboxylic acid.

Shaken bioreactors, like microtiter plates and shake flasks, are the cultivation vessels of choice for bioprocesses in the early stages of development [80]. Due to their high throughput and low costs, MTP are perfect for screening applications [74, 152] and strain characterization [76, 84]. On the other hand, shake flasks, with their ease of handling and increased filling volumes compared to MTP, allow for a range of offline analytics. In general, shaken bioreactors have been extensively studied, regarding for example power input [21, 81], energy dissipation rate [120], or OTR [33, 91, 104].

The OTR is a crucial parameter for microbial cultivations. It allows for the determination of biological phenomena such as diauxic growth, substrate limitations, or oxygen limitation, as it is directly coupled to the metabolic activity of the microbe [4]. It has repeatedly been used for the investigation of microbial growth and product formation and

is, therefore, the perfect parameter for bioprocess development in small scale [58, 108, 117]. The OTR can be monitored with the Respiratory Activity Monitoring System (RAMOS), which has been developed for shake flasks almost twenty years ago [4, 5]. Since then, it has been miniaturized for use in a 48-well MTP (µRAMOS) [42] and even combined with the BioLector technology [90]. However, for higher throughput, the recently published micro(µ)-scale transfer rate online measurement device (µTOM) for 96-well MTP can be used [33].

In this chapter, five engineered strains of *U. maydis* and *U. cynodontis* were screened regarding growth and product formation in defined media. One *U. cynodontis* and one *U. maydis* strain were then further used to investigate different side and waste streams from the local food industry, to find a suitable substrate for ITA production. In the next step, the carbon preference of the production organism was analyzed and the biologically available nitrogen content of thick juice and molasses was determined. In addition, the influence of osmolality and pH on ITA production was investigated.

## 2.2 Material and Methods

### *2.2.1 Microbial strains and media composition*

*Ustilago cynodontis* NBRC9727 Δfuz7r Δcyp3r $P_{ria1}$ria1 (*U. cynodontis* pre-gen), *Ustilago cynodontis* NBRC9727 Δfuz7r Δcyp3r $P_{etef}$mttA $P_{ria1}$ria1 (*U. cynodontis* ITA Max pH) [63], *Ustilago maydis* MB215 Δcyp3 Δ$P_{ria1}$::$P_{etef}$ Δfuz7 $P_{etef}$mttA (*U. maydis* ITA Max) [61], *Ustilago maydis* MB215 2229 Δcyp3 ΔMEL ΔUA Δdgat ria1↑ Δfuz7 (*U. maydis* ITA chassis) [11] and *Ustilago maydis* MB215 2229 Δcyp3 ΔMEL ΔUA Δdgat ria1↑ Δfuz7 mttA↑ (*U. maydis* Mutterschiff) [12] were used for the cultivation experiments. The strains were stored as cryogenic cultures at -80 °C, containing 30 % (v/v) of 500 g/L glycerol stock and 70 % (v/v) culture grown on modified Verduyn medium (see below), containing 50 g/L glucose and 4 g/L $NH_4Cl$. Cultivations were performed in modified Verduyn medium as described before by Geiser et al. [48]. If not stated otherwise, the medium was composed of 0.2 g/L $MgSO_4 \cdot 7\ H_2O$, 0.01 g/L $FeSO_4 \cdot 7\ H_2O$, 0.5 g/L $KH_2PO_4$, and 0.1 % (v/v) trace element solution. The trace element solution consisted of 15 g/L TitriplexIII©, 4.5 g/L $ZnSO_4 \cdot 7\ H_2O$, 0.84 g/L $MnCl_2 \cdot 2\ H_2O$, 0.3 g/L $CoCl_2 \cdot 6\ H_2O$, 0.3 g/L $CuSO_4 \cdot 5\ H_2O$, 0.4 g/L $Na_2MoO_4 \cdot 2\ H_2O$, 4.5 g/L $CaCl_2 \cdot 2\ H_2O$, 3 g/L $FeSO_4 \cdot 7\ H_2O$, 1 g/L $H_3BO_3$ and 0.1 g/L KI. Experiments additionally contained 0.1 or 0.03 M 2-(N-morpholino) ethane sulfonic acid

(MES). The media components were either sterile-filtered with a 0.2 µm cut-off filter (Millipore-Sigma, Burlington, USA) or autoclaved at 121 °C for 20 min.

An overview of the feedstocks used for experiments presented in Figure 2.2 and Appendix 1 is provided in Appendix 2.

The alternative feedstocks were kindly provided by Pfeifer & Langen Industrie- und Handel-KG (molasses, thin and thick juice), Zentis GmbH & Co. KG (fruit preparations) and GNT Europe GmbH (filtration retentate and permeate). Molasses, thin and thick juice originate from the sugar manufacturing process as a side (thin and thick juice) or waste streams (molasses). The "fruit preparation" is a waste stream from jam and marmalade production. Filtration retentate and permeate are both side streams in the pigment extraction from carrots.

*2.2.2 Cultivation in shaken systems*

Cultivations on a small scale were carried out either in 96 round deep-well MTP (riplate RW, 2.0 ml round deep-well plate, HJ-BIOANALYTIK GmbH, Erkelenz, Germany) or in 250 mL RAMOS shake flasks at 350 rpm, with a shaking diameter of 50 mm at 30 °C (Climo-Shaker ISF1-X, Kuhner, Birsfelden, Switzerland). Filling volumes ranged from 300 µL in MTP to 10 mL in shake flasks. For sterility, MTP were covered with gas-permeable sealing films (AeraSeal$^{TM}$, Sigma-Aldrich, St. Louis, USA). Online monitoring of the oxygen transfer rates was achieved using the RAMOS for shake flasks and the newly developed µTOM for MTP [4, 5, 33].

Pre-cultures were inoculated with 1 mL cryogenic stock (OD 5) per 10 mL pre-culture medium and cultivated overnight. Cultures were then centrifuged at 14,000 revolutions per minute (rpm) for 5 min at room temperature and resuspended in the main culture medium. Main cultures were inoculated to an OD of 0.8.

*2.2.3 Offline analytics*

Samples were analyzed regarding sucrose, fructose, glucose, and itaconic acid concentration using High-performance liquid chromatography (HPLC). Samples were centrifuged at 15,000 rpm for 10 min. The supernatant was diluted appropriately with deionized water and then filtered with a 0.2 µm cut-off filter (Millipore-Sigma, Burlington, USA). HPLC analysis was performed in three dilutions per biological sample using a Thermo Fisher Ultimate 3000 (Thermo Fisher Scientific Inc., Waltham, USA) equipped

with an ERC RefractoMax 520 RID (Shodex, Munich, Germany). Separation was achieved with a ROA-Organic Acid H+ (8 %) (300 x 7.8 mm) column (Phenomenex, Torrance, USA) heated to 30 °C and a mobile phase of 5 mM $H_2SO_4$ running at 0.8 mL/min. Optical density (OD) was measured using a Genesys 20 photometer (Thermo Fisher Scientific Inc., Waltham, USA) at a wavelength of 600 nm. pH was measured with a HI221 Basic pH (Hanna Instruments Deutschland GmbH, Voehringen, Germany). Osmolality was determined with a cryoscopic Osmometer OSMOMAT® 030 (Genotec, Berlin, Germany).

*2.2.4 Calculations*

As key performance indicator, the yield [$g_{ITA}/g_{sugar}$] was calculated based on the produced ITA [g] and the consumed sugar mass [g] of sucrose, glucose and fructose. Other compounds in the complex feedstock were not considered. Equation 2.1 shows the calculation of the mass balances for the substrates.

$$m_x(t) = c_x(t_0) \cdot V_L(t_0) - \sum_{t_0}^{t} c_x(t) \cdot V_{sample}(t) \quad (2.1)$$

Here, $m_x(t)$ [g] is the calculated mass at time point t, $c_x(t_0)$ [g/L] is the concentration of the different substrates (glucose, fructose or sucrose) at the beginning of the fermentation and $V_L(t_0)$ [L] is the initial filling volume. To consider sampling, the sum of the substrate concentrations ($c_x(t)$ [g/L]) times the sample volume ($V_{sample}(t)$ [L]) is subtracted. To calculate the mass balance for the produced ITA Equation 2.2 is used.

$$m_{ITA}(t) = c_{ITA}(t) \cdot V_L(t) + \sum_{t_0}^{t} c_{ITA}(t) \cdot V_{sample}(t) \quad (2.2)$$

The mass of ITA [g] is calculated by multiplying the ITA concentration $c_{ITA}(t)$ [g/L] by the filling volume $V_L(t)$ [L] at time point t. The sum of the ITA concentrations $c_{ITA}(t)$ [g/L] times the sample volume $V_{sample}(t)$ [L] considers the sampling.

The yield can then be calculated by dividing the mass of ITA [g] by the sum of the substrates glucose [g], fructose [g], and sucrose [g] (Equation 2.3).

$$Y(t) = m_{ITA}(t) \cdot \left(m_{glucose}(t) + m_{fructose}(t) + m_{sucrose}(t)\right)^{-1} \quad (2.3)$$

Yields on glucose were calculated by counting one mol of sucrose as two moles of glucose.

For all the above-mentioned calculation errors are based on Gaussian error propagation, when applicable.

Statistical analysis tools (*scypi.stats* and *statsmodels* modules in *Python 3.0*) were used to determine the significance of the data from experiments with biological triplicates (Figure 2.1 and 2.2, OD, ITA, titer, and yield). Normal distribution was assumed and homogeneity of variance was determined using Levene's test. Afterward, an ANOVA with a significance level of $\alpha = 0.05$ was used to determine whether there was a significant difference between the different strains. As all tested conditions showed a significant difference, Tukey's Honestly Significant Difference test was performed to determine between which groups the difference was significant. As statistical significance was determined between almost all groups, only the ones where no difference was determined are mentioned in the manuscript.

When comparing cultivations with different durations, maintenance has to be considered. The longer cultivation requires more carbon for maintenance, thus lowering the substrate yield. The amount of substrate used for maintenance during the production phase for *U. cynodontis* ITA Max pH and *U. maydis* Mutterschiff was estimated for experiments depicted in Figure 2.1. In the following calculation, only that part of the cultivations which are nitrogen limited and where there is no substantial growth is considered. Assuming a constant biomass ($m_{bio}$) for the whole production phase, the consumed substrate due to maintenance ($c_{S,m}$) [g] can be calculated according to Equation 2.4.

$$c_{S,m} = m_{bio} \cdot m_S \cdot t_{prod} \quad (2.4)$$

With $m_{bio}$ as biomass [g], $m_S$ as maintenance coefficient [$g_{substrate}/g_{biomass}/h$] and $t_{prod}$ as production time [h]. Further, assuming the same constant maintenance coefficient for both strains, the ratio of $c_{S,m}$ ($r_m$) [-] between the strains can be calculated according to Equation 2.5.

$$r_m = m_{bio,U.cynodontis} \cdot t_{prod,U.cynodontis} \cdot \left(m_{bio,U.maydis} \cdot t_{prod,U.maydis}\right)^{-1} \quad (2.5)$$

With $m_{bio,U.cynodontis}$ as biomass for *U. cynodontis* ITA Max pH [g or -], $t_{prod,U.cynodontis}$ as the production time of *U. cynodontis* ITA Max pH [h], $m_{bio,U.maydis}$ as biomass for *U. maydis* Mutterschiff [g or -] and $t_{prod,U.maydis}$ as the production time of *U. maydis* Mutterschiff [h]. Note that no specific values for $c_{S,m}$ are calculated and, therefore, OD can be used for $m_{bio}$. In addition, no specific maintenance coefficient is required.

## 2.3 Results

### *2.3.1 Screening for a suitable production organism and feedstock*

To compare the five *Ustilago* strains under the same conditions in a time-efficient manner, the newly developed µTOM for OTR measurement was used for an experiment with glucose as carbon source (Figure 2.1) [33]. To enable ITA production, the cultivation was performed under nitrogen-limiting conditions.

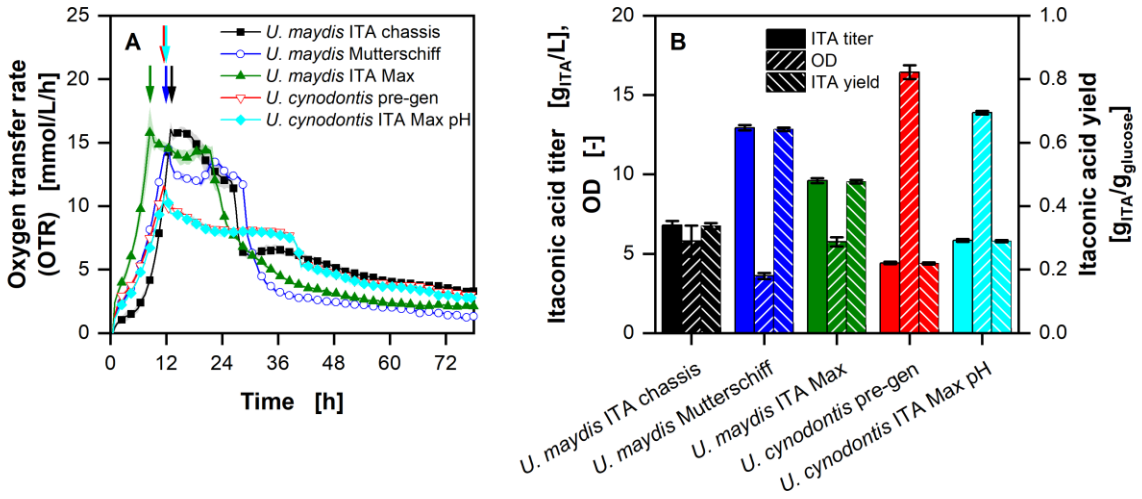


**Figure 2.1: Growth and production of different Ustilaginaceae strains grown on glucose with limiting ammonium chloride concentration (1 g/L $NH_4Cl$).**

(A) Course of the oxygen transfer rates. Arrows indicate the start of nitrogen limitation. (B) Itaconic acid titers, optical densities, and yields of ITA on glucose after 78 h of cultivation. Cultivations were performed in a 96 round deep-well MTP, filled with 300 µL modified Verduyn medium with 25 g/L glucose at 30 °C, 350 rpm shaking frequency, and a shaking diameter of 50 mm. 100 mM and 30 mM MES were added to the *U. maydis* and *U. cynodontis* cultivations, respectively. The initial pH was set to 6.5 for all cultures. Graphs in (A) show the mean of three replicates, with standard deviation as shaded area. Due to the high reproducibility of the measurements, the standard deviation might not be visible for every data point. For clarity, only every fourth data point is shown.

All five strains show three distinct phases: an exponential growth phase, a nitrogen-limited production phase, and a carbon depletion phase (Figure 2.1A). The typical phases of ITA production with Ustilaginaceae on glucose are illustrated in Appendix 3. During the first phase, the OTR increases exponentially until a drop is visible (Figure 2.1A). During the following phase, the Ustilaginaceae strains behave differently. The OTR of *U. maydis* ITA chassis indicates a short plateau at 15.8 mmol/L/h before it decreases to 6.5 mmol/L/h after 26 h. The OTR of both other *U. maydis* strains first decreases and then increases again during the nitrogen-limited production phase. The OTR of both *U. cynodontis* strains decreases slowly and then remains constant at ~8 mmol/L/h until 39.5 h. Once the glucose

is depleted, the OTR drops sharply for all strains. The total production time for *U. maydis* Mutterschiff is 14 h, while *U. cynodontis* ITA Max needed 28 h to consume all substrate. At the end of the cultivation, *U. maydis* ITA chassis and *U. maydis* ITA Max reached an OD of 5.8 (no significant difference) and ITA titers of 6.8 and 9.8 $g_{ITA}$/L, respectively (Figure 2.1B). *U. maydis* Mutterschiff had the lowest OD of 3.6 and the highest titer of 12.9 $g_{ITA}$/L. At the same time, *U. cynodontis* pre-gen and *U. cynodontis* ITA Max pH reached an OD of 16.4 and 13.9, as well as ITA titers of 4.4 and 5.9 $g_{ITA}$/L, respectively.

Figure 2.2 shows the OTR, ITA titers, and yields of *U. cynodontis* ITA Max pH on different carbon sources (Appendix 2). On the pure sugars glucose, fructose, and sucrose, the highest OTR reached is 12.5 mmol/L/h, which is considerably lower than the OTR reached with complex carbon sources (Figure 2.2A). OTR of ~13.5 mmol/L/h were reached with sugar beet thin juice, thick juice, and fruit preparation, while OTR of ~25.0 mmol/L/h could be reached with molasses and the filtration retentate (Figure 2.2B).

ITA production is shown in Figure 2.2C with all carbon sources, except filtration permeate due to no visible growth (data not shown). While titers of 23.9 $g_{ITA}$/L were reached with the filtration retentate, titers for the used fruit preparation were lower with 0.1 $g_{ITA}$/L. Even higher titers were reached with *U. maydis* Mutterschiff, while the strain was also able to produce increased amounts of ITA from the fruit preparation (Appendix 1). For *U. cynodontis* ITA Max pH, the highest yield of 0.30 $g_{ITA}/g_{sugar}$ was reached with filtration retentate, even outperforming production on glucose and fructose with yields of 0.22 and 0.21 $g_{ITA}/g_{sugar}$ (no significant difference), respectively. The yields on thin- and thick juice and molasses are between 0.13 and 0.17 $g_{ITA}/g_{sugar}$, with thin juice having the highest and molasses the lowest yield.

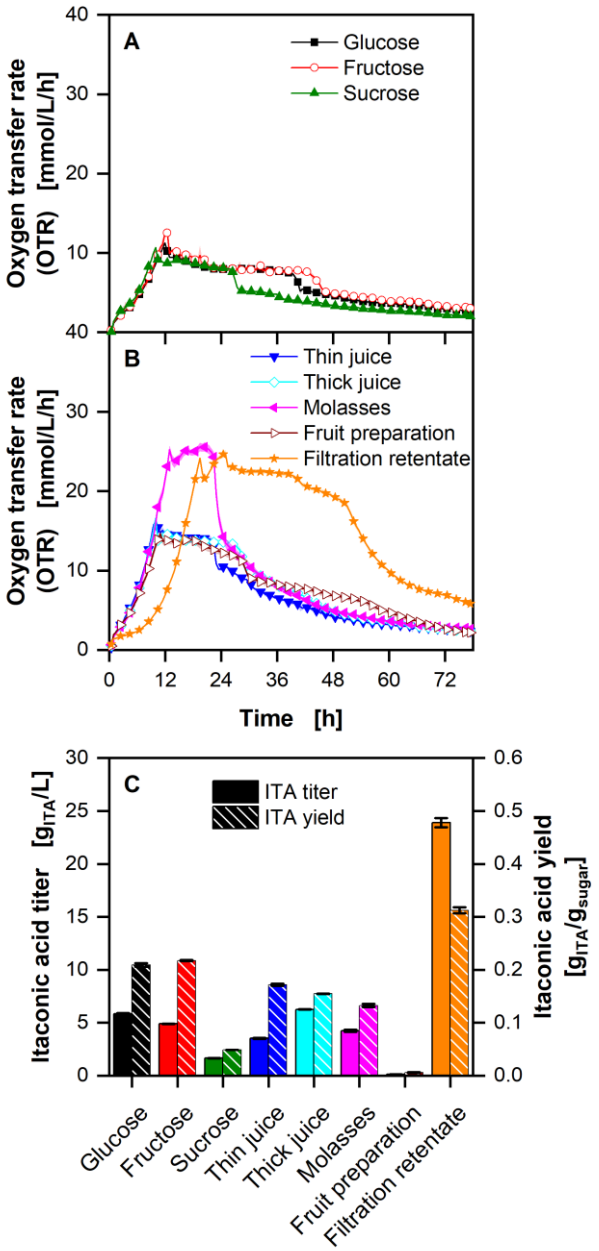


**Figure 2.2: Cultivation of *U. cynodontis* ITA Max pH on different carbon sources with limiting ammonium chloride concentration (1 g/L $NH_4Cl$).**

(A) Course of the oxygen transfer rates for cultivations with the pure sugars (glucose, fructose, and sucrose). (B) Course of the oxygen transfer rates for cultivations with complex substrates. (C) Itaconic acid titers and yields of the cultivations after 78 h of cultivation. Cultivations were performed in 96 round deep-well MTP, filled with 300 µL modified Verduyn medium at 30 °C, 350 rpm shaking frequency, and a shaking diameter of 50 mm. 30 mM MES were added to the cultivations. The initial pH was set to 6.5 for all cultivations. The different carbon sources are specified in Appendix 2. Graphs show the mean of three replicates, with standard deviation as shaded area. Due to the high reproducibility of the measurements, the standard deviation might not be visible for every data point. For clarity, only every fourth data point is shown.

To further analyze the possible substrates, *U. cynodontis* ITA Max pH was grown on different monomeric carbon sources available in thick juice and molasses (Figure 2.3). The OTR of all four cultivations shows similar behavior with an exponential increase until a sharp drop, which happens after 14 h for the reference and the cultivation with additional lactate. It is delayed by 2 h for the experiments with additional sugars (glucose and fructose).

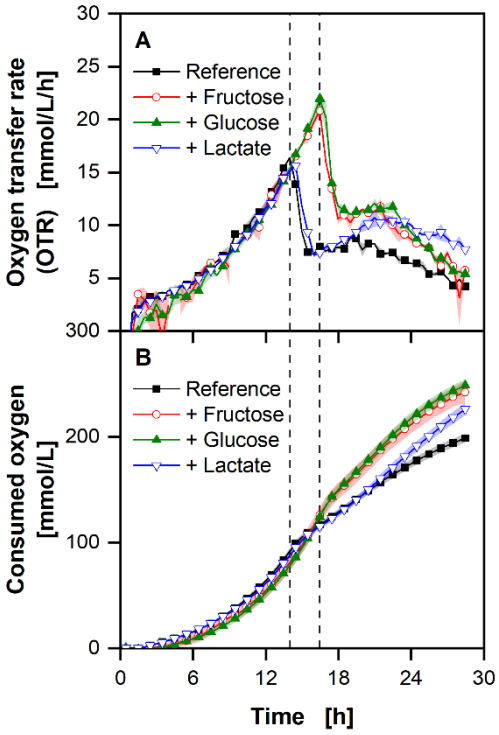


**Figure 2.3: Cultivation of *U. cynodontis* ITA Max pH on different carbon sources available in complex substrates without nitrogen limitation.**

The basic medium, denoted as "Reference" contained 5 g/L fructose, glucose, and lactate, each. The concentration of fructose, glucose, and lactate was each individually increased to 10 g/L compared to the reference. The curves in the figure are denoted by the type of additional carbon source. (A) Course of the oxygen transfer rates. (B) Consumed oxygen (integral of the data in (A)). Dashed vertical lines show the depletion of fructose and glucose. The first dashed line shows the depletion of fructose and glucose for the reference and the cultivation with increased lactate, while the second dashed line shows the depletion for the cultivations with increased sugars. Cultivations were performed in 250 mL RAMOS flasks filled with 10 mL modified Verduyn medium at 30 °C, 350 rpm shaking frequency, and a shaking diameter of 50 mm. 30 mM MES were added to the cultivations. The initial pH was set to 6.5 for all cultivations. The final pH reaches 6.37 ± 0.02, 6.22 ± 0.01, 6.23 ± 0.02, and 7.56 ± 0.03 for the reference, increased fructose, glucose, and lactate cultivations, respectively. Errors describe the deviation of the maximum and minimum pH value from the mean of duplicates. Graphs show the mean of duplicates. Shadows show the minimum and maximum values. Due to the high reproducibility of the measurements, the standard deviation might not be visible for every data point. For clarity, only every second data point is shown.

After the drop, the OTR increases slightly for the reference and the cultivations with additional sugars before slowly decreasing until the cultivations' end. Additional lactate prolongs the increase after the first OTR drop, compared to the reference. Correlating to the decline in the OTR (Figure 2.3A), the increase in the consumed oxygen decreases (Figure 2.3B). While it is similar for both runs with increased monosaccharide concentration, consumed oxygen for the reference and the cultivation with additional lactate differs after the drop. At the end of the cultivation, 250 mmol/L oxygen was consumed in the cultivations with added monosaccharides, 226 mmol/L with increased lactate, and 198 mmol/L in the reference. The pH at the end of the cultivations with additional sugars is lower than the reference, which in turn is significantly lower than the one with increased lactate.

### *2.3.2 Determination of biologically available nitrogen in molasses and thick juice*

Due to the necessary nitrogen limitation for ITA production, nitrogen availability in the feedstock plays a major role [151]. Therefore, the available nitrogen content in the complex substrate needs to be determined. The maximum OTR ($OTR_{N,max}$) is reached when the nitrogen limitation starts. A correlation between nitrogen concentration in the medium and the $OTR_{N,max}$ can be obtained on defined minimal media with known nitrogen concentrations. The correlation can be used to determine the unknown biologically available nitrogen concentration in thick juice and molasses.

*U. cynodontis* ITA Max pH was cultivated in defined medium with sucrose as carbon source (Figure 2.4A). With increasing ammonium concentrations, the resulting $OTR_{N,max}$ increases accordingly (Figure 2.4B). The $OTR_{N,max}$ reaches 4.7 mmol/L/h with 0.135 g/L ammonium and increases up to 19.8 mmol/L/h with 0.675 g/L ammonium (Figure 2.4A). Fitting a linear model through the $OTR_{N,max}$ values over the initially added ammonium ion concentration leads to a calibration curve, which can be used to determine the biologically available nitrogen concentration in any complex medium.

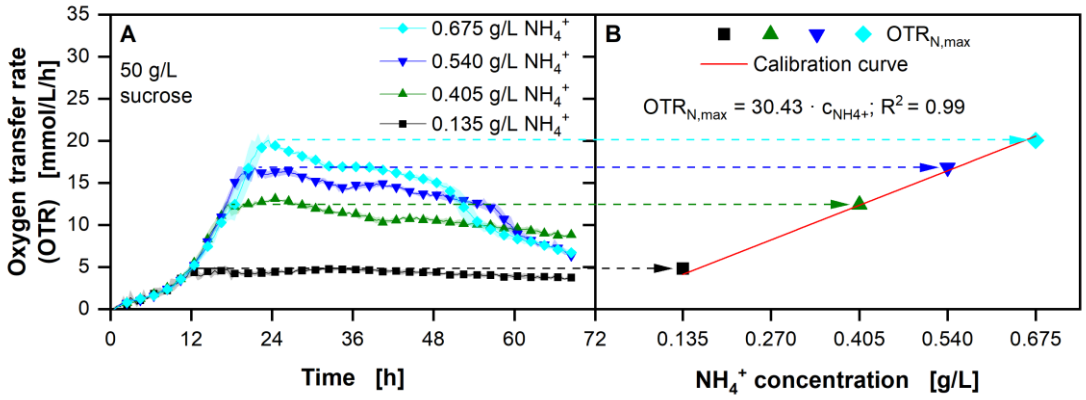


**Figure 2.4: Determination of a correlation between the maximum obtained oxygen transfer rate ($OTR_{N,max}$) and ammonium ion ($NH_4^+$) concentration using *U. cynodontis* ITA Max pH.**
(A) Course of the oxygen transfer rates with addition of specific $NH_4^+$ concentrations in modified Verduyn medium. (B) Correlation between $OTR_{N,max}$ and $NH_4^+$ concentration. Cultivations were performed in a 96 round deep-well MTP, filled with 300 µL modified Verduyn medium with 50 g/L sucrose and 0.135 – 0.675 g/L $NH_4^+$ (0.4 – 2.0 g/L $NH_4Cl$) at 30 °C, 350 rpm shaking frequency and a shaking diameter of 50 mm. 30 mM MES were added to the cultivations. The initial pH was set to 6.5 for all cultivations. Graphs show the mean of three replicates, with standard deviation as shaded area. Due to the high reproducibility of the measurements, the standard deviation might not be visible for every data point. For clarity, only every fourth data point is shown.

In a second step, *U. cynodontis* ITA Max pH was cultivated in the same medium, while the carbon source was replaced by thick juice (Figure 2.5A) or molasses (Figure 2.5C). While the general course of the OTR of the thick juice cultivations looks similar to the ones on pure sucrose (Figure 2.4A), the ones on molasses differ after the initial exponential increase that lasts for 18 h (Figure 2.5C). While the OTR for the condition with the lowest ammonium concentration drops, the other three stay either constant or increase. With the calibration curve from Figure 2.4B, the $OTR_{N,max}$ can be used to calculate the ammonium equivalents available in the media. From these, the initially added ammonium concentration needs to be subtracted to determine the biologically available nitrogen in the added thick juice or molasses. Hence, values of 2.3 ± 0.2 and 5.1 ± 0.1 g/L ammonium ion equivalents can be calculated and are available in thick juice and molasses, as indicated by vertical lines in Figure 2.5B and D, respectively.

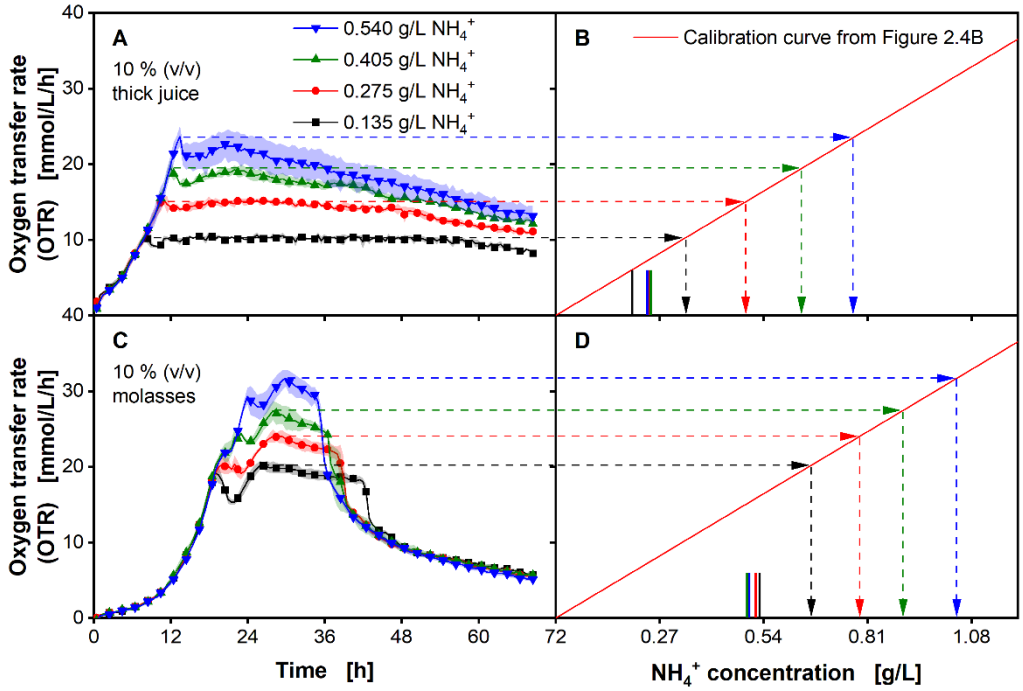


**Figure 2.5: Estimation of the biologically available ammonium ion concentration equivalents in thick juice (A) and molasses (C) using *U. cynodontis* ITA Max pH.**

(A, C) Course of the oxygen transfer rates with addition of specific $NH_4^+$ concentrations in modified Verduyn medium. Estimated $NH_4^+$ equivalents in the medium containing thick juice (B) or molasses (D). Arrows show available $NH_4^+$ concentrations in the respective medium. Solid colored vertical lines in Figure 2.5B and D indicate the biologically available $NH_4^+$ equivalents in modified Verduyn medium without added $NH_4^+$. Cultivations were performed in a 96 round deep-well MTP, filled with 300 µL modified Verduyn medium with 10 % (v/v) thick juice or molasses and 0.135 – 0.540 g/L $NH_4^+$ (0.4 – 1.6 g/L $NH_4Cl$) at 30 °C, 350 rpm shaking frequency and a shaking diameter of 50 mm. 30 mM MES were added to the cultivations. The initial pH was set to 6.5 for all cultivations. Graphs show the mean of three replicates, with standard deviation as shaded area. Due to the high reproducibility of the measurements, the standard deviation might not be visible for every data point. For clarity, only every fourth data point is shown.

### *2.3.3 Influence of osmolality, pH and ITA concentrations on U. cynodontis cultivations*

Replacing pure sugars with complex substrates inevitably increases the osmolality of the medium, which can significantly influence the process [150]. Therefore, defined media with increased osmolalities and their effect on growth and ITA production were investigated.

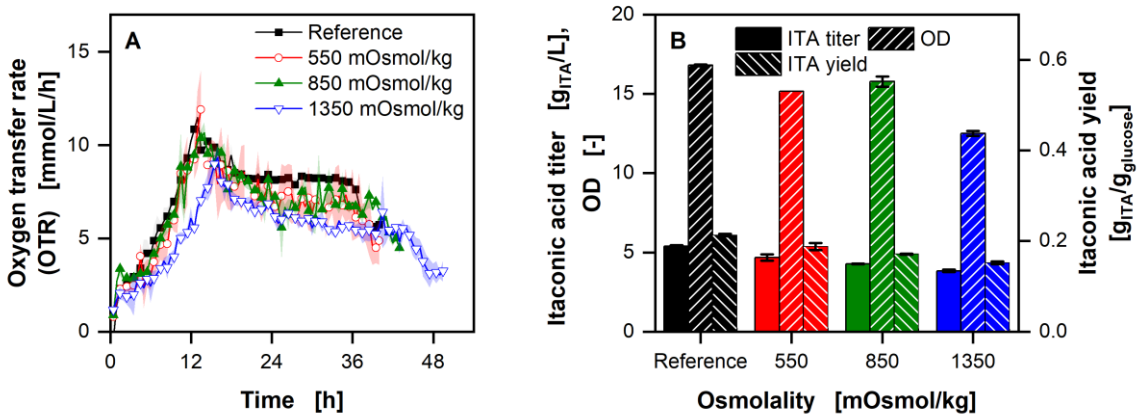


**Figure 2.6: Influence of osmolality on growth and productivity of *U. cynodontis* ITA Max pH with limiting ammonium chloride concentration (1 g/L $NH_4Cl$).**

(A) Course of the oxygen transfer rates. (B) Itaconic acid titer, OD, and yield at the end of the respective cultivations. Osmolality was increased by addition of 0.1, 0.25, and 0.5 M NaCl. The reference medium has an osmolality of 350 mOsmol/kg. Cultivations were performed in 250 mL RAMOS flasks filled with 10 mL modified Verduyn medium with 25 g/L glucose at 30 °C, 350 rpm shaking frequency, and a shaking diameter of 50 mm. 30 mM MES were added to the cultivations. The initial pH was set to 6.5 for all cultivations. The final pH reaches 2.80 ± 0.01, 2.77 ± 0.01, 2.70 ± 0.01, and 2.65 ± 0.01 for the reference, 550, 850, and 1350 mOsmol/kg cultivations, respectively. Graphs show the mean of duplicates. Shadows and error bars show the minimum and maximum values. For clarity, only every second data point is shown.

The OTR of the reference cultivation with 350 mOsmol/kg is similar to the ones with an osmolality of up to 850 mOsmol/kg (Figure 2.6A). However, higher osmolalities increase the time until the nitrogen limitation is reached by 33 % for 1350 mOsmol/kg. At the same condition, the OD decreased by 26 % from 16.8 ± 0.1 to 12.5 ± 0.2 (Figure 2.6B). The ITA titer decreases slightly with increasing osmolality from 5.4 ± 0.1 to 3.8 ± 0.1 g/L. With decreasing product concentration, the yield also decreases from 0.21 ± 0.00 for the reference to 0.15 ± 0.00 $g_{ITA}/g_{glucose}$ with an osmolality of 1350 mOsmol/kg.

Figure 2.7 shows the influence of increased initial ITA concentrations on OTR, final ITA titer, OD, and yield. To differentiate between possible cytotoxic effects of the acid itself and osmolality or pH effects, the added ITA concentrations were chosen to reach the same osmolalities as presented in Figure 2.6. The OTR peaks are shifted slightly from 19 to 22 h with the addition of 40 g/L ITA, compared to the reference and addition of 20 g/L ITA. With the initial addition of 80 g/L ITA, the peak is reached after 32 h. In addition, the biomass is decreased with increased initial ITA concentrations (Figure 2.7B). In the reference cultivation without the initial addition of ITA, the pH drops to 1.88 ± 0.04. With increasing ITA concentrations, the final pH increases to 4.42 ± 0.04, 5.08 ± 0.03, and 5.39 ± 0.01 for 20, 40, and 80 g/L ITA, respectively.

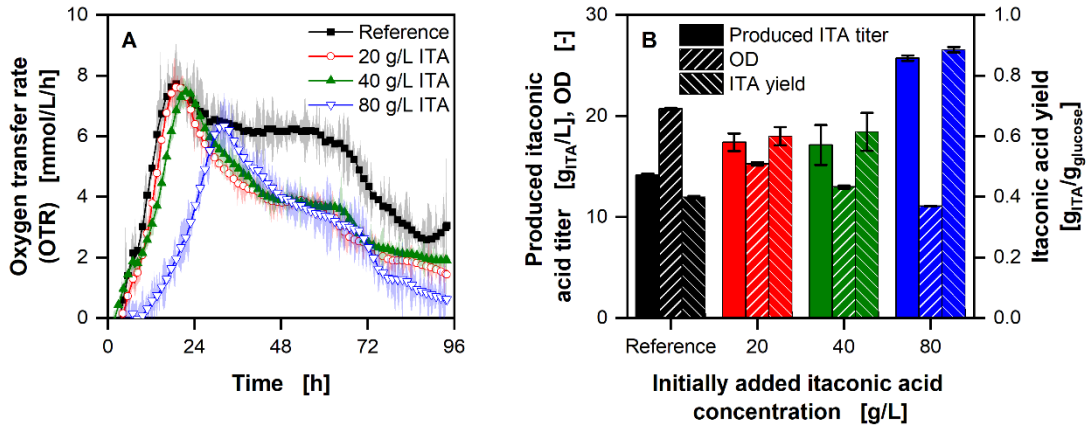


**Figure 2.7: Influence of itaconic acid concentrations on growth and productivity of on *U. cynodontis* ITA Max pH with limiting ammonium chloride concentration (1 g/L $NH_4Cl$).**

(A) Course of the oxygen transfer rates with increasing itaconic acid concentrations added at the beginning of the experiments. (B) Produced itaconic acid titer (in addition to the amount added at the beginning), optical density, and yield after 95 hours. Cultivations were performed in 250 mL RAMOS flasks filled with 10 mL modified Verduyn medium with ~25 g/L glucose at 30 °C, 350 rpm shaking frequency, and a shaking diameter of 50 mm. 30 mM MES were added to the cultivations. The initial pH was set to 6.5 for all cultivations. The final pH reached 1.88 ± 0.04, 4.42 ± 0.04, 5.08 ± 0.03, and 5.39 ± 0.01 for the reference, 20, 40 and 80 g/L added itaconic acid cultivations, respectively. (A) Graphs show the smoothed mean (Savatzky-Golay) of duplicates. Shadows show the minimum and maximum values of the unsmoothed data. (B) Error bars show the minimum and maximum value of duplicates. For clarity, only every fourth data point is shown.

## 2.4 Discussion

### *2.4.1 Screening for a suitable production organism and feedstock*

Production of ITA is generally possible with both *U. maydis* and *U. cynodontis*, and each of these has its own unique features that are relevant to process development [149]. Therefore, finding a suitable production strain is the first step in establishing a production process for ITA on alternative feedstocks. However, using complex substrates for cultivation introduces new challenges not seen with defined media [36]. These include impurities or excessive amounts of nitrogen sources, which might negatively influence productivity. Therefore, at first, strain selection was performed on a defined medium.

All tested strains show exponential growth until a drop indicates the onset of the nitrogen limitation, as described before (Figure 2.1) [77]. Once the nitrogen limitation starts, ITA production is induced [151]. During the production phase, *U. maydis* ITA Max and *U. maydis* Mutterschiff have an OTR that first decreases and then increases again, hinting

at a change in metabolism during the production phase. Nevertheless, *U. maydis* Mutterschiff reaches the highest ITA titers compared to the other two *U. maydis* strains. These results are not surprising, given the fact that *U. maydis* Mutterschiff is the most genetically engineered of the three strains. All three *U. maydis* strains have the *fuz7* and *cyp3* genes deleted to allow for yeast-like growth and hinder the transformation of ITA to 2-hydroxyparaconate. In addition, the strains overexpress the *ria* gene, which regulates the whole ITA gene cluster [11, 12, 61]. However, *U. maydis* ITA Max has an additional mttA transporter, which is an antiporter for malate and *cis*-aconitate in the mitochondrial membrane. In contrast, *U. maydis* chassis has deletions in the genes encoding mannosyl erythritol lipid (MEL), ustilagic acid (UA), and diacylglycerol acyltransferase (dgat) enzymes. While all these deletions increase production by either increasing the flux of precursor molecules towards ITA (mttA) or directing more carbon towards the product (ΔMEL ΔUA Δdgat), both strains show similar production profiles. *U. maydis* Mutterschiff consolidates the genetic modifications of the other two strains into one, leading to further increased ITA production.

The difference between the two *U. cynodontis* strains can also be explained by the genetic modifications. The only difference is the mttA antiporter for malate and *cis*-aconitate that is integrated into *U. cynodontis* ITA Max pH, allowing for increased ITA production.

The difference between *U. maydis* and *U. cynodontis* can, at least in part, be explained by the extended metabolic engineering of *U. maydis* Mutterschiff, compared to *U. cynodontis* ITA Max pH. Due to the deletion of by-product formation, higher ITA concentrations are expected for *U. maydis* Mutterschiff. As ITA production from sugars results in a net surplus of energy equivalents, such as NADH and ATP [55], the difference in ITA titer between *U. maydis* and *U. cynodontis* cannot be due to a difference in the diversion of energy for growth and production alone. Therefore, the available carbon needs to be the limiting factor. As described before, a nitrogen limitation is necessary for ITA production [151]. Because both strains exhibit product formation, the added nitrogen source was consumed. Therefore, with the same amount of available nitrogen, the higher biomass for *U. cynodontis* can only be reached with a higher biomass yield per nitrogen than *U. maydis*. Hence, less carbon is available for ITA production because more is used for biomass, leading to lower ITA titers and yields. However, this drawback of *U. cynodontis* can be handled by accordingly adjusting the nitrogen content of the media, thus allowing maximal ITA production and yield [12, 62].

In general, strains with higher specific production rates are considered good performers as they utilize less carbon for cell maintenance due to shorter production times. Assuming the same constant maintenance coefficient for both, *U. maydis* Mutterschiff and *U. cynodontis* ITA Max pH, the substrate consumption for maintenance during the production phase is about 7.7 times higher with *U. cynodontis*, under the tested conditions (compare Figure 2.1, and Equation 2.5). However, the assumption of a constant maintenance coefficient that is the same for both strains under changing cultivation conditions might not hold.

Cultivations with both *U. cynodontis* strains indicate a lower OTR with higher OD than the *U. maydis* strains, showing a lower oxygen consumption per biomass. This is especially favorable in large-scale fermentations, where oxygenation is difficult and gradients arise [52].

Finally, *U. cynodontis* is more tolerant to acidic pH values, compared to *U. maydis* [62, 63], which might be interesting for the following unit operations in downstream processing. Nowadays, crystallization at low pH is most commonly used [98, 112]. Therefore, using a strain that can withstand low pH values during the fermentation and, thus, reducing the costs of pH adjusting agents and saline wastes is beneficial [132]. Due to these reasons, *U. cynodontis* ITA Max pH was chosen for further process development.

The selection of a suitable feedstock is the next step of the process development. Growth and ITA production are possible on almost all tested crude feedstocks. However, the OTR increase indicates the availability of additional nitrogen in the complex substrates, which will negatively influence production. If the C/N ratio decreases, more carbon is used for biomass, up to a point where no nitrogen limitation is reached, and no ITA is produced. Based solely on the ITA yield, the filtration retentate should be used for further analysis. However, the experiment does not show the full potential of the substrates due to the different C/N ratios. The observed higher titer with filtration retentate can be explained by the fact that almost three times as much sugar was available in the medium compared to the pure sugar cultivations (Appendix 2). This increases the C/N ratio, which is strongly influenced by the initially added ammonium chloride, and leads to the increased ITA titer. Next to titer and yield, other aspects like tonnage, costs, and handling of the substrate need to be considered for the production process (Appendix 2). Due to the filtration retentate's low availability and high costs (personal discussion with GNT Europa GmbH, Aachen), it was discarded as a possible substrate. The fruit preparation only showed very low ITA titers

with *U. cynodontis* ITA Max pH, in addition to a high solid load, and was, therefore, ruled out as well. Thin juice had small loads of solids and a comparable yield to thick juice, leaving the latter and molasses as the preferable carbon sources. HPLC analysis revealed that both are mainly composed of sucrose and small amounts of the monomers glucose and fructose (data not shown). Molasses also contains significant amounts of lactate, likely due to acid fermentation during unsterile storage [137].

Growth of the production strain on the main carbon sources was further analyzed (Figure 2.3). The OTR clearly indicates the consumption of the three carbon sources glucose, fructose, and lactate, with a preference for the sugar monomers glucose and fructose, consuming these before the acid lactate. The change in pH further supports the assumption that lactate is consumed by the microorganism. Additionally, lactate consumption has been previously described for *U. maydis* [102]. The experiment shows that *U. cynodontis* ITA Max pH can also metabolize lactate, which is necessary for an economical production process on molasses.

### *2.4.2 Determination of biologically available nitrogen in molasses and thick juice*

Nitrogen availability and the resulting C/N ratio play a significant role in the ITA production with Ustilaginaceae due to the necessary nitrogen limitation [151]. Low nitrogen amounts have been shown to increase the yield while simultaneously decreasing productivity [12, 62]. To optimize the production process, the available nitrogen amount in the complex substrate needs to be determined. Due to differences in metabolism between strains and the wide range of possible nitrogen sources, the biologically available nitrogen might differ from the total amount of nitrogen in the media. Therefore, the production strain was used for the determination. Due to the nitrogen limitation reached at $OTR_{N,max}$, these values can be correlated with the ammonium concentration (Figure 2.4). Using this correlation, the nitrogen content in the alternative feedstock can be estimated (Figure 2.5). In addition, the OTR of the molasses cultivations indicate the presence of a secondary nitrogen source (Figure 2.5C). Because the strains behave the same with different ammonium concentrations until 18 h, this secondary nitrogen source must be consumed before the ammonium. The growth on the latter is, therefore, visible in the second increase of the OTR.

Even though the concentration of biologically available nitrogen is only twice as high in the molasses compared to the thick juice, the amount of added nitrogen is much higher in

a real production process. This is due to the lower sugar concentration and, therefore, the C/N ratio in the molasses, leading to a higher volumetric ratio that needs to be added to the fermentation to reach the desired sugar concentration. As higher nitrogen amounts are added with the feedstock molasses, thick juice was chosen as the substrate for the scale-up.

### *2.4.3 Influence of osmolality, pH and ITA concentrations on U. cynodontis cultivations*

Using complex substrates as carbon source increases the osmolality of the medium, which can significantly influence the process [150]. Even though there is no difference in the OTR and biomass formation between the reference and osmolalities up to 850 mOsmol/kg, there is a difference in ITA titer and, therefore, yield. This can be explained by increased energy demand for maintenance. In addition, the biomass yield per nitrogen is reduced with higher osmolalities, as is evidenced by the decreasing OD. The increase in osmolality also corresponds to a lower growth rate in *U. cynodontis* ITA Max pH, as visible in the decreased slope of the OTR. However, the same effects are only in part visible for *U. maydis* Mutterschiff (Appendix 4). While the growth rate shows a stronger dependency on the osmolality for this strain, the biomass and product yield remain constant with increasing osmolality. This is surprising because previous data by Klement et al. (2012) [77] showed that *U. maydis* is only impacted to a small extent by osmolalities up to 2.5 Osmol/L regarding growth. However, Klement et al. worked with wild-type strains, while in this study highly engineered strains are used, which might have a lower robustness towards high osmolalities. Due to the higher buffer concentration with *U. maydis* Mutterschiff, a pH effect might also explain the difference between the two strains. To investigate this effect further, in addition to potential product inhibition, experiments with different initial ITA concentrations were conducted (Figure 2.7). Here, a shift in the OTR peak with increasing initially added ITA concentration was observed. This is coherent with the observations for the experiments with increased osmolalities (Figure 2.6). In addition, a decrease in the biomass with increasing initially added ITA could be noticed for increased osmolality. However, the substantial decrease in the OTR visible in Figure 2.6B cannot be explained by an osmolality effect alone. Thus, the ITA itself has to negatively affect biomass formation, as has previously been described for *U. vetiveriae* in pH-controlled stirred tank reactors [152]. Because additional ITA is formed under all tested conditions – indicating that a nitrogen limitation is reached – the biomass yield per available nitrogen is reduced, resulting in lower biomass formation. Therefore, more glucose is available for product formation, as seen in the increased ITA titers.

Next to osmolality, the pH is critical for the production of weak acids. It has been shown that ITA concentrations are limited to ~80 g/L at low pH values by an effect called weak acid uncoupling [62, 77]. Compared to the reference, the higher pH with initially added ITA allows more ITA to be produced because the acid is not fully protonated (ITA $pK_a$ 5.55 and 3.83) and, therefore, exhibits lower stress to the cells [137]. The reason for the higher pH presumably also lies in the initial ITA addition, which buffers the media at the $pK_a$ value of 5.55.

The combination of reduced biomass and higher pH leads to increased ITA titers and, thus, increased yields. However, the calculated yield for the initial addition of 80 g/L ITA reaches $0.89 \pm 0.01$ $g_{ITA}/g_{glucose}$, which is considerably higher than the theoretical maximum of 0.72 $g_{ITA}/g_{glucose}$. This can be explained by evaporation, leading to higher concentrations and, thus, to the observed high yields. The concentration effect is more substantial the higher the initial ITA concentration. However, due to the use of humidified air during the experiment, only a minimal volume change is to be expected. Thus, the observed trend of increasing yield with higher initial ITA concentrations can be attributed to higher pH values during the experiment. This contradicts what has been shown for *U. maydis* wild type [77]. There, lower amounts of ITA were produced with increased initial ITA concentration. However, $CaCO_3$ was used as buffer, leading to precipitation for most of the initially added ITA [152]. Thus, the buffer capacity of the system was reduced dramatically, resulting in lower pH and stronger weak acid stress.

Based on these findings, the biggest influence on itaconic acid production is the pH due to weak acid stress, followed by osmolality and the itaconic acid itself.

These inherent challenges to the process need to be addressed in future research. *In-situ* product removal presents great potential, as it reduces the ITA concentration and the osmolality, allowing for increased production [98]. Alternatively, adaptive laboratory evolution experiments have increased the acid tolerance of *Saccharomyces cerevisiae* and could be used to induce the same effect for the Ustilaginaceae strains [154]. In addition, the fermentation medium could be further optimized by reducing the initially added components, as some of them might be contained in large excess and are added through the alternative feedstock. Lastly, the production process as a whole can be further optimized, for example, regarding optimal pH and purification route.

## 2.5 Conclusion

In this chapter, *U. maydis* and *U. cynodontis* strains were used to produce ITA on complex substrates from the local food industry. Thick juice was identified as the most suitable out of six alternative feedstocks, using the newly developed µTOM device for MTP. Here, nitrogen availability and C/N ratios were of key importance. For this, a method was developed to determine the biologically available nitrogen, which can also be used for any other component of a (complex) substrate. The presented method enables rapid screening of the suitability of different kinds or batches of substrates for production processes within a circular bioeconomy.

To further characterize the production process, the effect of medium characteristics, like osmolality, pH, and product inhibition, were examined in shake flasks. The pH, followed by the osmolality and then the itaconic acid itself, was determined to have the greatest impact on the production of itaconic acid.

In conclusion, valuable insights into the itaconic acid production process with Ustilaginaceae on alternative feedstocks were generated, which will lead to a fast scale-up to stirred tank fermenters.

Parts of the following chapter have been previously published as Sauer, K. M., Kiefel, R., Niehoff, P.-J., Hofstede, J., Ernst, P., Brockkötter, J., Gätgens, J., Viell, J., Noack, S., Wierckx, N., Büchs, J., Jupke, A. (2023). Holistic Approach to Process Design and Scale-Up for Itaconic Acid Production from Crude Substrates. *Bioengineering* 2023, *10*(6), 723. Sauer, Kiefel, and Niehoff contributed equally to this work. For this thesis, the publication has been revised with a focus on the fermentation experiments. These were conducted by Paul-Joachim Niehoff.

In addition, parts of the following chapter have been published in Niehoff, P.-J., Müller, W., Pastoors, J., Miebach, K., Ernst, P., Hemmerich, J., Noack, S., Wierckx, N., Büchs, J. Development of an Itaconic Acid Production Process With Ustilaginaceae on Alternative Feedstocks. *BMC Biotechnology* 23, 34 (2023). This includes Figure 3.1. The underlying experiments were performed by Paul-Joachim Niehoff.

# Chapter 3

# 3. Optimization and Scale-Up of the Itaconic Acid Production Process in Stirred Tank Reactors

## 3.1 Background

After successfully screening and identifying a suitable production strain and feedstock for itaconic acid production in shaken bioreactors (Chapter 2), a scale-up follows as the next step of process development. While shaken bioreactors, such as microtiter plates and shake flasks, are ideal for early-stage screening and characterization [80], stirred tank reactors offer several advantages for large-scale production.

STR are widely used in industrial bioprocessing due to their scalability, good process control, and high productivity [22, 51, 146]. These reactors provide efficient mixing, aeration, and heat transfer [46, 146]. Moreover, they offer the capability to continuously monitor and adjust process parameters like pH or dissolved oxygen tension (DOT) during production, leading to enhanced process stability and reproducibility.

Scale-up from shaken bioreactors to stirred tank reactors presents various challenges [105]. Increasing volumes can lead to changes in oxygen availability, shear stress, and nutrient distribution within the bioreactor, potentially affecting cell growth and product formation [45, 52]. A suitable scale-up criterion must be established to avoid these negative impacts [100]. However, STR fermentation have been described for *U. cynodontis* ITA Max pH [62] and *U. maydis* Mutterschiff [12] before, allowing for an easy use of the presented parameters in 2 L reactors. Further scale-up from small to large STR is based on the

volumetric power input, as no specific requirements regarding oxygen supply or shear stress were observed for the production strain [16, 62, 100].

In this chapter, the production process is scaled up to 2 L scale. The resulting process is optimized regarding substrate availability, pH, and pH adjusting agent, based on a holistic view on the overall process, including downstream processing (DSP). The resulting production process was then scaled up to a 150 L STR for proof of concept in large scale.

## 3.2 Material and Methods

### *3.2.1 Microbial strain and media composition*

For fermentation and cultivation, all chemicals were purchased from Carl Roth GmbH & Co. KG (Karlsruhe, Germany). *Ustilago cynodontis* NBRC 9727 Δ*fuz7* Δ*cyp3* $P_{etef}$*mttA* $P_{ria1}$*ria1* was used for all cultivation experiments [63].

Cultivations were performed in a modified Verduyn medium as described by Geiser et al. (2014) [48]. The medium was composed of 0.8 g/L $NH_4Cl$, 0.2 g/L $MgSO_4 \cdot 7\ H_2O$, 0.01 g/L $FeSO_4 \cdot 7$ H2O, 0.5 g/L $KH_2PO_4$, 0.1 vol% trace element solution and 0.1 vol% vitamin solution. The trace element solution contained 15 g/L TitriplexIII©, 4.5 g/L $ZnSO_4 \cdot 7\ H_2O$, 0.84 g/L $MnCl_2 \cdot 2\ H_2O$, 0.3 g/L $CoCl_2 \cdot 6\ H_2O$, 0.3 g/L $CuSO_4 \cdot 5\ H_2O$, 0.4 g/L $Na_2MoO_4 \cdot 2\ H_2O$, 4.5 g/L $CaCl_2 \cdot 2\ H_2O$, 3 g/L $FeSO_4 \cdot 7\ H_2O$, 1 g/L $H_3BO_3$ and 0.1 g/L KI. The vitamin solution contained 0.05 g/L D-biotin, 1 g/L D-calcium pantothenate, 1 g/L nicotic acid, 25 g/L myo-inositol, 1 g/L thiamine hydrochloride, 1 g/L pyridoxine hydrochloride, and 0.2 g/L para-aminobenzoic acid. Shake flask pre-cultures contained 0.03 M MES as a buffer at pH 6.5. Stirred tank reactor cultivations were supplemented with 1 g/L yeast extract and 0.05 vol% Antifoam 204. All media components were either autoclaved or sterile-filtered with a 0.2 µm cut-off filter (Millipore-Sigma, Burlington, VT, USA). Thick juice from sugar beets was kindly provided by Pfeifer & Langen GmbH & Co. KG (Jülich, Germany). It was autoclaved in undiluted form and used as the sole carbon source. The composition of thick juice used for all cultivations can be found in Appendix 5.

### *3.2.2. Cultivation Conditions*

*U. cyndontis* ITA Max pH was stored in cryogenic cultures at -80 °C, containing 30 vol% of 500 g/L glycerol stock and 70 vol% culture grown in modified Verduyn medium. For

each fermentation, one YEPS plate with 10 g/L yeast extract, 10 g/L peptone, 10 g/L sucrose, and 20 g/L agar-agar was inoculated from one fresh cryogenic vial and cultivated at 30 °C for 48 h. From this plate, 500 mL shake flasks with 50 mL filling volume, containing Verduyn medium with 50 g/L sucrose from thick juice and 2 g/L $NH_4Cl$, were inoculated as pre-culture. The flasks were cultivated overnight at 30 °C and 300 rpm with a shaking diameter of 50 mm. The culture broth was then centrifuged in a Rotina 35 R centrifuge (Andreas Hettich GmbH & Co. KG, Tuttlingen, Germany) at 4000 rpm for 10 min. The pellets were suspended in 3 mL of the resulting supernatant, and fermentations were inoculated with the resulting solution to an optical density ($OD_{600}$) of 0.25.

Small-scale cultivations were performed in a 2 L Sartorius BIOSTAT® stirred tank reactor (Sartorius AG, Göttingen, Germany) equipped with a six-blade Rushton turbine with a diameter of 45 mm and four baffles. The initial filling volume was 1 L, and the temperature was kept at 30 °C. Dissolved oxygen tension was regulated at > 30% by increasing the stirring frequency from 400 or 800 to 1200 rpm. pH was controlled by adding 5 M NaOH or 2.5 M $Mg(OH)_2$ as base or 1 M HCl as acid. Due to its low solubility in water, 2.5 M $Mg(OH)_2$ was pumped in a cycle to avoid settling of the crystals within the tubing for the respective fermentation. When necessary, a second pump delivered the $Mg(OH)_2$ solution from the primary cycle to the fermenter. Off-gas composition was determined with a DASGIP off-gas analyzer GA4 (Eppendorf SE, Hamburg, Germany). pH and DOT were measured using an Easyferm plus PHI K8 200 (Hamilton, Höchst, Germany) and a VisiFerm DO ECS 225 probe (Hamilton, Höchst, Germany).

Pre-cultures for the 100 L fermentation scale were performed in 2 L Sartorius fermenters as described above. The pre-culture was run with 50 g/L sucrose from thick juice and 2 g/L $NH_4Cl$. After 24 h, the whole filling volume was used to inoculate a 100 L fermenter (Frings GmbH, Rheinbach, Germany), which was equipped with three six-blade Rushton turbines with a diameter of 150 mm and four baffles. Cultivations were performed with an initial filling volume of 105 L at 30 °C and a stirring rate of 285 rpm. pH was controlled by adding 5 M NaOH. OTR and CTR were determined by measuring the off-gas with a Rosemount™X-STREAM XEFD exhaust gas analyzer (Emerson Automation Solutions, Langenfeld, Germany). pH and DOT were monitored using a Polylite Plus H VP 120 Pt100 (Hamilton, Hoechst, Germany) and a VisiPro DO Ex 120 H2 probe (Hamilton, Höchst, Germany).

### *3.2.3. Offline Analytics*

Samples for offline analysis were drawn from fermentation at regular intervals. All analyses were done in triplicates. For each sample, 2 mL fermentation broth was centrifuged at 14,000 rpm for 10 min in a Sigma 1–15 centrifuge (Sigma Laborzentrifugen GmbH, Osterode am Harz, Germany). The supernatant was filtered with a 0.2 µm cut-off filter (Millipore-Sigma, Burlington, MA, USA) and analyzed by HPLC for sugars and organic acid content. HPLC analysis was performed using a Thermo Fisher Ultimate 3000 (Thermo Fisher Scientific Inc., Waltham, MA, USA) equipped with an ERC RefractoMax 520 RID (Shodex, Munich, Germany). For separation, a ROA-Organic Acid H+ (8 %) column (300 x 7.8 mm) (Phenomenex, Torrance, USA) was heated to 30 °C and used with a mobile phase of 5 mM $H_2SO_4$ running at 0.8 mL/min. Cell pellets were dried at 80 ° C for 48 h and then weighed to determine cell dry weight (CDW).

### *3.2.4 Calculations*

To evaluate fermentation performance, yield, STY, CTR, OTR and the respiratory quotient (RQ) were calculated based on mass balances. Equation 3.1 shows how to calculate the mass balance for a compound from fermentation.

$$m_x(t) = c_x(t_0) \cdot V_L(t_0) + c_{x,feed} \cdot V_{feed}(t) - \sum_{t_0}^{t} c_x(t) \cdot V_{sample}(t) \qquad (3.1)$$

With $m_x(t)$ [g] as the calculated mass at time point t, $c_x(t_0)$ [g/L] as the concentration of x at the beginning of the fermentation, $V_L(t_0)$ [L] as the initial filling volume, $c_{x,\,feed}$ [g/L] as the concentration of x in the feed and $V_{feed}(t)$ [L] as the added feeding volume at time t. Sampling was considered by summing up the substrate concentration $c_x(t)$ [g/L] times the corresponding sample volume $V_{sample}(t)$ [L].

The yield Y(t) [$g_{ITA}/g_{substrate}$] was calculated by dividing the mass of ITA produced by the summed mass of the substrates glucose, fructose, and sucrose (Equation 3.2).

$$Y(t) = \frac{m_{ITA}(t)}{\left(m_{glucose}(t) + m_{fructose}(t) + m_{sucrose}(t)\right)} \qquad (3.2)$$

The yield was calculated in $g_{ITA}/g_{sucrose}$ and also converted to the amount of glucose equivalents in $g_{ITA}/g_{glucose\ eq.}$. For the calculation of glucose equivalents, it was assumed that water hydrolyzes sucrose into glucose and fructose, and the utilization of fructose proceeds similarly to glucose.

Space-time-yield (STY) [$g_{ITA}$/L/h] was calculated by dividing the mass of ITA $m_{ITA}(t)$ [g] by the sum of the filling volume $V_L(t)$ [L] of the fermenter and the total sample volume $V_{sample,total}(t)$ [L] times the fermentation time t [h] (Equation 3.3).

$$STY(t) = \frac{m_{ITA}(t)}{\left(V_L(t) + V_{sample,total}(t)\right) \cdot t} \quad (3.3)$$

As a critical fermentation parameter, the respiratory quotient [-] was calculated by dividing the carbon dioxide transfer rate (CTR) by the oxygen transfer rate. These parameters were used to draw conclusions on the organism's metabolic behavior, as has previously been demonstrated [59, 85, 118]. Equations 3.4 and 3.5 describe the calculation of CTR and OTR using the gas flow rate into the fermenter $q_{in}$ [L/h], the fermentation volume $V_L$ [L], the molar volume of an ideal gas $V_M$ [L/mmol] at 25 °C and the $O_2$ and $CO_2$ fractions in the inlet and outlet $y_{O2,in}$, $y_{O2,out}$, $y_{CO2,in}$ and $y_{CO2,out}$ [-], respectively.

$$CTR = \frac{q_{in}}{V_L \cdot V_M} \cdot \left(y_{CO2,out} \cdot \frac{1 - y_{O2,in} - y_{CO2,in}}{1 - y_{O2,out} - y_{CO2,out}} - y_{CO2,in}\right) \quad (3.4)$$

$$OTR = \frac{q_{in}}{V_L \cdot V_M} \cdot \left(y_{O2,in} - \frac{1 - y_{O2,in} - y_{CO2,in}}{1 - y_{O2,out} - y_{CO2,out}} \cdot y_{O2,in}\right) \quad (3.5)$$

Equation 3.6 describes the calculation of the RQ corresponding to CTR and OTR.

$$RQ = \frac{CTR}{OTR} \quad (3.6)$$

Equations 3.7 and 3.8 describe the RQ of growth on pure glucose. Calculations were based on the biomass composition from Klement et al. (2012) [77].

$$C_6H_{12}O_6 + 4.95 \cdot O_2 + 0.1 \cdot NH_4^+ = CH_{1.8}N_{0.1}O_{0.6} + 5\,CO_2 + 5.3\,H_2O \quad (3.7)$$

$$RQ = \frac{CTR}{OTR} = \frac{5}{4.95} = 1.01 \quad (3.8)$$

Equations 3.9 and 3.10 describe the theoretical RQ of itaconic acid production on pure glucose.

$$C_6H_{12}O_6 + 1.5 \cdot O_2 = C_5H_6O_4 + CO_2 + 3\,H_2O \quad (3.9)$$

$$RQ = \frac{CTR}{OTR} = \frac{1}{1.5} = 0.67 \quad (3.10)$$

The carbon balance included the sugars sucrose, fructose, and glucose, in addition to the products itaconic acid, biomass, and $CO_2$. For all included compounds, except $CO_2$, the balance was based on the mass calculations above (Equations 3.1 and 3.2). C-mol was

calculated by dividing the mass by the molar mass and multiplying by the number of carbons of the respective molecule. $CO_2$ was directly measured in C-mol with the off-gas analyzer (see 3.4.2). The biomass composition was based on Klement et al. [77].

## 3.3 Results and Discussion

### *3.3.1 Extended batch stirred tank reactor cultivation of U. cynodontis ITA Max pH with thick juice as carbon source*

Based on the findings in Chapter 2, a constant pH of 6.5 was used with *U. cynodontis* and thick juice as the sole carbon source for a first scale-up to an STR. Stirring and aeration rate, in addition to DOT control, are based on Tehrani et al. [62]. Extended-batch cultivations have the same advantages of reducing the osmolality and increasing the production time as fed-batch cultivations while allowing for maximum production rates [8]. Therefore, extended-batch mode was chosen. Figure 3.1 shows the results of an extended batch fermentation in a 2 L STR with *U. cynodontis* ITA Max pH and thick juice as sole carbon source. Next to substrate concentration as well as ITA and biomass production, oxygen transfer rate, carbon dioxide transfer rate, and respiratory quotient are monitored.

The OTR and CTR increase exponentially during the first 18.5 h, after which they increase linearly until 28 h (Figure 3.1A). During this time, the CTR is higher than the OTR, leading to a respiratory quotient of ~1.2. The high RQ indicates the production of a reduced product in addition to growth. These are likely intracellular lipids, which have previously been reported to be produced by members of the Ustilaginaceae family [49]. This is supported by the CDW, which increases from initially 5.4 to 32.3 g/L (Figure 3.1C). At the same time, sucrose is equally converted to its monomers, glucose and fructose. However, a higher accumulation of fructose can be observed after 10 h, likely due to catabolite repression of fructose uptake by glucose. Therefore, fructose accumulates while glucose is consumed.

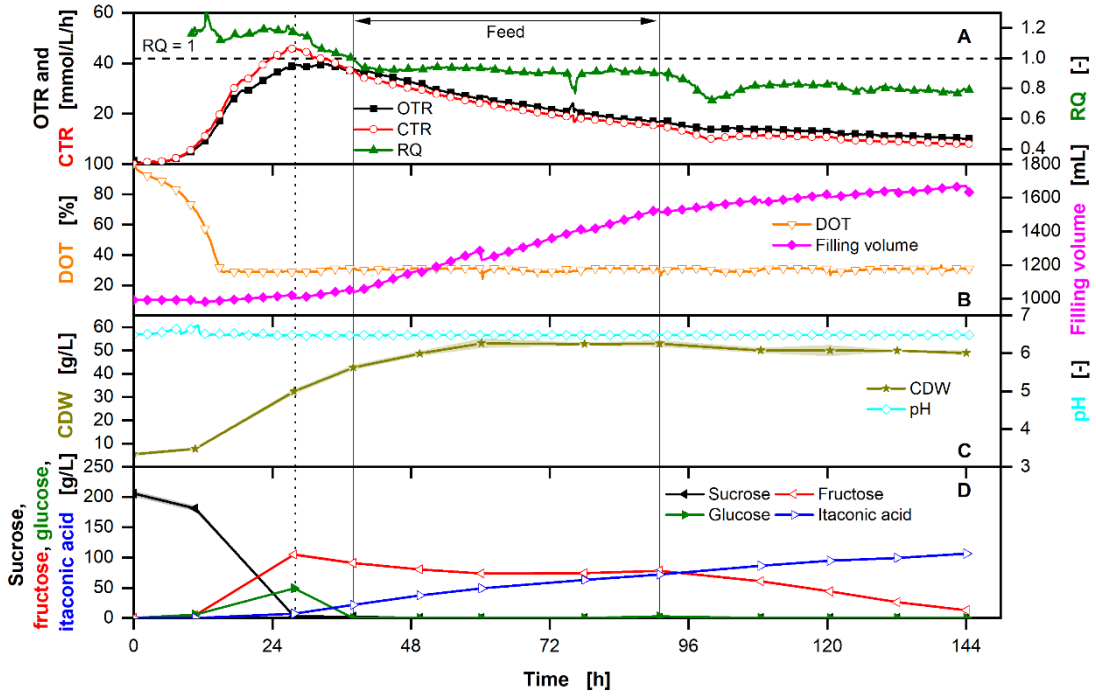


**Figure 3.1: Extended-batch fermentation of *U. cynodontis* ITA Max pH grown with thick juice as sole carbon source with limiting ammonium chloride concentration (4 g/L $NH_4Cl$).**

(A) Course of the oxygen and carbon dioxide transfer rates and respiratory quotient. The black dotted line indicates the start of the nitrogen limitation. The horizontal black dashed line indicates an RQ = 1. (B) Dissolved oxygen tension and filling volume. (C) Cell dry weight concentration and pH. (D) Sugar (sucrose, glucose, fructose) and itaconic acid concentrations. For the batch phase, 200 g/L sucrose from thick juice were initially added to the medium. During the feed phase (between the vertical solid lines) 200 g of additional sucrose in the form of thick juice were added to the fermentation vessel. Cultivation was performed in a 2 L Sartorius BIOSTAT® stirred tank reactor (Sartorius AG, Göttingen, Germany) with an initial filling volume of 1 L at 30 °C. Dissolved oxygen tension was kept > 30 % by increasing the stirring frequency from 800 to 1200 rpm. pH was kept constant at 6.5 by addition of 1 M HCl and 5 M NaOH. RQ values are only shown for OTR values > 5 mmol/L/h. Samples were taken regularly and analyzed via HPLC. Concentrations are shown as mean values of triplicates and standard deviations as shaded areas. Due to high reproducibility of the measurements, the standard deviation might not be visible for every data point. For clarity, only every 15$^{th}$ data point is shown for the online data.

After 28 h, the OTR and CTR start to decrease, indicating the start of the nitrogen limitation (Figure 3.1A) [62]. In accordance, the ITA concentration starts to increase at this time (Figure 3.1D). Interestingly, the CDW continues to increase after nitrogen is depleted. This is likely due to a change in the biomass composition, which has previously been observed in *U. maydis* [29, 77]. Through the reduction of necessary nitrogen per carbon, more biomass is formed. This hypothesis is underlined by the RQ (Figure 3.1A), which decreases from 1.2 to 0.9 between 28 h and the beginning of the feed phase, showing the metabolic shift from lipid formation and growth to ITA formation (compare Equations 3.8 and 3.10).

During the feed phase, thick juice and, thus, nitrogen and carbon is fed into the reactor with a constant feed rate of 5.5 ml/h. This corresponds to 0.013 ± 0.001 g/h $NH_4^+$ equivalents (compare Chapter 2.4.22.3.2 Determination of biologically available nitrogen in molasses and thick juice). Even though the CDW increases during this time, the cells continue to produce ITA, showing that nitrogen is still limiting (Figure 3.1C). The RQ < 1.0 emphasizes the hypothesis that nitrogen is limiting, thus allowing ITA to be formed even though growth is visible. At the same time, the sugar concentrations remain almost constant, showing the immediate conversion of sucrose and consumption of glucose (Figure 3.1D). However, it is noteworthy that during the whole cultivation, especially during the feed phase, the filling volume increases from 1 L to 1.65 L due to feeding and pH adjustments (Figure 3.1B). This leads to a constant dilution effect of the substrate, product, and CDW concentrations. Thus, the increase in fructose and CDW mass is masked by the increasing filling volume. Once the feed ends, fructose concentrations start to decrease and reach 13.2 g/L at the end of the fermentation. At the same time, the RQ decreases from 0.9 to 0.8, showing stronger ITA formation with less growth compared to the feed phase. This is again supported by the increasing biomass, which is masked in the constant CDW by the previously mentioned dilution effect.

A carbon balance of the process showed that almost 20 % of the carbon present in the products (ITA, biomass, and $CO_2$) is unaccounted for and does not originate from the sugars. This is unsurprising, as thick juice likely contains further carbon sources like amino acids or other organic acids [132]. Due to the large error, carbon balances were not considered for the following fermentations.

In the end, a final concentration of 106.4 ± 0.1 g/L ITA was reached. In total, 194.9 ± 0.2 g ITA with a STY of 0.72 ± 0.00 $g_{ITA}/L/h$ were produced. This corresponds to a yield of 0.48 ± 0.02 $g_{ITA}/g_{sucrose}$ or 0.46 ± 0.02 $g_{ITA}/g_{glucose,eq.}$. KPI are summarized in Table 3.1. In a similar experiment, *U. maydis* Mutterschiff reached titers of 99.8 ± 0.7 g/L with a yield of 0.66 ± 0.02 $g_{ITA}/g_{sucrose}$ (0.63 ± 0.02 $g_{ITA}/g_{glucose,eq.}$) and a STY of 0.92 ± 0.00 $g_{ITA}/L/h$ (Appendix 6). In an optimized process, no sugar should be left in the medium due to high costs. Thus, excluding the excess fructose, theoretical yields of 0.50 ± 0.02 $g_{ITA}/g_{sucrose}$ (0.48 ± 0.02 $g_{ITA}/g_{glucose,eq.}$) and 0.72 ± 0.02 $g_{ITA}/g_{sucrose}$ (0.66 ± 0.02 $g_{ITA}/g_{glucose,eq.}$) were reached with *U. cynodontis* ITA Max pH and *U. maydis* Mutterschiff, respectively. For both strains, the yields are in the same range as the highest values previously published [12, 62]. Compared to reference fermentations on glucose at a constant pH of 3.6, the titer and

yield increased by 139 % and 28 % for *U. cynodontis* ITA Max pH [62]. The increase of both ITA titer and yield is likely due to the lower product toxicity at higher pH. The reference cultivation was performed at pH 3.6, which leads to a higher ratio of protonated to unprotonated ITA and, thus, stronger weak acid stress [86]. The pH of 6.5, therefore, allows ITA titers above ~80 g/L. However, for an optimized process, the purification method of ITA has to be taken into account. Recently, it has been shown that lower titers due to low pH are more cost-effective if the next unit operation demands a low pH, like crystallization [132]. A low pH during the fermentation drastically reduced the costs for pH-adjusting agents and saline waste, improving the economy of the process.

### *3.3.2 Introduction of a pH shift and reduction of added nitrogen*

A techno-economic analysis by Saur et al. [132] has shown that reduced costs of a low pH fermentation indeed outweigh the cost of lower product titers. This is due to the necessary low pH in the following downstream process. On glucose, the growth phase of *U. cynodontis* ITA Max pH is not strongly affected by pH and can be conducted equally at pH 6.5 and 3.6 [61]. With thick juice as a substrate, even the acid-tolerant *U. cynodontis* ITA Max pH did not grow properly (data not shown), which might be attributed to the lactic acid present in thick juice (Appendix 5) exhibiting weak organic acid stress during the growth phase [141]. Therefore, the pH is kept > 6.5 at the beginning of the fermentation to ensure improved growth. A pH shift is then introduced during the production phase, allowing the pH to naturally drop to 3.6, where it is then kept until the end of the fermentation.

It has previously been shown that an increased yield could be achieved by decreasing the available nitrogen [62]. As thick juice introduces additional nitrogen sources, therefore reducing the yield, the initially added ammonium was reduced to compensate for the addition. Figure 3.2 shows the extended batch fermentation of *U. cynodontis* ITA Max pH with a pH shift and reduced initial ammonium using thick juice as sole carbon source.

The exponential growth phase is mirrored in the exponential increase of OTR and CTR (Figure 3.2A). The drop in the CTR after 15.2 hours indicates the start of the nitrogen limitation [62], where the pH shift is introduced. The pH subsequently increases for a short time before rapidly dropping to the desired pH of 3.6, where it is kept constant for the rest of the fermentation (Figure 3.2C). It is noteworthy that this reduced the needed volume of pH adjustment agent about fivefold from ~600 mL to ~120 mL. As seen in the previous

fermentation, the biomass increases further from 9 to 18 g/L between 15.2 and 43.1 h of fermentation after a nitrogen limitation is reached (Figure 3.2C). This is likely because the cells reduce their nitrogen content [29, 77]. During this time, the RQ is slightly above 1 and slowly decreases, showing combined cell growth and increasing ITA production.

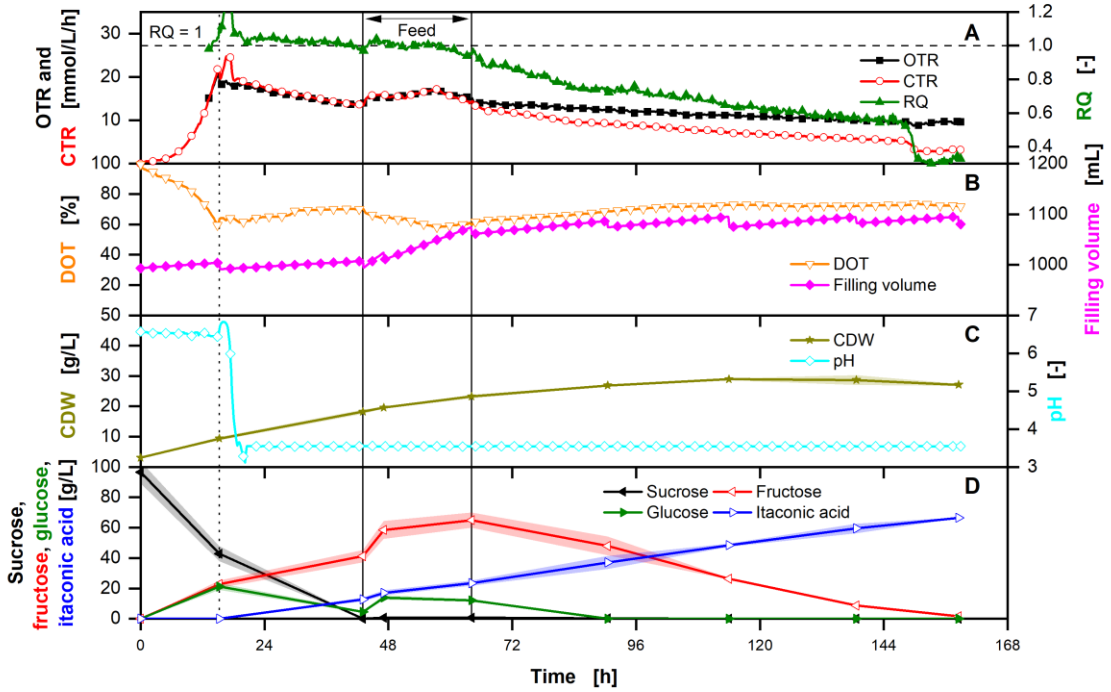


**Figure 3.2: Extended-batch fermentation of *U. cynodontis* ITA Max pH with pH shift and thick juice as sole carbon source.**

(A) Course of the oxygen and carbon dioxide transfer rates and respiratory quotient. The black dotted line indicates the start of the nitrogen limitation. The horizontal dashed line shows RQ = 1. RQ values are only shown for OTR values > 5 mmol/L/h. (B) Dissolved oxygen tension and filling volume. (C) Cell dry weight concentrations and pH. (D) Sugar (sucrose, glucose, fructose) and itaconic acid concentrations. For the batch phase, 100 g/L sucrose were initially added to the medium. During the feed phase (between the vertical solid lines) 60 g of additional sucrose were added to the fermentation vessel. Cultivation was performed in a 2 L Sartorius BIOSTAT® stirred tank reactor (Sartorius AG, Göttingen, Germany) with an initial filling volume of 1 L at 30 °C with constant aeration and stirring rate of 1 L/min and 800 rpm, respectively. pH was kept above 6.5 or 3.6 before and after the pH shift (indicated by a vertical dotted line) by adding 5 M NaOH. Concentrations are shown as mean values of triplicates and standard deviation as shaded area. Due to small errors, the standard deviation might not be visible for every data point. For clarity, only every 15$^{th}$ measured online data point is shown.

Until the start of the feed, sucrose is hydrolyzed to its monomers (Figure 3.2D). Nearly equimolar amounts of fructose accumulate during this time, while glucose is used up, underlining that the latter is the preferred substrate for ITA production. Continuous overfeeding for a constant glucose concentration leads to a reduced substrate yield, as not all substrate is converted over the fermentation time due to product inhibition [62, 137].

Therefore, the feed is started after glucose is nearly depleted at 43.1 h and terminated after 64.1 h when 62.1 g sucrose has been fed into the fermenter. This termination allows a switch from glucose to fructose metabolism and, thus, a complete substrate conversion until the end of the fermentation. The RQ increases during the feeding (Figure 3.2A), showing cell growth on the additional nitrogen in thick juice (Appendix 5). Simultaneously, the biomass increases further to reach a cumulative concentration of 27 g/L at the end of the fermentation (Figure 3.2C). As both CTR and OTR decline until the end of fermentation, it can be assumed that cell viability decreases due to weak organic acid stress. At the end of the fermentation, a titer of 66.6 ± 0.2 $g_{ITA}/L$ and a yield of 0.48 ± 0.02 $g_{ITA}/g_{sucrose}$ is reached (Figure 3.2D). Converted to glucose equivalents, the yield is 0.46 ± 0.02 $g_{ITA}/g_{glucose,eq.}$ (compare Table 3.1). Compared to the previous extended batch fermentation, the same yield – albeit at lower titers – was reached. Considering the additional biomass formation from nitrogen in thick juice, this is comparable to fermentations on glucose with a constant feeding profile and an ammonium chloride concentration of 4 g/L [62]. The yield of the process increases to 0.52 ± 0.02 $g_{ITA}/g_{sucrose}$ (0.49 ± 0.02 $g_{ITA}/g_{glucose,eq.}$) when only the actual production time, starting from the pH shift until the end of the fermentation, is taken into account. This once again highlights the potential for *in-situ* product removal [38, 85], where the production phase is extended, leading to higher fermentation yields. The STY decreased compared to the previous fermentation from 0.72 ± 0.00 $g_{ITA}/L/h$ to 0.40 ± 0.01 $g_{ITA}/L/h$. This can be explained by the lower biomass concentration in the fermentation with reduced initially added ammonium. However, for the economic feasibility of the process, the increased yield is more important than the reduced STY [132].

The theoretical yield of ITA production on glucose is at 0.72 $g_{ITA}/g_{glucose}$. To allow more ITA production, increasing the substrate concentration is necessary (Appendix 7). However, ITA concentrations above 80 g/L could not be reached, even when glucose and fructose are still available. This is due to weak acid stress and has been described before [62, 77, 86, 88]. In addition, no limitation in oxygen transfer due to high substrate concentration and osmolarity has been observed, underlining the results from Chapter 2.4.3.

### *3.3.3 Evaluation of using $Mg(OH)_2$ for pH control*

To increase the overall process yield, $Mg(OH)_2$ provides a viable alternative as a pH-adjusting agent, as the fermentation broth can be further concentrated in the downstream

process [132]. To investigate the tolerance of *U. cynodontis* ITA Max pH towards $Mg(OH)_2$ [95], an extended-batch fermentation on thick juice with *U. cynodontis* ITA Max pH is carried out with $Mg(OH)_2$ as a base (Figure 3.3).

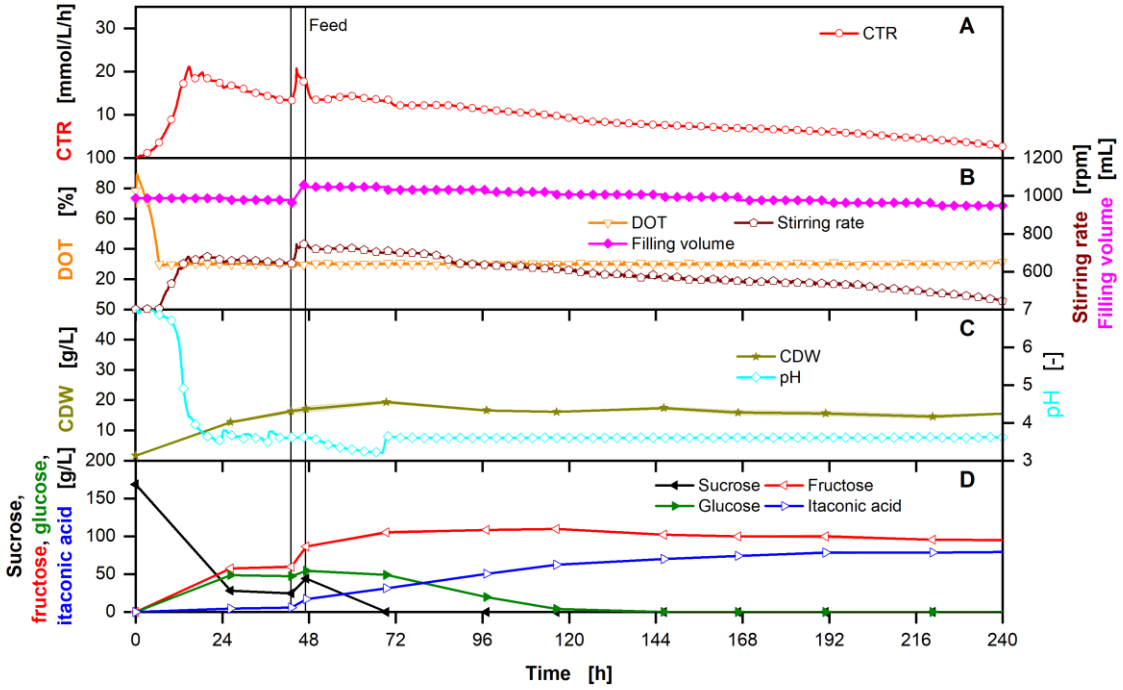


**Figure 3.3: Extended-batch fermentation of *U. cynodontis* ITA Max pH with magnesium hydroxide as pH adjusting agent and thick juice as sole carbon source.**

(A) Course of the carbon dioxide transfer rate. (B) Dissolved oxygen tension, stirring rate, and filling volume. (C) Cell dry weight concentrations and pH. (D) Sugar (sucrose, glucose, fructose) and itaconic acid concentrations. For the batch phase, 160 g/L sucrose were initially added to the medium. During the feed phase (between the vertical solid lines) 100 g of additional sucrose were added into the fermentation vessel. Cultivation was performed in a 2 L Sartorius BIOSTAT® stirred tank reactor (Sartorius AG, Göttingen, Germany) with an initial filling volume of 1 L at 30 °C with a constant aeration rate of 1 L/min. Dissolved oxygen tension was kept > 30 % by increasing the stirring frequency from 400 to 1200 rpm. pH was kept above 3.6 by addition of 2.5 M $Mg(OH)_2$. Concentrations are shown as mean values of triplicates and standard deviation as shaded area. Due to small errors, the standard deviation might not be visible for every data point. For clarity, only every 20$^{th}$ measured online data point is shown. Due to technical errors, no OTR is available.

As before, the CTR increases exponentially during the growth phase until a drop is visible after 14.5 hours, indicating the start of the nitrogen limitation (Figure 3.3A). Afterward, the CTR decreases until the beginning of the feed phase, at which point it increases up to 20.7 mmol/L/h due to the newly available nitrogen in the feed. As indicated by the CTR, the CDW increases from initially 1.7 g/L to 16.4 g/L at the beginning of the feed phase (Figure 3.3C). Afterward, it increases further to 19.4 g/L, staying constant until the end of

the fermentation. Until the nitrogen limitation starts, the pH drops from initially 7.8 to 4.6 and decreases further to 3.6 afterward due to ammonium consumption and ITA production (Figure 3.3C). The further decrease after 48 h is due to a burst tube in the second peristaltic pump of the control loop. At 70 hours, the tubing was replaced, and the controller was adjusted for a smoother control, as can be seen by comparing the pH between 24 and 48 hours with the pH between 72 and 240 hours. As described in the previous experiments, the filling volume changes because of sampling as well as the addition of feed and $Mg(OH)_2$. Again, the available sucrose is converted to its monomers, glucose, and fructose (Figure 3.3D). During the feed phase, the sucrose concentration increases from 24.8 g/L to 44.1 g/L because of a faster feed rate compared to the extended batch fermentation with pH shift (Figure 3.2). Glucose and fructose concentrations increase to 54.4 g/L and 86.6 g/L until the end of the feed phase, respectively (Figure 3.3D). After the feed phase, fructose increases to 106.6 g/L with decreasing sucrose concentrations. At the same time, glucose is being fully consumed until 146 h. After glucose is depleted, fructose slowly decreases, again showing a repression of the fructose utilization. Fructose concentrations reach 95.6 g/L after 220 hours and stay at this level until the end of the fermentation. ITA concentrations start to increase once the nitrogen limitation is reached and increase with a decreasing slope until 78.5 g/L are reached after 190 hours. Afterward, no further accumulation of the product was detected.

In total, 79.3 ± 1.6 $g_{ITA}$/L with an overall yield of 0.33 ± 0.01 $g_{ITA}/g_{sugar}$ and a STY of 0.31 ± 0.01 $g_{ITA}$/L/h were produced. This describes a lower yield and STY compared to the pH shift cultivation (Figure 3.2). However, assuming no leftover sugar, a theoretical overall yield of 0.51 ± 0.01 $g_{ITA}/g_{sugar}$ was reached. Further, looking only at the production phase starting from 26 hours until 190 hours, the theoretical yield increases to 0.66 ± 0.02 $g_{ITA}/g_{sugar}$ with a STY of 0.48 ± 0.02 $g_{ITA}$/L/h. This increase in yield, compared to the pH shift cultivation (Table 3.1 and Figure 3.2), is due to the fact that the maximal possible ITA concentration was reached. Therefore, a higher proportion of the substrate could be used for ITA production instead of growth.

While the experiment shows that growth and ITA production are possible with $Mg(OH)_2$, the salt has low solubility in water at high pH values. It must be fed as a suspension, which presents challenges, especially regarding the blocking of tubing and pipes. Due to the increased difficulty in handling, further scale-up experiments are conducted with NaOH as a base to alleviate the proof-of-concept.

*3.3.4 Scale-Up to 150 L Bioreactor*

A 150 L stirred tank reactor was used to show the feasibility of using thick juice as sole carbon source for the production of ITA in pilot scale. The fermentation at elevated scale is performed using NaOH as a base. To allow for scale comparability, the stirring frequency is adapted to keep the volumetric power input constant during scale-up [16]. The aeration, however, is set to 1 vvm as in laboratory scale experiments. As the volume of the fermenter decreases throughout operation due to evaporation, the aeration is adjusted accordingly. The filling volume is determined via the weight of the fermenter, and spikes in the filling volume are visible when samples are taken (Figure 3.4). There is no effect of substrate overfeeding on *U. cynodontis* ITA Max pH metabolism observed in this work (Appendix 7). Additionally, sufficient oxygen transfer can be realized (Appendix 7). Thus, a batch process with an initial substrate concentration of 137 $g_{sucrose}$/L from thick juice is performed to facilitate the first scale-up. Similar to laboratory scale experiments, biomass formation, ITA production, OTR, CTR, and RQ are monitored to reflect the overall metabolic activity (Figure 3.4). The following section will discuss the effects of the scale-up and the switch to batch fermentation mode.

The first 20 h of fermentation are comparable to fermentations in laboratory scale. Fluctuations in CTR during this time are due to changes in pH value, as illustrated in Appendix 8. The higher initial CDW is due to inoculation with 1 vol% instead of a specific OD. However, after the initiation of the nitrogen limitation, no increase in biomass is observed, resulting in a low CDW of 12.1 ± 0.4 g/L (Figure 3.4C). The inoculation with a fully grown culture can partially explain the deviation from laboratory scale experiments. The cells already experienced nitrogen limitation and may have changed their composition to adapt to nitrogen-limited conditions [77]. This difference in metabolic state is also reflected in OTR and CTR (Figure 3.4A). Between 24 h and 125 h, the CTR and OTR decreased from 17.8 to 9.4 mmol/L/h and from 18.2 to 11.4 mmol/L/h, respectively. This leads to a constant RQ, which stays around the theoretical value for ITA formation at ~0.66 (compare Equation 3.10), indicating increased product formation compared to small-scale fermentation. As a result, nearly twice the amount of ITA per g CDW is produced, and the productivity normalized to CDW is higher as in laboratory scale (Table 3.1). However, the product concentration stops increasing after reaching 60.3 $g_{ITA}$/L at 116.5 h (Figure 3.4D). Subsequently, there is only a small increase in the ITA titer to 66.4 g/L until the end of the fermentation.

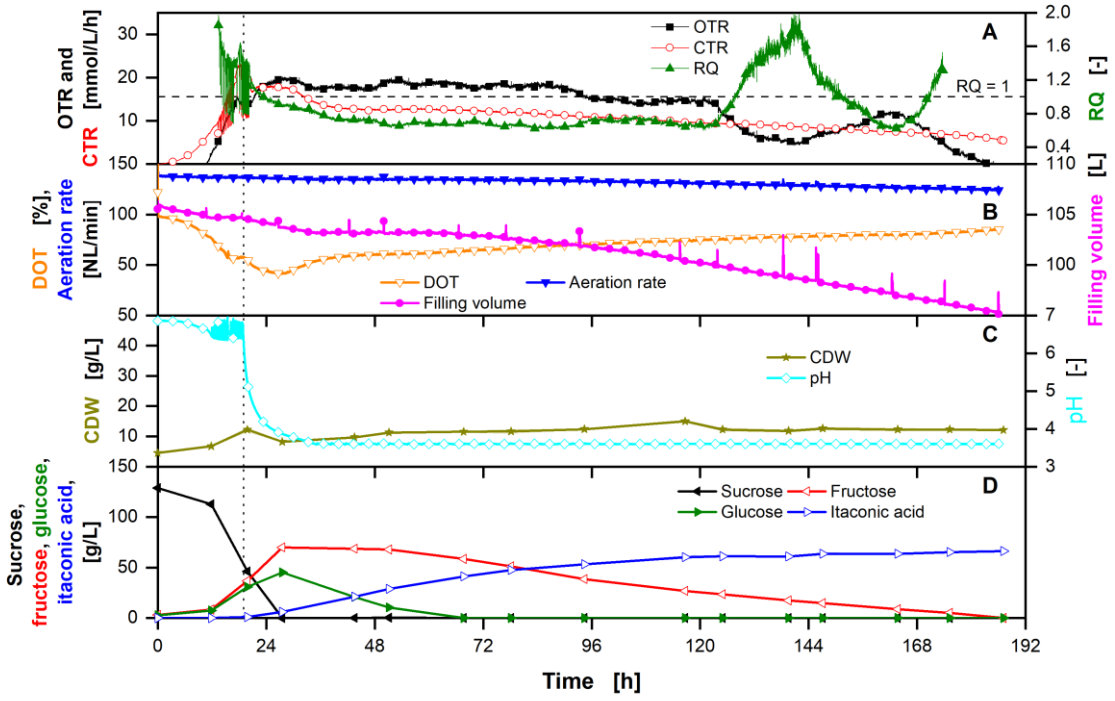


**Figure 3.4: 100 L batch fermentation of *U. cynodontis* ITA Max pH with pH shift and thick juice as sole carbon source**.

(A) Course of the oxygen and carbon dioxide transfer rates and respiratory quotient. The black dotted line indicates the start of the nitrogen limitation. The horizontal dashed line shows RQ = 1. RQ values are only shown for OTR values > 5 mmol/L/h. (B) Dissolved oxygen tension, absolute aeration rate, and filling volume. (C) Cell dry weight concentrations and pH. (D) Sugar (sucrose, glucose, fructose) and itaconic acid concentrations. 130 g/L sucrose were initially added to the medium. Cultivation was performed in a 150 L stirred tank pressure reactor (Frings Elektrotechnik und Anlagenbau GmbH, Alsdorf, Germany) with an initial filling volume of 105 L at 30 °C with a stirring rate of 285 rpm. pH was kept above 6.5 or 3.6 before and after the pH shift (indicated by a vertical dotted line) by adding 5 M NaOH. Concentrations are shown as mean values of triplicates and standard deviation as shaded area. Due to small errors, the standard deviation might not be visible for every data point. For clarity, only every 200$^{th}$ measured online data point is shown.

At the same time, about 25 g/L of fructose were consumed. It is unlikely that this is just used for maintenance due to the short time frame and no increase in the CTR. However, it correlates with the drop in the OTR, leading to an RQ well above 1. This would indicate the production of a more reduced compound like hydrocarbons. It has previously been shown that species of the Ustilaginacea family produce different lipids as storage molecules, with *U. cynodontis* being able to produce glycolipids [1, 106]. This thesis is further supported by gas chromatography measurements, which did not reveal any accumulation of small molecules below 1,000 Da (data not shown). Determination of which specific molecules were produced and what caused the metabolic switch will be subject of future research.

At the end of the fermentation, 6.4 ± 0.1 kg ITA with a yield of 0.44 ± 0.01 $g_{ITA}/g_{glucose,eq.}$ and an STY of 0.35 ± 0.01 $g_{ITA}/L/h$ were produced. Considering overall yield, STY, and titer, the batch fermentation at 150 L scale and the extended-batch fermentation in laboratory scale behaved similarly (Table 3.1).

**Table 3.1: Comparison of fermentation KPI in laboratory and 150 L scale.**

| | **Reference [62]** | **Constant pH** | **pH Shift** | **$Mg(OH)_2$** | **150 L fermentation** |
|---|---|---|---|---|---|
| Carbon source | Glucose | Thick juice | Thick juice | Thick juice | Thick juice |
| Mode | Batch | Extended-Batch | Extended-Batch | Extended-Batch | Batch |
| Ammonium added [g/L] | 4.0 | 4.0 | 0.8 | 0.8 | 0.8 |
| pH [-] | 3.6 | 6.5 | 6 → 3.6 | 6 → 3.6 | 6 → 3.6 |
| Titer [$g_{ITA}/L$] [a] | 83.0 ± 0.8 | 106.4 ± 0.1 | 66.6 ± 0.2 | 79.3 ± 1.6 | 66.4 ± 0.4 |
| $Y_{P/S}$ [$g_{ITA}/g_{glucose,eq}$] [b] | 0.30 ± 0.0 | 0.46 ± 0.02 | 0.46 ± 0.02 | 0.32 ± 0.01 | 0.44 ± 0.01 |
| $Y_{P/S,max}$ [$g_{ITA}/g_{glucose,eq}$] [c] | 0.36 ± 0.0 | 0.52 ± 0.02 | 0.52 ± 0.02 | 0.66 ± 0.02 | 0.66 ± 0.03 |
| STY [$g_{ITA}/L/h$] [d] | 0.59 ± 0.0 | 0.72 ± 0.02 | 0.40 ± 0.01 | 0.31 ± 0.01 | 0.35 ± 0.01 |
| $STY_{max}$ [$g_{ITA}/L/h$] [e] | 1.4 ± 0.0 | 0.82 ± 0.02 | 0.43 ± 0.02 | 0.48 ± 0.02 | 0.61 ± 0.02 |
| Product normalized to CDW [$g_{ITA}/g_{CDW}$] | No data available | 2.0 ± 0.2 | 2.3 ± 0.2 | 2.5 ± 0.3 | 5.4 ± 0.4 |
| $STY_{norm}$ [$g_{ITA}/h/g_{CDW}$] [f] | No data available | 0.014 ± 0.005 | 0.015 ± 0.004 | 0.010 ± 0.005 | 0.029 ± 0.005 |

[a] Titer: itaconic acid concentration at the end of the respective fermentation

[b] $Y_{P/S}$: overall yield of itaconic acid on glucose (equivalents)

[c] $Y_{P/S,max}$: maximum yield during production phase without leftover sugars

[d] STY: overall space-time-yield

[e] $STY_{max}$: maximum space-time-yield during production phase

[f] $STY_{norm}$: space-time-yield normalized to cell dry weight

As described previously [78, 86], ITA exhibits weak acid stress at pH 3.6, limiting cultivations to the observed maximum titers in this study (Table 3.1, Figure 3.3 and Figure 3.4). To overcome this, *in-situ* product removal by reactive extraction [85], salt precipitation [61], or adsorption processes could be employed [117]. With these, longer

production times and higher titers could be achieved – increasing yield and STY – making ITA production from alternative feedstocks economically even more interesting [132].

To reach the above-mentioned maximum yields ($Y_{P/S,max}$, Table 3.1), no sugars need to be left at the end of the fermentation. In addition, the inherent challenge of seasonal fluctuations in crude substrates needs to be met [84]. To tackle both challenges simultaneously, online analytics are indispensable for accurate feeding protocols. Here, optical methods such as Raman spectroscopy show great potential, as they do not interfere with the process and provide highly time-resolved data [37, 69]. Even though first results have been promising for measuring the sugars (glucose, fructose, sucrose) and ITA in media containing thick juice, further research is necessary to establish a feeding profile based on Raman measurements [132].

## 3.4 Conclusion

Based on the findings from Chapter 2, a successful scale-up to a 2 L fermenter was performed with thick juice as the sole carbon source at a constant pH of 6. High titers of 106.4 ± 0.1 g/L and 99.8 ± 0.7 g/L with yields of $0.50 \pm 0.02$ $g_{ITA}/g_{sucrose}$ ($0.48 \pm 0.02$ $g_{ITA}/g_{glucose,eq.}$) and $0.69 \pm 0.02$ $g_{ITA}/g_{sucrose}$ ($0.66 \pm 0.02$ $g_{ITA}/g_{glucose,eq.}$) for *U. cynodontis* ITA Max pH and *U. maydis* Mutterschiff were reached, respectively.

However, a low pH is necessary for efficient downstream process integration. Therefore, a pH shift was introduced to allow natural acidification of the medium during the fermentation. In addition, the initially added ammonium chloride concentration was reduced to compensate for the added nitrogen sources in thick juice. Even though the titer was reduced in the experiment with pH shift, a constant yield was observed compared to the fermentation at a constant, high pH. However, higher yields are expected for fermentations that reach the maximum product concentration of ~80 $g_{ITA}$/L. This showcases the need for online analytics of the substrates and products to allow for better feeding control.

As a holistic approach has shown that aligning the pH-adjusting agents in fermentation and DSP is necessary to improve the overall process yield, a fermentation with $Mg(OH)_2$ was run. While the experiment showed that growth and ITA production with $Mg(OH)_2$ are possible, the salt has a low solubility in water at high pH values and must be fed as a

suspension. This presents challenges, especially regarding the blocking of tubing and pipes, which makes specialized equipment necessary for large-scale production.

In the last step, a scale-up to a 150 L STR was performed. With a maximum yield of $0.66 \pm 0.03$ $g_{ITA}/g_{glucose,eq.}$ and product and STY normalized to CDW around twice as high as in small scale, the fermentation showcased the feasibility of the scale-up of an ITA fermentation with thick juice as the sole carbon source in batch mode.

In the future, *in-situ* product removal will be implemented to alleviate the product toxicity and, thus, increase the yield and STY even further. In addition, online analytics of the substrates and products are necessary to allow for better process control, especially regarding the feed.

# Chapter 4

## 4. Procedural Analysis of Commercially Available Shake Flasks from 50 – 5000 mL

### 4.1 Background

Shake flasks are a simple and versatile tool for parallel studies in bioprocess development. Former major disadvantages of shake flasks compared to stirred tank reactors, like missing online monitoring capabilities or the possibility to feed substrates, have been remedied [4, 5, 43, 75, 121, 135], making flasks an interesting alternative for STR cultivations in small scale.

In addition, shake flasks have been extensively studied regarding ‘in-phase’ shaking conditions [6, 18], power input [17, 18], energy dissipation rate [120], OTR or maximum oxygen transfer capacity ($OTR_{max}$) [104, 107] and heat transfer [138].

While ‘in-phase’ shaking parameters lead to the liquid volume following the rotation of the shaker, ‘out-of-phase’ conditions lead to a major part of the liquid remaining at the bottom of the shake flask [6, 18]. This results in significantly reduced oxygen transfer and mixing in the liquid and, thus, in unreproducible outcomes of screening experiments [18, 119].

The volume specific power input strongly influences culture performance and repeatability of experiments [19]. It generally increases with shaking frequency, shaking diameter, viscosity of the medium, and vessel size [17, 18, 125] and is a major contributor to heat generation within the shaken bioreactor [123]. Although the volume specific power input is often used as a scale-up criterion for shear-sensitive organisms [100], the maximum energy dissipation rate might be better suited. Interestingly, it is about tenfold lower in shake flasks than in STR cultivations with the same volumetric power input [120].

Alternatively, the $OTR_{max}$ can be used as a scale-up criterion to ensure a comparable oxygen supply [100]. This is especially interesting for cultivations where oxygen consumption is of key importance. In shake flasks, the $OTR_{max}$ can be predicted based on Meier et al. (2016) [104]. Here, the transfer resistance of the sterile barrier is normally not limiting to the overall mass transfer [107]. However, the resistance is highly dependent on the type and form of the sterile barrier used for cultivation, and thus, it should be considered for the determination of $OTR_{max}$ [79].

The shaking of the flasks, in addition to the biological activity of the microbes, results in hydromechanical heat generation [25, 123]. However, the heat transfer in shake flasks is generally dismissed because the heat loss over the flask wall is considered sufficient to ensure a constant liquid temperature. Nevertheless, it has previously been shown for large shaken reactors that the heat sources lead to a temperature difference between liquid and surrounding air due to a limited heat transfer [125]. Sumino and Akiyama (1987) [141] published an empirical estimation of the heat transfer coefficient for shake flasks.

Despite the advances in shake flask characterization, the importance of engineering characteristics such as volumetric power input or OTR is often underestimated [79, 139]. However, these are important for the development of the bioprocess, as mistakes made during this stage are costly to undo in later stages. It is, therefore, of key importance to critically evaluate the screening conditions in shake flask scale.

In this chapter, standard shake flasks from 50 – 5000 mL are procedurally analyzed regarding the engineering parameters described above. Here, only narrow-neck unbaffled shake flasks are considered. Even though baffles might increase the $OTR_{max}$ and hydromechanical stress, they show a low reproducibility, often wet the sterile barrier, thus reducing the mass transfer and benefit ‘out-of-phase‘ conditions [19]. On the one hand, small flasks could be used to increase throughput. Large flasks, on the other hand, might be used to produce increased amounts of biomass, for example, for subsequent inoculation of STR cultivations.

The shaking frequency (n) and shaking diameter ($d_0$) are two key parameters for running experiments in shake flasks. To allow for a comparison between the different flask sizes, two key assumptions must be met:

1. The center of rotation should be at the same relative point for each flask size.
2. The centrifugal forces should be constant between different flask sizes.

The assumptions lead to a constant ratio between $d_0$ and the flask diameter and a constant axial Froude number [18]. As a reference, a common 250 mL narrow neck shake flask with 10 mL filling volume at 350 revolutions per minute and a shaking diameter of 25 mm is used.

The filling volume is another key parameter that influences most engineering parameters. In this study, three different cases are compared:

1. A constant relative filling volume of 4 % (according to 10 mL in 250 mL flask)
2. A constant volumetric gas transfer coefficient ($k_La$)
3. A constant maximum oxygen transfer capacity regarding sterile barrier resistance ($OTR_{max,plug}$)

## 4.2 Material and Methods

*4.2.1 Determination of the shaking diameter, the shaking frequency, and the filling volume*

A 250 mL narrow-neck Erlenmeyer flask with a shaking diameter ($d_0$) of 25 mm, a shaking frequency (n) of 350 rpm, and a filling volume ($V_L$) of 10 mL was used as a reference for the calculations.

Two assumptions were used to determine the shaking diameter ($d_0$) and the shaking frequency (n) for each flask size. First, the center of rotation should be at the same relative point for each flask size. This results in a constant ratio between $d_0$ and the flask diameter (d). Using the standard 250 mL narrow-neck Erlenmeyer flask results in a value of ~0.3075. From this, $d_0$ can be calculated for the other flask sizes according to Equation 4.1:

$$\frac{d_0}{d} = 0.3075 \quad \leftrightarrow \quad d_0 = 0.3075 \cdot d \tag{4.1}$$

with $d_0$ as shaking diameter [m] and d as flask diameter [m].

The second assumption is that the centrifugal forces should be constant between the different flasks, leading to a constant axial Froude number [18].

$$Fr_a = \frac{(2 \cdot \pi \cdot n)^2 \cdot d_0}{2 \cdot g} \approx 1.712 \tag{4.2}$$

Equation 4.2 shows the calculation of the axial Froude number ($Fr_a$) [-] with n as the shaking frequency [1/s] and g as the gravitational acceleration (9.81) [$m/s^2$]. For the

reference $Fr_a$ is determined to be approximately 1.712. Rearranging the equation allows to determine n for the other flask sizes:

$$n = \sqrt{\frac{1.712 \cdot 2 \cdot g}{d_0}} / (2 \cdot \pi) \quad (4.3)$$

The filling volume of each flask size depends on the observed case. Three different cases were analyzed in this study:

1. A constant relative filling volume of 4 % (according to 10 mL in 250 mL flask)
2. A constant volumetric gas transfer coefficient ($k_La$)
3. A constant maximum oxygen transfer capacity regarding plug resistance ($OTR_{max,plug}$)

The determination of the filling volume for each flask in case one is trivial. For case two, first, the maximum oxygen transfer capacity [mol/L/h] has to be determined according to Equation 4.4 [104]:

$$OTR_{max} = 3.72 \cdot 10^{-7} \cdot Osmol^{0.05} \cdot n^{\left(1.18 - \frac{Osmol}{10.1}\right)} \cdot V_L^{-0.74} \cdot d_0^{0.33} \cdot d^{1.88} \cdot p_R \cdot y_{0_2}^* \quad (4.4)$$

Here, Osmol describes the osmolality of the medium [Osmol/kg], n the shaking frequency [rpm], $V_L$ the filling volume [mL], $d_0$ the shaking diameter [mm], d the flask diameter [mm], $p_R$ the ambient pressure (1.013) [bar] and $y_{O2}^*$ the oxygen mole fraction in the gas phase [mol/mol]. For the osmolality, a value of 0.68 Osmol/kg is assumed, which corresponds to the classic Wilms-MOPS media containing glucose [104]. In addition, 0.20942 mol/mol (air) is assumed for $y_{O2}^*$.

The correlation between the oxygen transfer rate (OTR) [mol/L/h] and $k_La$ [1/s] (gas-liquid transfer) is described by Equation 4.5:

$$OTR = k_L a \cdot p_R \cdot L_{O_2} \cdot (y_{O_2,inside}^* - y_{O_2,L}) \quad (4.5)$$

with $L_{O_2}$ as the solubility of oxygen in the liquid (0.001) [mol/L/bar], $y_{O_2,inside}^*$ as oxygen mole fraction of the gas inside the flask [mol/mol] and $y_{O2,L}$ as oxygen mole fraction in the liquid phase [mol/mol]. In the case of OTR = $OTR_{max}$ $y_{O2,L}$ becomes zero and $k_La$ can easily be determined using Equation 4.6.

$$k_L a = \frac{OTR_{max}}{p_R \cdot L_{O_2} \cdot y_{O_2,inside}^*} \quad (4.6)$$

Note that for this case, the gas inside the flask is assumed to be normal air (no influence of the sterile barrier). Thus, a $y_{O2,inside}$ of 0.20942 mol/mol is assumed. In addition, it has previously been shown by Maier et al. (2004) [99] that the dissolved oxygen concentration inside the liquid does not reach zero in the catalyzed sulfite system, which is normally used to determine $OTR_{max}$. It is, therefore, unlikely that the concentration will reach zero in a microbial setting. Nevertheless, the 'true' maximum oxygen transfer capacity is calculated in this study. This is reached when the driving force of the OTR is at its maximum, thus, when the dissolved oxygen concentration inside the liquid is zero.

Using the parameters from the 250 mL flask reference, a $k_La$ of 237.2 1/s was determined. To determine the filling volumes for the other flask sizes, the *Solver* provided by *Microsoft Excel* was employed. As the filling volume changes $OTR_{max}$ and, thus, $k_La$, it was iteratively in- or decreased until the calculated $k_La$ for the respective flask size was 273.2 1/s.

For the case of a constant $OTR_{max,plug}$, not only the gas-liquid transfer (Equation 4.5) needs to be considered, but also the mass transfer through the cotton plug. This is described by Equation 4.7:

$$OTR = \frac{k_{pl}}{V_L} \cdot (y^*_{O_2,outside} - y^*_{O_2,inside}) \tag{4.7}$$

with $k_{pl}$ as the mass transfer coefficient for the sterile barrier (cotton plug) [mol/s] and $y^*_{O_2,outside}$ as the oxygen mole fraction in the gas phase outside of the flask [mol/mol].

Rearranging Equation 4.7 for $y^*_{O_2,inside}$ yields:

$$y^*_{O_2,inside} = y^*_{O_2,outside} - \frac{OTR \cdot V_L}{k_{pl}} \tag{4.8}$$

Calculation of the OTR regarding the sterile closure ($OTR_{plug}$) [mol/L/h] is then possible by inserting Equation 4.8 into 4.5 [79]:

$$OTR_{plug} = \frac{k_La \cdot p_R \cdot L_{O_2} \cdot (y^*_{O_2,outside} - y_{O_2,L})}{1 + \frac{k_La \cdot p_R \cdot L_{O_2} \cdot V_L}{k_{pl}}} \tag{4.9}$$

with

$$k_{pl} \approx \frac{D_{O_2,eff} \cdot A_{pl}}{H_{pl} \cdot V_{mo}} \tag{4.10}$$

Here, $D_{O2,eff}$ is the effective oxygen diffusion coefficient (approximately 80 % of the coefficient in air ~$1.256 \cdot 10^{-5}$ $m^2/s$ (personal communication with Prof. Jochen Büchs))

[$m^2/s$], $A_{pl}$ the base area of the cotton plug inside the flask neck [$m^2$], $H_{pl}$ the height of the cotton plug inside the flask neck (= flask neck height) [m] and $V_{mo}$ the molar gas volume (22.414) [L/mol]. To calculate $A_{pl,}$ the flask neck diameter ($d_N$) [m] is used according to Equation 4.11:

$$A_{pl} = \pi \cdot \left(\frac{d_N}{2}\right)^2 \tag{4.11}$$

The flask dimensions for each size used in this study are given in Appendix 9.

As before, $y_{O2,L}$ becomes zero when $OTR_{plug} = OTR_{max,plug}$, which then yields an $OTR_{max,plug}$ of 47.4 mmol/L/h for the reference 250 mL flask. Note, that $y^*_{O_2,inside}$ (Equation 4.8) is used to calculate $k_La$ (Equation 4.6). As these depend on each other, an iterative approach is needed to calculate $OTR_{max,plug}$. As in case two, the filling volume for each flask size was calculated using the *Microsoft Excel Solver*.

The filling volumes for each case and flask size are given in Table 4.1.

**Table 4.1: Calculated filling volumes for each flask sizes depending on the observed case.**

| Nominal flask volume ($V_F$) [mL] | Filling volume ($V_L$) [mL] | | |
|---|---|---|---|
| | Constant $V_L/V_F$ | Constant $k_La$ | Constant $OTR_{max,plug}$ |
| 50 | 2.0 | 3.3 | 3.4 |
| 100 | 4.0 | 5.1 | 5.1 |
| 250 | 10.0 | 10.0 | 10.0 |
| 500 | 20.0 | 16.2 | 15.6 |
| 1000 | 40.0 | 27.0 | 24.7 |
| 2000 | 80.0 | 47.3 | 42.4 |
| 5000 | 200.0 | 89.1 | 67.4 |

The fluid volume per tray can be calculated by multiplying $V_L$ with the number of flasks of each size that can be mounted on a shaking tray. The number is given in Appendix 9.

To verify ‘good’ shaking conditions (e.g. the bulk liquid circulates ‘in-phase’ with the shaking tray), Büchs et al. (2000) [18] have introduced the phase number (Ph) [-]:

$$Ph = \frac{d_0}{d} \cdot \left(1 + 3 \cdot log_{10}\left(Re_f\right)\right) > 1.26 \quad (4.12)$$

with

$$Re_f = Re \cdot \frac{\pi}{2} \cdot \left(1 - \sqrt{1 - \frac{4}{\pi} \cdot \left(\frac{{V_L}^{1/3}}{d}\right)^2}\right)^2 \quad (4.13)$$

and

$$Re = \frac{\rho \cdot n \cdot d^2}{\eta} \quad (4.14)$$

Here, $Re_f$ is the liquid film Reynolds number [-], Re is the flask Reynolds number [-], ρ is the density of the liquid (1000 kg/m$^3$ [144]) [kg/m$^3$], and η is the dynamic viscosity of the liquid (0.001 Pa·s [64]) [Pa·s]. It has been shown that the inner flask diameter (d) is a suitable characteristic length scale for flasks [17]. To reach 'in-phase' conditions, Ph needs to be greater than 1.26 with an axial Froude number greater than 0.4 [18]. In this study, only the Phase number needs to be calculated, as all conditions show $Fr_a$ = 1.712 (compare Equation 4.2 and 4.3).

*4.2.2 Volume specific power input and energy dissipation rate*

A modified Newton number has been introduced for stirred tank reactor by Clark and Vermeulen (1964) [23]. This has been further modified by Büchs et al. (2000) [17] to Equation 4.15:

$$Ne' = Ne \cdot \frac{d}{h} \approx Ne \cdot \frac{d}{{V_L}^{1/3}} = \frac{P}{\rho \cdot n^3 \cdot d^4 \cdot {V_L}^{1/3}} \quad (4.15)$$

with Ne' as the modified Newton number [-], Ne as the Newton number [-], h as the vertical length scale for the friction area between liquid and flask wall [m] and P as the power [W]. Rearranging for P and dividing by the filling volume yields the volume specific power input ($P_V$) [W/m$^3$]:

$$P_V = Ne' \cdot \frac{\rho \cdot n^3 \cdot d^4}{{V_L}^{2/3}} \quad (4.16)$$

The modified Newton number can be calculated according to Equation 4.17 [18]:

$$Ne' = 70 \cdot Re^{-1} + 25 \cdot Re^{-0.6} + 1.5 \cdot Re^{-0.2} \quad (4.17)$$

Using Equations 4.15, 4.16 and 4.17 allows to calculate the volume specific power input for each parameter set according to the different observed cases.

The average energy dissipation rate (εØ) [W/kg] can be described by:

$$\varepsilon_{Ø} = \frac{P}{V_L \cdot \rho} = Ne' \cdot \frac{n^3 \cdot d^4}{{V_L}^{2/3}} \quad (4.18)$$

Liepe et al. (1988) [92] introduced a general relationship to quantify the maximum energy dissipation rate ($\varepsilon_{max}$) [W/kg]:

$$\varepsilon_{max} = 0.1 \cdot \frac{u^3}{h_1} \quad (4.19)$$

with u as the velocity of the turbulence generating element relative to the liquid volume [m/s] and $h_1$ as the characteristic length of the same element [m]. This equation is, however, only valid for fully developed turbulent flow. Peter et al. (2006) [120] have shown that full turbulence is reached with $Re_{crit} > 60{,}000$ in unbaffled shake flasks. In addition, $\varepsilon_{max}$ can be calculated according to Equation 4.19 with u as the velocity of the flask (compare Equation 4.22) [m/s] and $h_1$ as the liquid height of the bulk liquid inside the flask [m]. The liquid height was calculated according to the liquid distribution model from Büchs et al. (2007) [20] and can be found in Appendix 10.

### *4.2.3 Heat transfer coefficients and temperature change*

The overall heat transfer and temperature change were compared based on three different correlations and one constant UA value.

1. An empirical correlation for the heat transfer coefficient (UA) in shake flasks
2. An empirical correlation for the heat transfer coefficient (UA) in large orbitally shaken cylindrical bioreactors
3. Calculation of the overall heat transfer coefficient (U) for a cylinder model
4. An empirically determined UA of 0.39 W/K for a 250 mL shake flask

Sumino and Akiyama (1987) [138] were the first (and to date only) to investigate the heat transfer in shake flask. They developed empirical equations for three different geometries of flasks. Their so-called S-type resembles a 250 mL Erlenmeyer shake flask. However, it only had a nominal volume of 200 mL and, therefore, also slightly different dimensions, compared to a standard 250 mL flask. The empirical correlation for the heat transfer coefficient (UA) [W/K] is given by Equation 4.20.

$$UA = 5.3 \cdot {W_F}^{-0.26} \cdot {V_L}^{-0.62} \cdot n^{0.19} \cdot {v_F}^{0.25} \quad (4.20)$$

Here, $W_F$ is the weight of the flask [g] (Appendix 9), $V_L$ is the filling volume [mL], n is the shaking frequency [rpm] and $v_F$ is the velocity of the flask on the tray (Equation 4.22) [m/s]. Note that the empirical correlation yields UA in J/(ml·min·K).

Raval et al. (2014) [125] have studied the heat transfer in large orbitally shaken cylindrical bioreactors (30 – 50 L nominal volume). Using the extended temperature method [124], an empirical correlation for UA was determined [125]:

$$UA = 5.3 \cdot {V_L}^{0.25} \cdot n^{0.55} \cdot {v_{air}}^{0.5} \quad (4.21)$$

with $v_{air}$ as the velocity of the lateral airflow [m/s]. The lateral airflow in the study is introduced through additional fans [125]. However, the motion of the vessel also produces airflow. In this study, as there is no additional lateral airflow, the velocity of the flask through the shaker is used as $v_{air}$.

$$v_F = \pi \cdot n \cdot d_0 = v_{air} \quad (4.22)$$

Here, $v_F$ is the velocity of the flask due to shaking [m/s].

A shake flask can be modeled as a rotating cylinder with lateral airflow. The rotation with the lateral airflow then describes the influence of the shaking movement on the heat transfer in flasks. Calculating the overall heat transfer coefficient (U) [W/m$^2$/K] instead of UA removes the influence of the heat transfer area (A) and, hence, does not need to be considered by the model. Jeng et al. (2014) [68] described the Nusselt number in rotating cylinders with lateral air flow ($Nu_{rj}$) [-]:

$${Nu_{rj}}^m = {Nu_r}^m + {Nu_j}^m \quad (4.23)$$

with $Nu_r$ as the Nusselt number for pure rotation without lateral air flow [-] and $Nu_j$ as the Nusselt number for pure lateral air flow without rotation [-]. The factor m is used for the superposition of the two parts and is described by:

$$m = 4.726 \cdot \frac{D}{w}^{-0.362} \quad (4.24)$$

Here, D is the diameter of the cylinder [m] and w is the width of the nozzle used to produce the lateral air flow [m]. Because in our case the flask is moving through the shaker, thus, creating the air flow, the nozzle width is described by the flask diameter (d), as the diameter of the cylinder. $Nu_r$ is then described by:

$${Nu_r} = 0.226 \cdot {Re_r}^{0.607} \quad (4.25)$$

with

$$Re_r = \frac{\rho_{air} \cdot \pi \cdot n \cdot D^2}{120 \cdot \eta_{air}} \quad (4.26)$$

$Re_r$ describes the Reynolds number of the rotating cylinder [-], $\rho_{air}$ the density of the surrounding fluid (air) (1.2041 kg/m$^3$ [147]) [kg/m$^3$], n the rotational (shaking) frequency [rpm] and $\eta_{air}$ the dynamic viscosity of the surrounding fluid (air) ($1.822 \cdot 10^{-5}$ Pa·s [70]) [Pa·s]. $Nu_j$ is calculated according to:

$$Nu_j = 0.995 \cdot Re_j^{0.560} \cdot \left(\frac{L}{w}\right)^{-0.341} \cdot \left(\frac{D}{w}\right)^{-0.768 \cdot \left(\frac{L}{w}\right)^{-0.516}} \quad (4.27)$$

with

$$Re_j = \frac{\rho_{air} \cdot v_{air} \cdot D}{\eta_{air}} \quad (4.28)$$

Here, $Re_j$ describes the Reynolds number of the lateral air stream [-] and L the shortest distance of the air nozzle to the cylinder [m]. For L, the shaking diameter of each flask size is used, as it describes the maximum displacement of the flasks inside the shaker. Like before, the velocity of the airflow is approximated with the velocity of the flask (Equation 4.22).

The Nusselt number (Nu) [-] is generally defined as:

$$Nu = \frac{\alpha \cdot L}{\lambda} \quad (4.29)$$

with α as heat transfer coefficient between wall and fluid (here: air) [W/m$^2$/K], L as characteristic length (flask diameter) [m], and λ as thermal conductivity of the fluid (0.0262 W/m/K [136]) [W/m/K]. Rearranging Equation 4.29 for α yields:

$$\alpha = \frac{Nu \cdot \lambda}{L} \quad (4.30)$$

The overall heat transfer coefficient can be described as the sum of the liquid side heat transfer coefficient, the wall heat transfer coefficient, and the gas side heat transfer coefficient. In turn, the wall heat transfer coefficient is the rate of thermal conductivity of the flask wall to the wall thickness. This results in Equation 4.31:

$$\frac{1}{U} = \frac{1}{h_L} + \frac{l}{k} + \frac{1}{h_g} \quad (4.31)$$

with U as the overall heat transfer coefficient [W/m$^2$/K], $h_L$ as the liquid side heat transfer coefficient [W/m$^2$/K], l as the thickness of the flask wall [m], k as the thermal conductivity of the flask material [W/m/K] and $h_g$ as gas side heat transfer coefficient [W/m$^2$/K].

Assuming a cylindrical geometry of the flask, $h_L$ can be correlated to the power consumption:

$$\frac{h_L}{\rho \cdot c_p} = 0.13 \cdot \left(\frac{\frac{P}{V_L} \cdot \eta}{\rho^2}\right)^{\frac{1}{4}} \cdot P_r^{-2/3} \quad (4.32)$$

with

$$P_r = c_p \cdot \frac{\eta}{\lambda} \quad (4.33)$$

Here, ρ is the density of the fluid [kg/m$^3$], $c_p$ is the specific heat capacity of the fluid [J/kg/K], $P/V_L$ is the volume specific power input [W/m$^3$], η is the dynamic viscosity of the fluid [Pa·s] and λ as the thermal conductivity of the fluid [W/m/K].

U can then be calculated according to 4.31, with α as $h_g$, for rotating cylinders with lateral airflow. The assumed values are given in Appendix 11.

To compare the different (overall) heat transfer coefficients they are converted to each other by dividing by or multiplying with the heat transfer area (A) [m$^2$] according to Equation 4.34:

$$UA = U \cdot A \leftrightarrow U = \frac{UA}{A} \quad (4.34)$$

Note that, due to liquid film formation, it is assumed that the whole area that is wetted and not only the bulk liquid area contributes to heat transfer and is, therefore, used as A (Appendix 10).

The temperature change (ΔT) [K] inside each flask is due to an accumulation of heat inside the flask that cannot be diverted outside the flask over the flask wall. It can easily be calculated by dividing the total power per flask ($P_{total}$) [W] by the heat transfer coefficient (UA) [W/K]:

$$\Delta T = \frac{P_{total}}{UA} \quad (4.35)$$

The total power per flask is the sum of the power introduced into the liquid by the shaking motion (mechanical heat generation, $P_s$) [W] and the biological heat production through microbial activity ($P_{bio}$) [W]:

$$P_{total} = P_S + P_{bio} \tag{4.36}$$

It is assumed, that the whole power from the shaking motion is converted to heat. Therefore, $P_S$ can be calculated from the volume specific power input (Equation 4.16) [W/m$^3$] by multiplication with the filling volume of each flask size [m$^3$]:

$$P_S = \frac{P}{V_L} \cdot V_L \tag{4.37}$$

The microbial heat generation is due to the oxidation of substrates (e.g. carbohydrates) as part of the cells' metabolism. The respiration activity, therefore, gives a direct correlation between consumed oxygen and microbial heat generation [25]. Using the oxycaloric equivalent ($\Delta H_{ox}$) [kJ/mol] of -469 kJ/mol$_{O2}$ [74, 126] and $OTR_{max,plug}$ the biological heat generation can be calculated according to Equation 4.38.

$$P_{bio} = -\Delta H_{ox} \cdot OTR_{max,plug} \cdot V_L \tag{4.38}$$

Table 4.2 shows the calculated total power, biological power, and mechanical power through shaking per flask, depending on the three observed cases.

**Table 4.2: Total ($P_{total}$), biological ($P_{bio}$) and mechanical power through shaking ($P_S$) per flask for each flask volume and observed case.**
All values are given in $10^{-2}$ W.

| Nominal flask volume ($V_F$) [mL] | Constant $V_L/V_F$ | | | Constant $k_La$ | | | Constant $OTR_{max,plug}$ | | |
|---|---|---|---|---|---|---|---|---|---|
| | $P_{total}$ | $P_{bio}$ | $P_S$ | $P_{total}$ | $P_{bio}$ | $P_S$ | $P_{total}$ | $P_{bio}$ | $P_S$ |
| 50 | 2.8 | 1.9 | 0.9 | 3.2 | 2.1 | 1.1 | 3.2 | 2.1 | 1.1 |
| 100 | 4.7 | 3.0 | 1.7 | 5.0 | 3.2 | 1.8 | 5.0 | 3.2 | 1.8 |
| 250 | 10.5 | 6.2 | 4.3 | 10.5 | 6.2 | 4.3 | 10.5 | 6.2 | 4.3 |
| 500 | 18.6 | 10.2 | 8.4 | 17.6 | 9.7 | 7.9 | 17.4 | 9.6 | 7.8 |
| 1000 | 34.1 | 17.0 | 17.0 | 30.5 | 15.6 | 14.9 | 29.8 | 15.3 | 14.5 |
| 2000 | 66.6 | 30.1 | 36.5 | 57.4 | 26.8 | 30.6 | 55.7 | 26.1 | 29.5 |
| 5000 | 141.6 | 51.3 | 90.3 | 113.0 | 44.0 | 69.0 | 104.5 | 41.6 | 62.9 |

## 4.3 Results and Discussion

*4.3.1 Determination of shaking frequency, shaking diameter and filling volume*

For the comparison of the different flask sizes, $d_0/d$ and $Fr_a$ are kept constant. The resulting shaking frequencies (n) and shaking diameters ($d_0$) are shown in Table 4.3.

**Table 4.3: Calculated shaking diameter ($d_0$) and shaking frequency (n) for the different flask sizes.** Calculations are based on Equations 4.1 and 4.3.

| Nominal flask volume ($V_F$) [mL] | Shaking diameter ($d_0$) [mm] | Shaking frequency (n) [rpm] |
|---|---|---|
| 50 | 15.3 | 448 |
| 100 | 18.5 | 407 |
| 250 | 25.0 | 350 |
| 500 | 31.1 | 314 |
| 1000 | 39.0 | 280 |
| 2000 | 49.5 | 249 |
| 5000 | 66.5 | 215 |

With increasing flask volume and, therefore, increasing inner diameter (d) (shake flask dimensions in Appendix 9), the shaking diameter ($d_0$) increases. Due to this increase in $d_0$, the shaking frequency (n) needs to decrease to keep the axial Froude number ($Fr_a$) constant (Equation 4.2). Even though the assumptions are reasonable and allow for the comparison of the different scales, it needs to be mentioned that only shakers with shaking frequencies up to 400 rpm are currently commercially available.

The filling volumes of the different flask sizes are dependent on the three cases that are compared. The relative filling volumes, in addition to the fluid volume per tray, are shown in Figure 4.1.

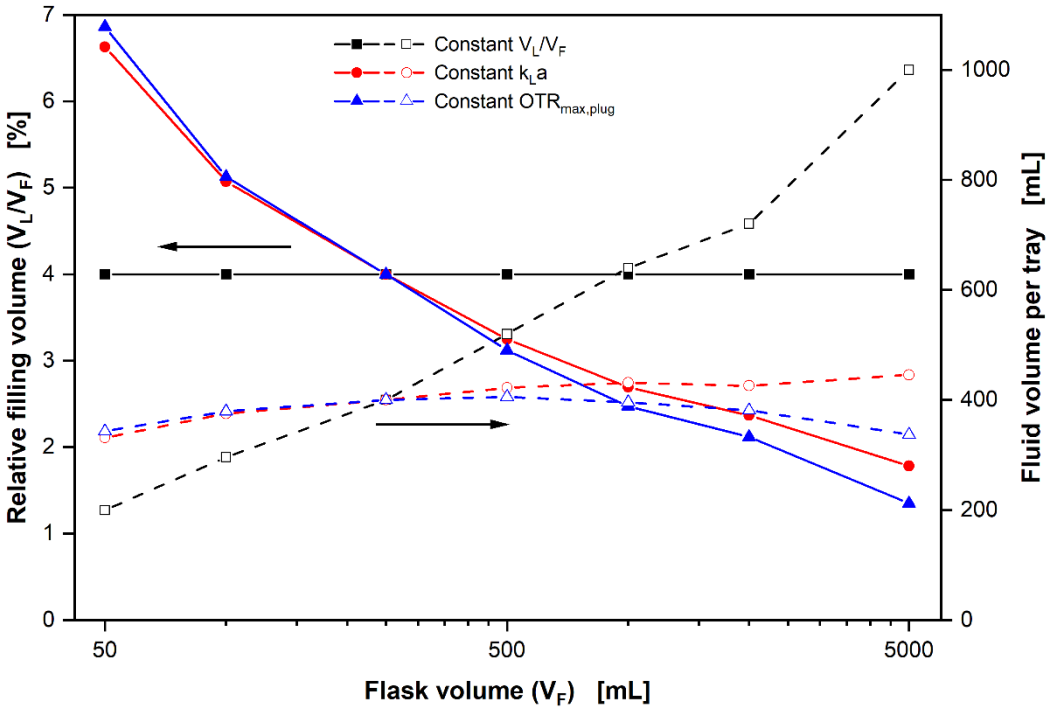


**Figure 4.1: Relative filling volume ($V_L/V_F$) and the fluid volume per tray for the three different cases in dependance of the flask volume ($V_F$).**

The reference point of the 250 mL shake flask can clearly be seen as the intersection of the curves of the different cases. Below this flask volume, the relative filling volume increases for constant $k_La$ and $OTR_{max,plug}$ conditions, up to 6.6 and 6.9 %, respectively. With increasing flask volume, the relative filling volume decreases significantly to values of 1.8 and 1.3 %, showing a 73 and 81 % reduction for constant $k_La$ and $OTR_{max,plug}$ conditions, respectively. Due to the different base areas, a different number of flasks can be placed on the tray for each flask size (compare Appendix 9). This leads to the almost constant total fluid volume per tray for constant $k_La$ and $OTR_{max,plug}$ conditions, independent of the flask size. Using a constant relative filling volume, however, the total fluid volume per tray increases from 200 to 1000 mL. Using large flask sizes to produce more inoculation biomass for stirred tank reactors compared to small flasks is, therefore, only possible with a constant relative filling volume.

Once the parameters ($d_0$, n, and $V_L$) were determined for each flask size, the phase number (Ph) could be calculated for the three different cases to verify that the chosen assumptions ($d_0/d$ and $Fr_a$ constant) result in sound shaking parameters (Figure 4.2).

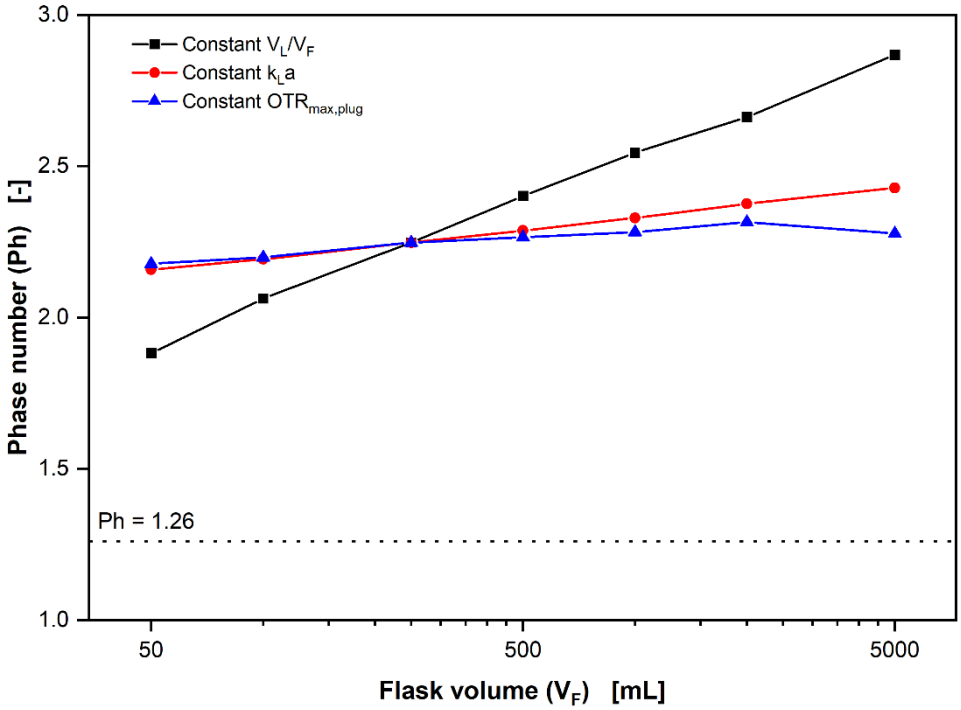


**Figure 4.2: Phase numbers for the three different cases in dependance of the flask volume ($V_F$).**

Calculations are based on Equation 4.12. The black dotted line indicates the critical phase number of 1.26.

While the phase number in small flasks is lowest with a constant relative filling volume, this case shows a higher increase with increasing flask volume compared to the other two cases. This is not surprising, as this difference is due to the filling volume and the shaking frequency (viscosity and $d_0/d$ are constant). While the shaking frequency more than halves from small- to large-scale flasks (constant $Fr_a$), the filling volume spans up to two orders of magnitude, depending on the observed case (Table 4.1), and, therefore, shows the bigger influence on the phase number. Nevertheless, all calculated phase numbers are higher than the critical phase number of 0.91 by Azizan et al. (2019) [6] and even the more conservative 1.26 by Büchs et al. (2000) [18]. Note that $Fr_a$ is = 1.712 and, therefore, bigger than the necessary 0.4 for all conditions. This suggests that the chosen parameter sets for the three different cases are suitable, and further analysis is possible.

### *4.3.2 Volume specific power input and energy dissipation rate*

The power consumption strongly influences culture performance and is considered to be crucial for the characterization of biological cultures [17].

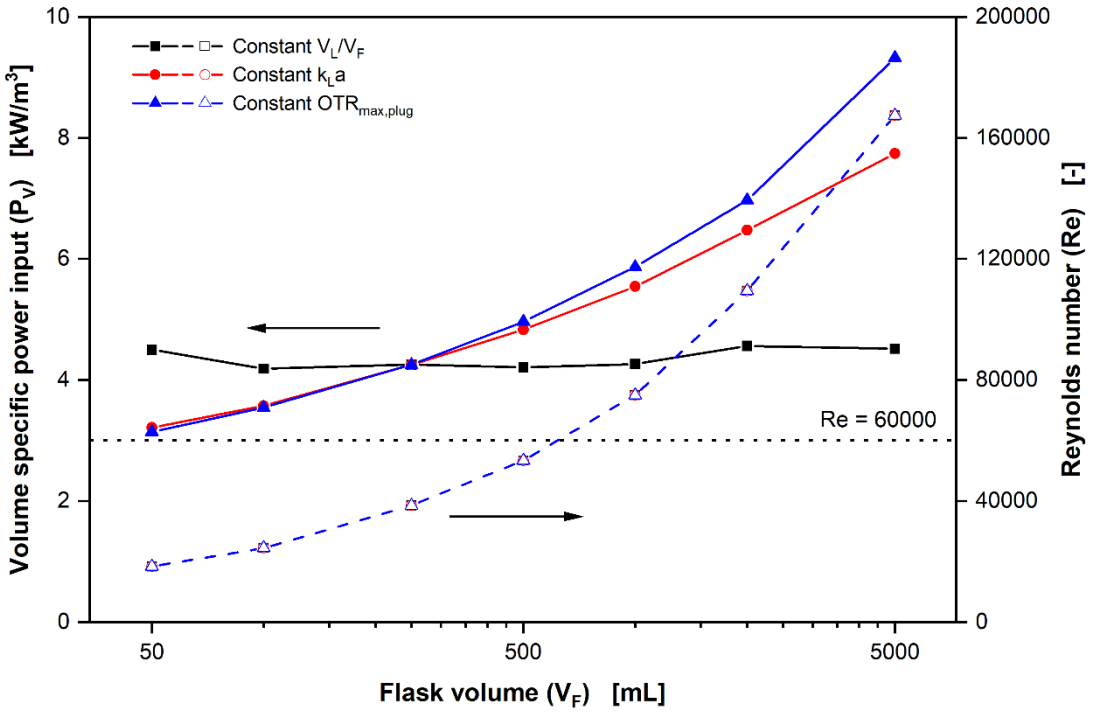


**Figure 4.3: Volume specific power input ($P_V$) and Reynolds number (Re) for the three different cases in dependance of the flask volume ($V_F$).**

Calculations are based on Equations 4.14 and 4.16. The black dotted line indicates a critical Reynolds number of 60,000.

Figure 4.3 shows the volume specific power input ($P_V$) of the three different cases in dependance of the flask volume (Equation 4.16). Surprisingly, $P_V$ stays almost constant at 4.2 – 4.5 kW/m$^3$ over all flask volumes, with a constant relative filling volume. In comparison, $P_V$ increases from 3.2 and 3.1 to 7.7 and 9.3 kW/m$^3$ with constant $k_La$ and $OTR_{max,plug}$ conditions, respectively. This describes a 2.4- and 3-fold increase in volume specific power input. Independent of the observed case, the Reynolds number behaves similarly over the different flask sizes. The liquid in flask volumes over 500 mL exceeds the critical Reynolds number of 60000 and is, therefore, in turbulent flow while in a transitional range for smaller flasks [120]. Thus, the hydromechanical stress qualitatively changes between the flask sizes due to a change in flow regime.

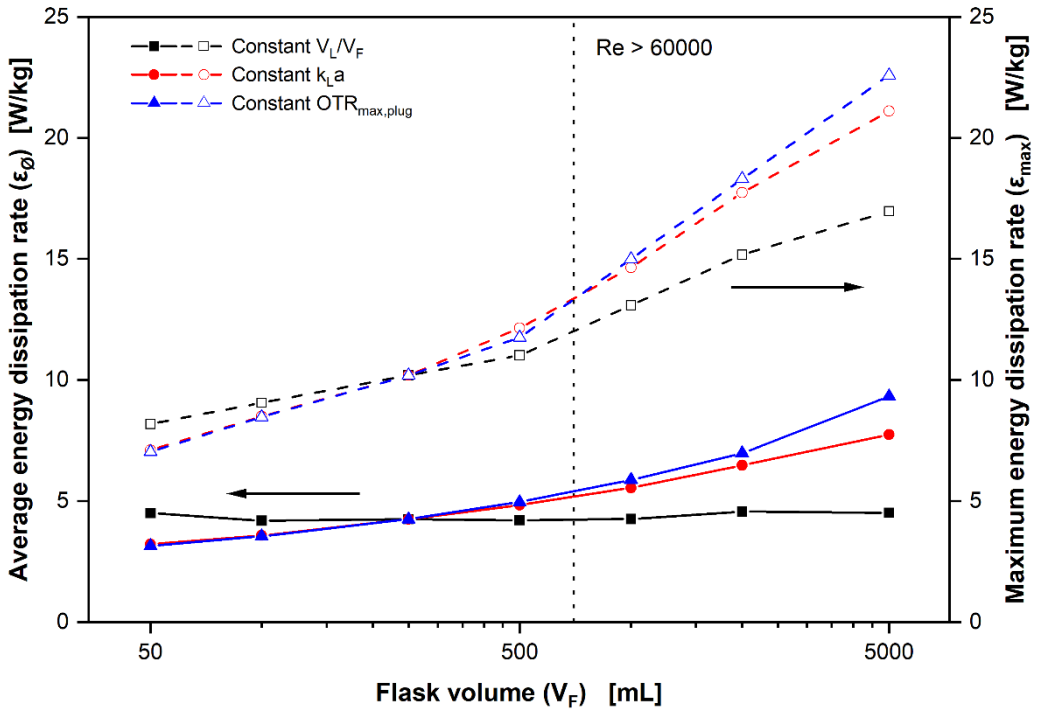


**Figure 4.4: Average ($\varepsilon_Ø$) and maximum energy dissipation rate ($\varepsilon_{max}$) for the three different cases in dependance of the flask volume ($V_F$).**

Calculations are based on Equations 4.18 and 4.19. The black dotted line indicates exceeding the critical Reynolds number ($Re_{crit}$) of 60000 and, therefore, a shift in energy dissipation [120].

Figure 4.4 shows the average energy dissipation rate $\varepsilon_Ø$ and maximum energy dissipation rate $\varepsilon_{max}$ for the different cases. The average energy dissipation rate behaves comparable to the volumetric power input. It stays almost constant over all flask sizes for the constant relative filling volume, while it starts lower and increases for the other two cases. However, the maximum energy dissipation rate behaves differently. Here, an almost linear increase from 7.0 and 8.2 to ~12.0 and 11.0 W/kg for 50 mL flasks up to 500 mL flasks is visible for the constant $k_La$ and $OTR_{max,plug}$ conditions and a constant relative filling volume, respectively. With flasks bigger than 500 mL, the slope of the curve increases compared to smaller flask sizes for all three cases. Even though the correlation for $\varepsilon_{max}$ is only valid for Re > 60000 [120], the change in the slopes before and after reaching this critical value underlines the qualitative change in energy dissipation. For 5000 mL flasks, maximum energy dissipation rates of 17.0, 21.1, and 22.6 $m^2/s^3$ are calculated for constant $k_La$, $OTR_{max,plug}$, and relative filling volume, respectively. It has previously been shown that the maximum energy dissipation rate in shake flasks is about tenfold lower compared to stirred tank reactors at the same volume specific power input [120]. Nevertheless, the maximum

energy dissipation rate increases with flask size, especially with lower relative filling volumes (compare Figure 4.1). Therefore, if large flasks are used, higher filling volumes are necessary for bioprocesses in which high energy dissipation is unfavorable [93, 129]. However, it must be kept in mind that this might drastically decrease the maximum oxygen transfer rate.

### *4.3.3 Maximum oxygen transfer capacity ($OTR_{max,plug}$) and oxygen availability*

The $OTR_{max}$ is a crucial parameter not only for microbial cultivations but also for cell-free reactions. The resistance of the cotton plug, used for sterility for most shaken flasks, needs to be considered, as it changes with the size of the flask, thus changing the mass transfer resistance of the plug. The resulting $OTR_{max,plug}$, in addition to the fraction of oxygen inside the flask, is shown in Figure 4.5.

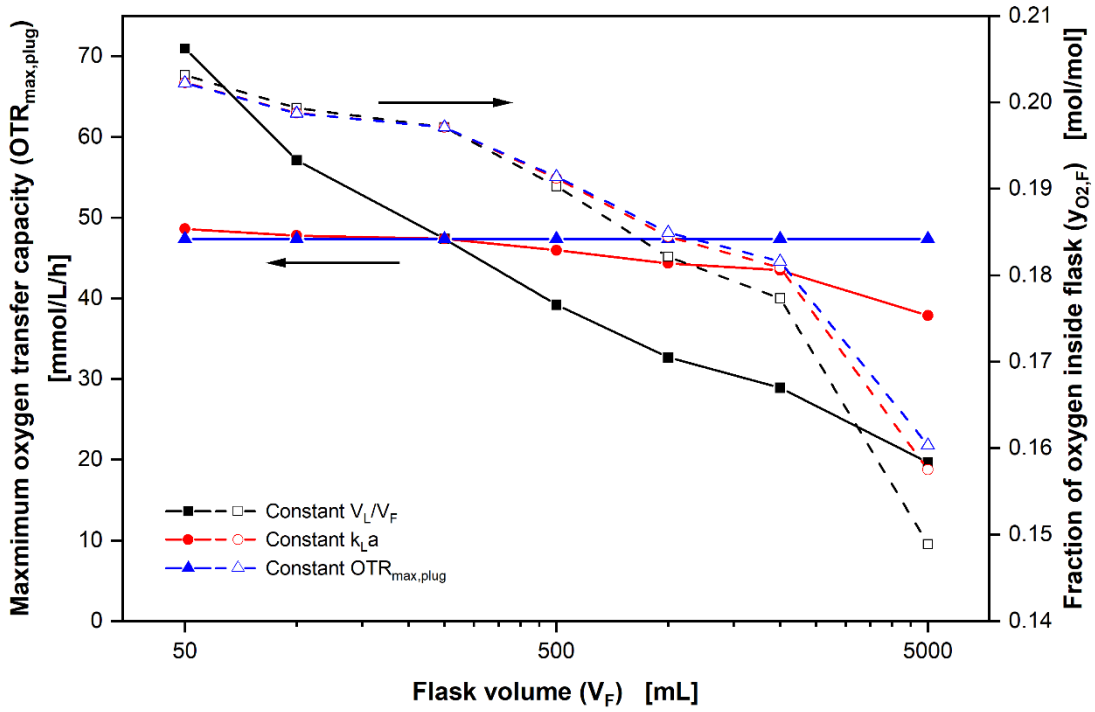


**Figure 4.5: Maximum oxygen transfer capacity ($OTR_{max,plug}$) and the fraction of oxygen inside the flask ($y_{O2,F}$) for the three different cases in dependance of the flask volume ($V_F$).**
Calculations are based on Equations 4.8 and 4.9.

As stipulated, the $OTR_{max,plug}$ stays constant in the case of a constant $OTR_{max,plug}$. With a constant relative filling volume, the $OTR_{max,plug}$ decreases from 70.9 mmol/L/h in 50 mL flasks to 19.7 mmol/L/h in 5000 mL flasks, which corresponds to a reduction of 72 %. With constant $k_La$ conditions, the decrease is not as pronounced, from 48.6 to 37.9 mmol/L/h

(decrease of 22 %) for 50 to 5000 ml flasks, respectively. Especially for fast-growing organisms that reach high oxygen transfer rates (OTR), the $OTR_{max,plug}$ is of key importance [54]. Oxygen limitation can not only impede the growth of the organism but also change the entire cultivation process, leading, for example, to overflow metabolism and reduced product concentrations [53, 96, 103]. However, the low $OTR_{max,plug}$ reached with constant relative filling volumes and large flask sizes could be used for organisms that only need a limited amount of oxygen, like CHO cells [66, 67].

The oxygen fraction inside the flask decreases from ~0.20 mol/mol in 50 mL flask for all three cases to 0.160, 0.158, and 0.149 mol/mol for constant $OTR_{max,plug}$, $k_La$, and relative filling volume, respectively. This reduces the driving force of the mass transfer into the liquid, which must be compensated by lowering the filling volume (compare Chapter 4.2.1). Interestingly, the oxygen fraction inside the flask for large flasks is also low with a constant $OTR_{max,plug}$. To achieve the same oxygen mol fraction inside the 5000 mL as in the 250 mL flask – with a constant neck height to diameter ratio – the neck height and diameter of the large flask need to be increased to 354.1 and 267.0 mm, respectively. As this would mean that the neck of the flask is bigger than the flask itself (Appendix 9), the low oxygen mol fraction in the headspace of the flask is an inherent challenge of the large flasks and, thus, limits its application to cultivations with low oxygen consumption. According to the decrease in $O_2$, $CO_2$ must accumulate inside the flasks. This might even be beneficial to some microbial processes as a higher dissolved $CO_2$ has been shown to be beneficial in some cases due to anapleurotic reactions [10]. On the other hand, high concentration of $CO_2$ is used for the prevention of food spoilage and could be detrimental to the cultivation [27, 32]. However, the determined oxygen concentrations inside the flasks are rather low and need to be verified experimentally, as the calculations are based on correlations that are extended beyond their validity range.

### *4.3.4 Overall heat transfer and temperature change inside liquid volume*

Heat is produced inside the liquid volume of the flask through power input by the shaking motion, in addition to the microbial activity. Therefore, the heat transfer out of the flask is an important aspect of the experimental design using different shake flask sizes. To the best of our knowledge, there is only one publication concerning heat transfer in shake flasks by Sumino and Akiyama (1987) [138], providing an empirical correlation estimation of the heat transfer coefficient (UA) (Equation 4.20) [138]. Additionally, Dinger et al. (2023) [34] have experimentally determined the heat transfer coefficient to be at ~0.39 W/K in shake

flasks, which is in the same range as values from Sumino and Akiyama (1987) [138]. However, all experiments in both studies were performed in 200 or 250 mL shake flasks, reducing the validity range of these results. Alternatively, a shake flask can be described as a rotating cylinder with lateral airflow. The determination of the overall heat transfer coefficient (U) in this model has been described by Jeng et al. (2014) [68]. In addition, the heat transfer coefficient is compared to a correlation for large, orbitally shaken cylindrical vessels described by Raval et al. (2014) [125].

Figure 4.6 shows the overall heat transfer and the heat transfer coefficients (U and UA) calculated with the different correlations. Note that the heat transfer area (A) is already included in UA. An overview of A is given for each flask size and the three different conditions in Appendix 10. In addition, it needs to be mentioned that Jeng et al. (2014) [68] describe the calculation of the overall heat transfer coefficient (U), while the other correlations determine the heat transfer coefficient (UA), already including the heat transfer area. Multiplying by A thus results in UA in the case of Jeng et al. (2014) [68]. For the other correlations, the heat transfer coefficient must be divided by the heat transfer area to get the overall heat transfer coefficient.

All determined heat transfer coefficients increase with the flask size (Figure 4.6A). However, the absolute values differ quite strongly between the different correlations. While the correlation by Sumino and Akiyama (1987) [138] (shake flasks) results in UA between 0.11 and 0.27 W/K, values from 0.65 to 2.00 W/K are reached for 50 and 5000 mL flasks with the correlation from Raval et al. (2014) [125] (large, cylindrical vessels). Using the cylinder as a model (Jeng et al. (2014) [68]), UA values show the biggest difference between the different flask sizes from 0.16 to 2.3 W/K in 50 and 5000 mL flasks, respectively. With all correlations, a constant filling volume shows the lowest UA in small and the highest in big flasks, compared to the other two cases (Figure 4.6, black curves). This is not surprising, as the heat transfer area (A) gets smaller with lower filling volumes (Table 4.1 and Appendix 10), thus reducing UA. Interestingly, the curve for the cylindrical model (Jeng et al. (2014) [68]) intersects the constant UA determined by Dinger et al. at ~250 mL flask volume. As this constant value was determined for 250 mL shake flasks with a filling volume of 20 mL, this hints at the validity of the model system. However, it needs to be kept in mind that different shaking diameters were used by Dinger et al. (2023) [34] ($d_0$ = 50 mm) and in this study ($d_0$ = 25 mm).

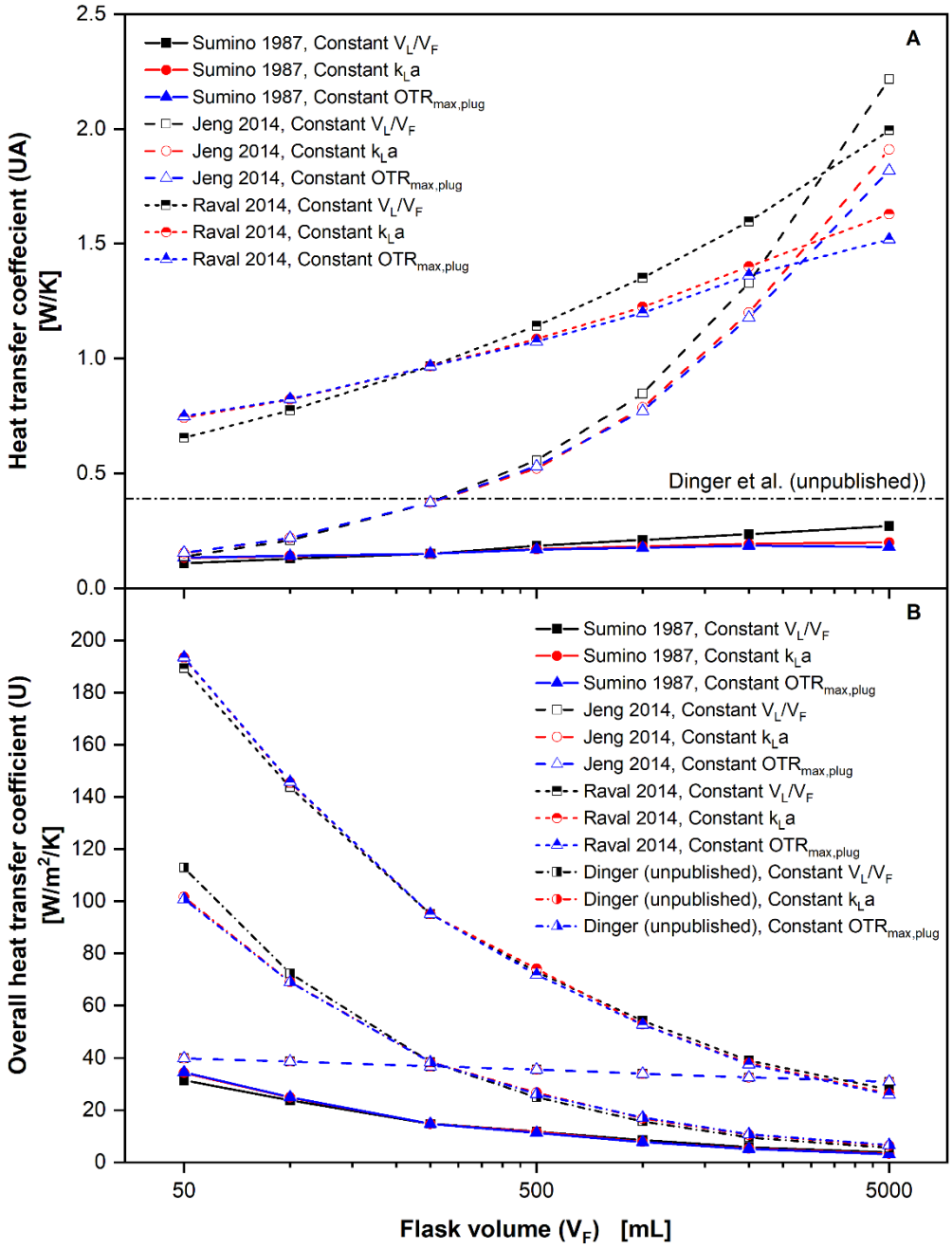


**Figure 4.6: Comparison of the overall heat transfer coefficient (UA) [A] and the heat transfer coefficient (U) [B] calculated after Sumino and Akiyama, Jeng et al., Raval et al. and Dinger et al. for the three different cases in dependance of the flask volume ($V_F$).**

Calculations are based on Equations 4.20 and 4.21. To determine U, UA was divided by the heat transfer area (A) (Equation 4.31) for all correlations, except Jeng et al. (2014) [68]. For this model, U was determined according to Equation 4.31. UA was then calculated by multiplying U with the heat transfer area (A) (Equation 4.34). The horizontal, black dotted-dashed line in [A] indicates the UA value of 0.368, determined by Dinger et al. (2023) [34].

The overall heat transfer coefficient decreases in all calculated cases (Figure 4.6B), mirroring the results from UA. There is also a difference between the different cases for each correlation, except for the cylindrical model (Jeng et al. (2014) [68]). This is

surprising, as the overall heat transfer coefficient should stay constant between the cases because the gas side heat transfer coefficient should have the biggest influence on U, as has previously been shown [72, 125]. The validity of the assumption is further explained in Appendix 11. Because only the filling volume (e.g. heat transfer area) changes between the cases – which is not included in U – the overall heat transfer coefficient should be constant between the cases. This can only be seen in the cylindrical model. However, the assumption of a constant overall heat transfer over all flask volumes might not hold true as the ratio of the heat transfer area that is covered by clamps, fixing the flask on the shaking tray, to the 'un-clamped' area changes. This might change the overall heat transfer coefficient between the flask sizes. As a measure of this, the maximal height of the liquid volume relative to the overall flask height was determined (Appendix 10). In addition, it was assumed that a constant relative height results in a constant ratio between the 'clamped' and 'un-clamped' heat transfer area. While the relative liquid height decreased from ~25 to 18.6 and 17.4 % with a constant $k_La$ and $OTR_{max,plug}$, respectively, it showed no specific trend and stayed at 22.4 ± 0.6 % for the constant relative filling volume. Therefore, no difference due to different heat transfer areas would be expected for this latter case. The difference between the cases, thus, might be a mathematical relict because UA is correlated instead of U, leading to a determination of the overall heat transfer coefficient from this value.

As the gas side heat transfer coefficient mostly determines U (Appendix 11), the movement of the flask through the shaker has the biggest influence on the overall heat transfer coefficient. This value depends on the shaking frequency (n) and shaking diameter ($d_0$) of the flask and does not change between the three observed cases. With increasing flask size, the velocity of the flask increases accordingly from 0.36 to 0.75 m/s for 50 – 5000 mL flasks. At the same time, the Reynolds number of the surrounding air reached tenfold higher values for the largest flasks compared to the smallest (10,000 vs. 1,000). The latter suggests a qualitative change of the gas side heat transfer coefficient from small to large flask sizes due to the change in flow regime, thus increasing U. However, the calculated overall heat transfer values for none of the correlations show an increase with increasing flask sizes. Nonetheless, it needs to be kept in mind that the actual difference between small and large flasks, based on the change in Re, is not researched and could potentially be quite small.

With the heat transfer coefficients and the overall power input, the temperature difference between the liquid inside the flask and the shaker can be calculated. The overall power input is the sum of the power input through the shaking motion of the flask and the

biological heat generation (Equation 4.36). Interestingly, the biological heat generation outweighs the power input through shaking in all three cases in small flasks (compare Chapter 4.3.2 and Table 4.2). This changes, however, with increasing flask size. With a constant relative filling volume, 1000 mL flasks have about the same power input through shaking motion as biological heat. The same is true for the constant $k_La$ case, while the 2000 mL flasks show the same behavior for the last case. This is unsurprising, as the microbial heat is a function of the filling volume and the $OTR_{max,plug}$.

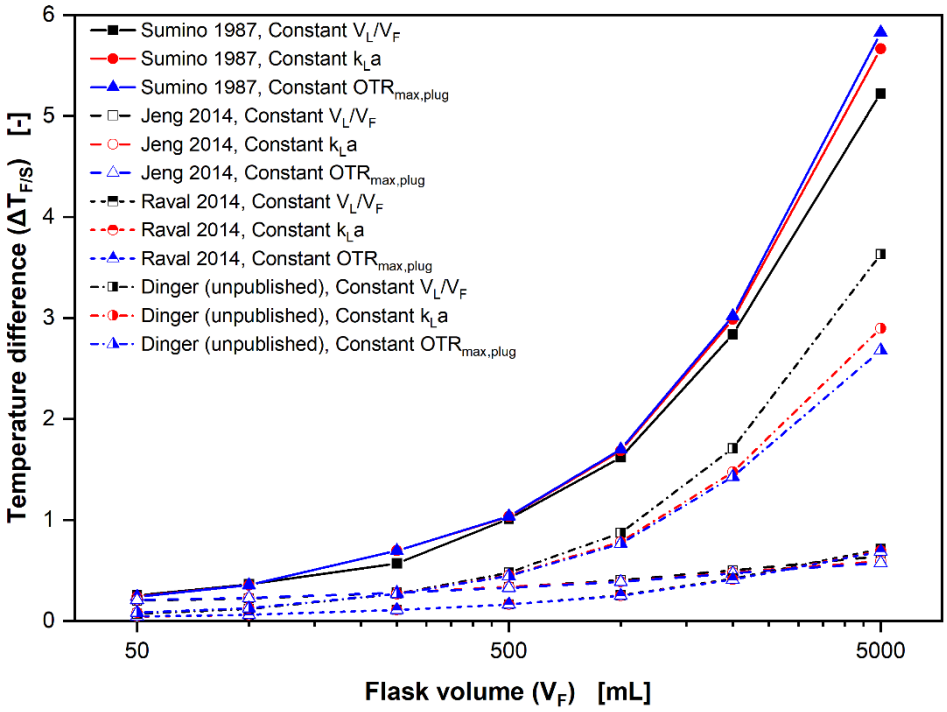


**Figure 4.7: Temperature difference between flask and surrounding air ($\Delta T_{F/S}$) calculated with UA after Sumino and Akiyama, Jeng et al., Raval et al. and Dinger et al. for the three different cases in dependance of the flask volume ($V_F$).**

Calculations are based on Equations 4.37. UA values can be found in Figure 4.6. and values for $P_{total}$ in Table 4.2.

The results for the temperature differences with the different UA correlations are shown for each of the three cases in Figure 4.7. For all correlations, $\Delta T_{F/S}$ increases with increasing flask size. While the direction of the curves is the same between the different correlations, the absolute values differ quite a lot. Using the calculations according to Sumino and Akiyama (1987) [138], small temperature differences of 0.25 K are expected in small-scale flasks. However, with increasing flask size, the difference increases exponentially up to 5.8 K in 5000 mL flasks. Using the constant UA of Dinger et al. (2023) [34], lower

temperatures in small scale (0.07 K) and large scale (3.63 K) are reached. For the last two correlations, the spread between the different flask sizes is much lower. While the temperature difference ranges between 0.04 K in small flasks and 0.71 K in large flasks with the correlation for large orbitally shaken bioreactors [125], it only ranges between 0.19 and 0.61 K with the cylinder model [68].

With a constant UA (Dinger et al. (2023) [34]), this is solely dependent on the increase in overall power input. It can be seen that this leads to higher temperature differences in the case with the highest filling volumes at each flask size (compare Figure 4.1). This can partly be attributed to the fact that the only difference between the cases is the filling volume. Therefore, it greatly influences the power input through the shaking motion. In addition, the filling volume is coupled to the calculated OTR values and, thus, directly affects the microbial heat production. However, once UA is not constant, the temperature difference in each flask size is no longer influenced by the filling volume only.

All correlations used to assess the heat transfer in shake flasks are extended beyond their validity range and, therefore, likely none of them are correct. However, all correlations, except the constant UA, include the lateral airflow towards the flask or the velocity of the flask itself. As the gas side heat transfer is the limiting step, this is necessary to ensure a base line of validity. For 250 mL flasks, it has been shown that UA is about 10-fold lower compared to large orbitally shaken bioreactors [34, 125, 138]. However, this 10-fold decrease is well described by Equation 4.21 (Raval et al. (2014) [125]) with the parameters for small shake flasks. The correlation of Sumino and Akiyama (1987) [138] uses the weight of the flask as an approximation for the wall thickness. However, the heat transfer effect through the flask wall is likely not limiting (Appendix 11), thus restricting the validity of this correlation for large flasks. The cylindrical model (Jeng et al. (2014) [68]) might be a good estimator for the actual heat transfer, as it fits well with the correlation by Sumino and Akiyama (1987) [138] for small and with the correlation by Raval et al. (2014) [125] in large flasks.

In all, independent of the used correlation and case, the temperature difference between liquid volume and shaker increases with increasing flask size. Depending on the model, the temperature change might be almost negligible in small flasks, while it is not in large flasks, independent of the model. The higher temperature might lead to changes in the microbials' metabolism, resulting in subpar growth and production or even cell death [130]. For the

different cases, no clear trend is visible. However, a constant relative filling volume likely leads to slightly higher temperature differences in large flasks (compare Jeng et al. (2014) [68], Figure 4.7).

## 4.4 Conclusion

In this chapter, a systematic analysis of the commercially available narrow neck shake flasks with nominal volumes of 50 – 5000 ml was performed. First, the shaking diameter and frequency were determined for all flask sizes, with a conical 250 mL flask as a reference ($d_0$ = 25 mm, n = 350 rpm). This was followed by calculating the filling volumes based on the three different cases. As all the resulting parameter combinations resulted in 'in-phase' conditions, further analysis was possible.

In general, the volume specific power input and the maximum energy dissipation rate decreased with the filling volume for each flask size, as is visible between the different cases. However, with flask sizes bigger than 500 mL, the maximum energy dissipation rate increases dramatically due to the change in flow behavior (keep in mind that $\varepsilon_{max} = \varepsilon_{Ø}$ for Re < 60,000). At the same time, the maximum oxygen transfer rate regarding the sterile barrier behaves similarly to the volume specific power input.

Independent of the observed model, the temperature difference between liquid and surrounding air increases with increasing flask sizes. While the difference might not lead to a significant change in the microbials' behavior in small flasks, this likely changes in flasks bigger than 1000 mL. However, all models used in this study are extended far beyond their validity range. In the future, a study regarding the heat transfer in different flask sizes might give better insights into whether temperature differences between the liquid and the surrounding air are to be expected.

This chapter shows the importance of engineering parameters for the successful use of shake flasks. While the volume specific power input, energy dissipation, and $OTR_{max}$ are well described in flasks, the heat transfer is not. More experimental data is necessary to determine a correlation that is valid for all observed flask sizes. In addition, this chapter highlights that no general recommendation for a specific parameter set can be made, which is valid for all cultivations. It rather shows that the parameters change depending on the microorganism's prerequisites. For example, a high relative filling volume in all flask sizes

is counterproductive for organisms that need high $OTR_{max,plug}$. On the other hand, it might be good for low-breathing strains that are shear-sensitive, like CHO cells.

# Chapter 5

## 5. Summary and Outlook

The first goal of this thesis was the development of a cost-efficient production process for itaconic acid from industrial side and waste streams using *Ustilago sp.* as production hosts.

Using the oxygen transfer rate as the main criterion, a fast and efficient strain characterization and process development was possible in small-scale, shaken cultivation systems. Out of five strains, *U. cynodontis* ITA Max pH was established as the most promising production host because of its low oxygen demand per biomass and low susceptibility to acidic pH values. Growth and production of the strain were then determined for a number of different side and waste streams from the local food industry as substrate. Thick juice and beet molasses, both originating in the sugar manufacturing process, were demonstrated to be the most suitable feedstocks for itaconic acid production. Due to the necessary nitrogen limitation, the nitrogen content of the feedstock is of key importance. Therefore, a simple method based on online monitoring of the OTR was developed to determine the biologically available nitrogen in any (complex) feedstock. Thick juice was then chosen as substrate for the scale-up because of its lower nitrogen content and higher C/N ratio. The effects of complex substrate characteristics, like osmolality, pH, and product inhibition, were then demonstrated in shake flasks. Here, the pH showed the greatest impact on itaconic acid production, followed by the osmolality and then the itaconic acid itself.

Following early-stage process development in MTP and shake flasks, the production process was scaled up to 2 L stirred tank reactors. After demonstrating the use of thick juice as sole carbon source in an STR cultivation, the process was further optimized. As thick juice introduces nitrogen into the fermentation medium, the initially added ammonium was

decreased. In addition, a holistic approach showed that low pH during the fermentation is necessary for cost-efficient ITA production because of the following downstream processing [132]. Therefore, a natural pH shift was introduced after the growth phase. Even though the titer was lower with this shift, the yield stayed constant compared to the fermentation at a constant, high pH. The maximum product concentration of ~80 $g_{ITA}/L$ was not reached, so higher yields are expected in future experiments. For these, online analytics of the substrates and products should be implemented to allow for better feeding control. In addition to a low pH, the choice of the pH-adjusting agent used during the fermentation greatly impacts the DSP [132]. This study demonstrated that the use of $Mg(OH)_2$ instead of NaOH is feasible. However, the salt has low solubility in water at high pH values and must be fed as a suspension. This presents challenges, especially regarding the blocking of tubing and pipes, which makes specialized equipment necessary for large-scale production. Finally, a scale-up to a 150 L STR was demonstrated. With a maximum yield of $0.66 \pm 0.03$ $g_{ITA}/g_{glucose,eq.}$ and product as well as STY normalized to CDW around twice as high as in small scale, the fermentation showcased the feasibility of the scale-up of an ITA fermentation with thick juice as the sole carbon source.

Inherent process challenges were demonstrated in this study, which need to be addressed in future research. *In-situ* product removal shows great potential, as it reduces the ITA concentration and the osmolality, thus allowing for an increased yield and STY [98]. In addition, the fermentation medium will be further optimized by reducing the initially added components, as some of them might be contained in large excess and are added through the alternative feedstock. For this purpose, the newly developed method for determination of the biologically available nitrogen content will be adapted. Lastly, online analytics of the substrates and products will be implemented to allow for better process control, especially regarding the feed.

The second aim of the study was the procedural analysis of the commercially available shake flasks from 50 – 5000 mL. First, comparable parameter sets for all flask sizes were determined using a conical 250 mL flask as a reference ($d_0$ = 25 mm, n = 350 rpm, $V_L$ = 10 mL). All of these parameter combinations resulted in ‘in-phase’ conditions, allowing for further analysis. The influence of flask size and different filling volumes on volume specific power input, energy dissipation rate, and maximum oxygen transfer capacity has been demonstrated. While all of these parameters are well described in literature, the heat transfer is not. Depending on the used model, temperature differences

up to 5.9 K were determined. However, all models used to determine the heat transfer in this study are extended well beyond their validity range. To reliably determine whether overheating of a culture is possible with a given parameter set, experimental research is needed to establish a new model.

In conclusion, this study demonstrates the use of alternative, complex feedstocks, and waste products from the local food industry for the production of ITA with Ustilaginaceae, without drawbacks in either titer or yield, compared to glucose fermentations. By combining the knowledge gained from the shaken bioreactor screening and the optimization and scale-up studies in stirred tank reactors, an efficient and robust ITA production process suitable for industrial implementation was established. The main goal is to contribute to the sustainable production of this valuable compound, facilitating its application in various industries, from bio-based chemicals to biodegradable polymers and beyond. In addition, this study shows the importance of engineering parameters for the successful use of shake flasks. It highlights that no general recommendation for a specific parameter set can be made, which is valid for all cultivations. These are rather depending on the microorganism’s prerequisites and change for each process.

# 6. Bibliography


[1] Aguilar, L. R., Pardo, J. P., Lomeli, M. M., Bocardo, O. I. L., Oropeza, M. A. J., and Sanchez, G. G., "Lipid droplets accumulation and other biochemical changes induced in the fungal pathogen *Ustilago maydis* under nitrogen-starvation", *Archives of Microbiology,* Article vol. 199, no. 8, pp. 1195-1209, Oct 2017.

[2] Ahmad, A., Banat, F., and Taher, H., "A review on the lactic acid fermentation from low-cost renewable materials: Recent developments and challenges", *Environmental Technology & Innovation,* Review vol. 20, pinc. 21, Nov 2020, Art. no. 101138.

[3] Akerberg, C. and Zacchi, G., "An economic evaluation of the fermentative production of lactic acid from wheat flour", *Bioresource Technology,* Article vol. 75, no. 2, pp. 119-126, Nov 2000.

[4] Anderlei, T. and Büchs, J., "Device for sterile online measurement of the oxygen transfer rate in shaking flasks", *Biochemical Engineering Journal,* Article; Proceedings Paper vol. 7, no. 2, pp. 157-162, Mar 2001.

[5] Anderlei, T., Zang, W., Papaspyrou, M., and Büchs, J., "Online respiration activity measurement (OTR, CTR, RQ) in shake flasks", *Biochemical Engineering Journal,* vol. 17, no. 3, pp. 187-194, 2004.

[6] Azizan, A., Sieben, M., Wandrey, G., and Buchs, J., "Reassessing the out-of-phase phenomenon in shake flasks by evaluating the angle-dependent liquid distribution relative to the direction of the centrifugal acceleration", *Biotechnol Bioeng,* vol. 116, no. 11, pp. 2983-2995, Nov 2019.

[7] Bambouskova, M. *et al.*, "Electrophilic properties of itaconate and derivatives regulate the IκBζ–ATF3 inflammatory axis", *Nature,* vol. 556, no. 7702, pp. 501-504, 2018.

[8] Battling, S. *et al.*, "Development of a novel defined minimal medium for Gluconobacter oxydans 621H by systematic investigation of metabolic demands", *Journal of Biological Engineering,* Article vol. 16, no. 1, pinc. 18, Nov 2022, Art. no. 31.

[9] Bauer, F., Coenen, L., Hansen, T., McCormick, K., and Palgan, Y. V., "Technological innovation systems for biorefineries: a review of the literature", *Biofuels Bioproducts & Biorefining-Biofpr,* Review vol. 11, no. 3, pp. 534-548, May-Jun 2017.

[10] Bäumchen, C. *et al.*, "Effect of elevated dissolved carbon dioxide concentrations on growth of *Corynebacterium glutamicum* on D-glucose and L-lactate", *Journal of Biotechnology,* Article vol. 128, no. 4, pp. 868-874, Mar 2007.

[11] Becker, J., Hosseinpour Tehrani, H., Gauert, M., Mampel, J., Blank, L. M., and Wierckx, N., "An *Ustilago maydis* chassis for itaconic acid production without by-products", *Microb Biotechnol,* vol. 13, no. 2, pp. 350-362, Mar 2019.

[12] Becker, J., Hosseinpour Tehrani, H., Ernst, P., Blank, L. M., and Wierckx, N., "An Optimized *Ustilago maydis* for Itaconic Acid Production at Maximal Theoretical Yield", *Journal of Fungi,* vol. 7, no. 1, pinc. 20, 2021.

[13] Behera, B. C., "Citric acid from *Aspergillus niger*: a comprehensive overview", *Critical Reviews in Microbiology,* Review vol. 46, no. 6, pp. 727-749, Nov 2020.

[14] Bento, L. S. M., "Application of ion exchange resins for sugar liquors decolourisation", in *Proceedings of the XXIII ISSCT Congress, New Delhi, India, 22-26 February, 1999. Volume 1*, 1999, pp. 68-75: Sugar Technologists' Association of India.

[15] Bera, R., Dey, A., and Chakrabarty, D., "Synthesis, Characterization, and Drug Release Study of Acrylamide-CoD-Itaconic Acid Based Smart Hydrogel", *Polymer Engineering and Science,* Article vol. 55, no. 1, pp. 113-122, Jan 2015.

[16] Bohm, L., Hohl, L., Bliatsiou, C., and Kraume, M., "Multiphase Stirred Tank Bioreactors - New Geometrical Concepts and Scale-up Approaches", *Chemie Ingenieur Technik,* Review vol. 91, no. 12, pp. 1724-1746, Dec 2019.

[17] Büchs, J., Maier, U., Milbradt, C., and Zoels, B., "Power consumption in shaking flasks on rotary shaking machines: I. Power consumption measurement in unbaffled flasks at low liquid viscosity", *Biotechnology and Bioengineering,* Article vol. 68, no. 6, pp. 589-593, Jun 2000.

[18] Büchs, J., Maier, U., Milbradt, C., and Zoels, B., "Power Consumption in Shaking Flasks on Rotary Shaking Machines: II. Nondimensional Description of Specific Power Consumption and Flow Regimes in Unbaffled Flasks at Elevated Liquid Viscosity", *Biotechnology and Bioengineering,* vol. 68, no. 6, pp. 594-601, 2000.

[19] Büchs, J., "Introduction to advantages and problems of shaken cultures", *Biochemical Engineering Journal,* Article; Proceedings Paper vol. 7, no. 2, pp. 91-98, Mar 2001.

[20] Büchs, J., Maier, U., Lotter, S., and Peter, C. P., "Calculating liquid distribution in shake flasks on rotary shakers at waterlike viscosities", *Biochemical Engineering Journal,* Article vol. 34, no. 3, pp. 200-208, Jun 2007.

[21] Büchs, J. Z., B., "Evaluation of Maximum to Specific Power Consumption Ratio in Shaking Bioreactors", *Journal of Chemical Engineering of Japan,* vol. 34, no. 5, pp. 647-653, 2001.

[22] Chu, L. and Robinson, D. K., "Industrial choices for protein production by large-scale cell culture", *Current Opinion in Biotechnology,* Review vol. 12, no. 2, pp. 180-187, Apr 2001.

[23] Clark, M. W. and Vermeulen, T., "Incipient Vortex Formation in Baffled Agitated Vessels", *Aiche Journal,* Letter vol. 10, no. 3, pp. 420-422, 1964.

[24] Coca, M., Garcia, M. T., Mato, S., Carton, A., and Gonzalez, G., "Evolution of colorants in sugarbeet juices during decolorization using styrenic resins", *Journal of Food Engineering,* Article vol. 89, no. 4, pp. 429-434, Dec 2008.

[25] Cooney, C. L., Wang, D. I. C., and Mateles, R. I., "Measurement of Heat Evolution and Correlation With Oxygen Consumption During Microbial Growth", *Biotechnology and Bioengineering,* Article vol. 11, no. 3, pp. 269-&, 1969.

[26] Cordes, T., Michelucci, A., and Hiller, K., "Itaconic Acid: The Surprising Role of an Industrial Compound as a Mammalian Antimicrobial Metabolite," in *Annual Review of Nutrition, Vol 35*, vol. 35, Bowman, B. A. and Stover, P. J., Eds. (Annual Review of Nutrition, Palo Alto: Annual Reviews, 2015, pp. 451-473.

[27] Couvert, O., Koullen, L., Lochardet, A., Huchet, V., Thevenot, J., and Le Marc, Y., "Effects of carbon dioxide and oxygen on the growth rate of various food spoilage bacteria", *Food Microbiology,* Article vol. 114, pinc. 7, Sep 2023, Art. no. 104289.

[28] de Witt, J., Ernst, P., Gategens, J., Noack, S., Hiller, D., Wynands, B., and Wierckx, N., "Characterization and engineering of branched short-chain dicarboxylate metabolism in Pseudomonas reveals resistance to fungal 2-hydroxyparaconate", *Metabolic Engineering,* Article vol. 75, pp. 205-216, Jan 2023.

[29] Demir, H. T., Bezirci, E., Becker, J., Tehrani, H. H., Nikerel, E., Wierck, N., and Turker, M., "High level production of itaconic acid at low pH by *Ustilago maydis* with fed-batch fermentation", *Bioprocess Biosyst Eng,* vol. 44, no. 4, pp. 749-758, Apr 2021.

[30] Demmelmayer, P. and Kienberger, M., "Reactive extraction of lactic acid from sweet sorghum silage press juice", *Separation and Purification Technology,* Article vol. 282, pinc. 8, Feb 2022, Art. no. 120090.

[31] Devi, N., Singh, S., Manickam, S., Cruz-Martins, N., Kumar, V., Verma, R., and Kumar, D., "Itaconic Acid and Its Applications for Textile, Pharma and Agro-Industrial Purposes", *Sustainability,* Review vol. 14, no. 21, pinc. 24, Nov 2022, Art. no. 13777.

[32] Devlieghere, F. and Debevere, J., "Influence of dissolved carbon dioxide on the growth of spoilage bacteria", *Lebensmittel-Wissenschaft Und-Technologie-Food Science and Technology,* Article vol. 33, no. 8, pp. 531-537, 2000.

[33] Dinger, R., Lattermann, C., Flitsch, D., Fischer, J. P., Kosfeld, U., and Büchs, J., "Device for respiration activity measurement enables the determination of oxygen transfer rates of microbial cultures in shaken 96-deepwell microtiter plates", *Biotechnology and Bioengineering,* vol. 119, no. 3, pp. 881-894, 2022.

[34] Dinger, R., Lauterbach, T., Finger, M., and Büchs, J., "Miniaturized temperature sensors reveal a temperature increase in liquid media of shake flasks caused by biological and hydromechanical heat generation", *Submitted to xyz for publication,* 2023.

[35] Dragone, G., Kerssemakers, A. A. J., Driessen, J., Yamakawa, C. K., Brumano, L. P., and Mussatto, S. I., "Innovation and strategic orientations for the development of advanced biorefineries", *Bioresource Technology,* Review vol. 302, pinc. 12, Apr 2020, Art. no. 122847.

[36] Dupont-Inglis, J. and Borg, A., "Destination bioeconomy - The path towards a smarter, more sustainable future", *New Biotechnology,* Article vol. 40, pp. 140-143, Jan 2018.

[37] Echtermeyer, A., Marks, C., Mitsos, A., and Viell, J., "Inline Raman Spectroscopy and Indirect Hard Modeling for Concentration Monitoring of Dissociated Acid Species", *Applied Spectroscopy,* Article vol. 75, no. 5, pp. 506-519, May 2021.

[38] Eggert, A., Maßmann, T., Kreyenschulte, D., Becker, M., Heyman, B., Büchs, J., and Jupke, A., "Integrated in-situ product removal process concept for itaconic acid by reactive extraction, pH-shift back extraction and purification by pH-shift crystallization", *Separation and Purification Technology,* vol. 215, pp. 463-472, 2019.

[39] Esmaeili, S. A. H., Sobhani, A., Ebrahimi, S., Szmerekovsky, J., Dybing, A., and Keramati, A., "Location Allocation of Biorefineries for a Switchgrass-Based Bioethanol Supply Chain Using Energy Consumption and Emissions", *Logistics-Basel,* Article vol. 7, no. 1, pinc. 22, Mar 2023, Art. no. 5.

[40] European Commission, *A sustainable bioeconomy for Europe : strengthening the connection between economy, society and the environment : updated bioeconomy strategy*. Publications Office, 2018.

[41] Feng, J., Li, C. Q., He, H., Xu, S., Wang, X., and Chen, K. Q., "Construction of cell factory through combinatorial metabolic engineering for efficient production of itaconic acid", *Microbial Cell Factories,* Article vol. 21, no. 1, pinc. 10, Dec 2022, Art. no. 275.

[42] Flitsch, D. *et al.*, "Respiration activity monitoring system for any individual well of a 48-well microtiter plate", *J Biol Eng,* vol. 10, pinc. 14, 2016.

[43] Flitsch, D., Ladner, T., Lukacs, M., and Büchs, J., "Easy to use and reliable technique for online dissolved oxygen tension measurement in shake flasks using infrared fluorescent oxygen-sensitive nanoparticles", *Microbial Cell Factories,* Article vol. 15, pinc. 11, Feb 2016, Art. no. 45.

[44] Gao, Q., Liu, J., and Liu, L. M., "Relationship Between Morphology and Itaconic Acid Production by *Aspergillus terreus*", *Journal of Microbiology and Biotechnology,* Article vol. 24, no. 2, pp. 168-176, Feb 2014.

[45] Garcia-Ochoa, F. and Gomez, E., "Bioreactor scale-up and oxygen transfer rate in microbial processes: an overview", *Biotechnol Adv,* vol. 27, no. 2, pp. 153-76, Mar-Apr 2009.

[46] Garcia-Ochoa, F., Santos, V. E., and Gomez, E., "2.15 - Stirred Tank Bioreactors," in *Comprehensive Biotechnology (Second Edition)*, Moo-Young, M., Ed. Burlington: Academic Press, 2011, pp. 179-198.

[47] Geilen, F. M. A., Engendahl, B., Harwardt, A., Marquardt, W., Klankermayer, J., and Leitner, W., "Selective and Flexible Transformation of Biomass-Derived Platform Chemicals by a Multifunctional Catalytic System", *Angewandte Chemie-International Edition,* Article vol. 49, no. 32, pp. 5510-5514, 2010.

[48] Geiser, E., Wiebach, V., Wierckx, N., and Blank, L. M., "Prospecting the biodiversity of the fungal family Ustilaginaceae for the production of value-added chemicals", *Fungal Biology and Biotechnology,* vol. 1, no. 1, pinc. 2, 2014/11/01 2014.

[49] Geiser, E. *et al.*, "Genetic and biochemical insights into the itaconate pathway of *Ustilago maydis* enable enhanced production", *Metab Eng,* vol. 38, pp. 427-435, Nov 2016.

[50] Geiser, E., Przybilla, S. K., Friedrich, A., Buckel, W., Wierckx, N., Blank, L. M., and Bolker, M., "*Ustilago maydis* produces itaconic acid via the unusual intermediate trans-aconitate", *Microb Biotechnol,* vol. 9, no. 1, pp. 116-26, Jan 2016.

[51] Gomes, D. G., Coelho, E., Silva, R., Domingues, L., and Teixeira, J. A., "8 - Bioreactors and engineering of filamentous fungi cultivation," in *Current Developments in Biotechnology and Bioengineering*, Taherzadeh, M. J., Ferreira, J. A., and Pandey, A., Eds.: Elsevier, 2023, pp. 219-250.

[52] Hajian, C. S. S., Haringa, C., Noorman, H., and Takors, R., "Predicting By-Product Gradients of Baker's Yeast Production at Industrial Scale: A Practical Simulation Approach", *Processes,* Article vol. 8, no. 12, pinc. 19, Dec 2020, Art. no. 1554.

[53] Hansen, S., Hariskos, I., Luchterhand, B., and Büchs, J., "Development of a modified Respiration Activity Monitoring System for accurate and highly resolved measurement of respiration activity in shake flask fermentations", *Journal of Biological Engineering,* Article vol. 6, no. 1, pinc. 12, 2012, Art. no. 11.

[54] Hansen, S., Gumprecht, A., Micheel, L., Hennemann, H. G., Enzmann, F., and Bluemke, W., "Implementation of Perforated Concentric Ring Walls Considerably Improves Gas-Liquid Mass Transfer of Shaken Bioreactors", *Frontiers in Bioengineering and Biotechnology,* Article vol. 10, pinc. 13, May 2022, Art. no. 894295.

[55] Hartmann, S. K. *et al.*, "Online in vivo monitoring of cytosolic NAD redox dynamics in Ustilago maydis", *Biochimica Et Biophysica Acta-Bioenergetics,* Article vol. 1859, no. 10, pp. 1015-1024, Oct 2018.

[56] Federal Institute for Occupational Safety and Health. (2016). *Classification of Fungi into Risk Groups*.

[57] Helm, T. *et al.*, "Molasses as an alternative feedstock into itaconate production using Ustilago sp", *New Biotechnology,* Research Article vol. 77, no. 25, pp. 30-39, 25.11.2023 2023.

[58] Heyman, B., Lamm, R., Tulke, H., Regestein, L., and Büchs, J., "Shake flask methodology for assessing the influence of the maximum oxygen transfer capacity

on 2,3-butanediol production", *Microbial Cell Factories,* Article vol. 18, pinc. 16, May 2019, Art. no. 78.

[59] Heyman, B., Tulke, H., Putri, S. P., Fukusaki, E., and Buchs, J., "Online monitoring of the respiratory quotient reveals metabolic phases during microaerobic 2,3-butanediol production with Bacillus licheniformis", *Eng Life Sci,* vol. 20, no. 3-4, pp. 133-144, Mar 2020.

[60] Holtz, A., Gortz, J., Kocks, C., Junker, M., and Jupke, A., "Automated measurement of pH-dependent solid-liquid equilibria of itaconic acid and protocatechuic acid", *Fluid Phase Equilibria,* Article vol. 532, pinc. 9, Mar 2021, Art. no. 112893.

[61] Hosseinpour Tehrani, H. *et al.*, "Integrated strain- and process design enable production of 220 g L(-1) itaconic acid with *Ustilago maydis*", *Biotechnol Biofuels,* vol. 12, pinc. 263, 2019.

[62] Hosseinpour Tehrani, H., Saur, K., Tharmasothirajan, A., Blank, L. M., and Wierckx, N., "Process engineering of pH tolerant *Ustilago cynodontis* for efficient itaconic acid production", *Microb Cell Fact,* vol. 18, no. 1, pinc. 213, Dec 12 2019.

[63] Hosseinpour Tehrani, H., Tharmasothirajan, A., Track, E., Blank, L. M., and Wierckx, N., "Engineering the morphology and metabolism of pH tolerant *Ustilago cynodontis* for efficient itaconic acid production", *Metab Eng,* vol. 54, pp. 293-300, Jul 2019.

[64] Huber, M. L. *et al.*, "New International Formulation for the Viscosity of $H_2O$", *Journal of Physical and Chemical Reference Data,* Review vol. 38, no. 2, pp. 101-125, 2009.

[65] Huber, M. L. *et al.*, "New International Formulation for the Thermal Conductivity of $H_2O$", *Journal of Physical and Chemical Reference Data,* Article vol. 41, no. 3, pinc. 23, Sep 2012, Art. no. 033102.

[66] Ihling, N. *et al.*, "Time-Resolved Monitoring of the Oxygen Transfer Rate of Chinese Hamster Ovary Cells Provides Insights Into Culture Behavior in Shake Flasks", *Frontiers in Bioengineering and Biotechnology,* Article vol. 9, pinc. 14, Aug 2021, Art. no. 725498.

[67] Ihling, N. *et al.*, "Non-invasive and time-resolved measurement of the respiration activity of Chinese hamster ovary cells enables prediction of key culture parameters in shake flasks", *Biotechnology Journal,* Article vol. 17, no. 8, pinc. 13, Aug 2022, Art. no. 2100677.

[68] Jeng, T. M., Tzeng, S. C., and Xu, R., "Heat transfer characteristics of a rotating cylinder with a lateral air impinging jet", *International Journal of Heat and Mass Transfer,* Article vol. 70, pp. 235-249, Mar 2014.

[69] Jones, R. R., Hooper, D. C., Zhang, L. W., Wolverson, D., and Valev, V. K., "Raman Techniques: Fundamentals and Frontiers", *Nanoscale Research Letters,* Review vol. 14, pinc. 34, Jul 2019, Art. no. 231.

[70] Kadoya, K., Matsunaga, N., and Nagashima, A., "Viscosity and Thermal Conductivity of Dry Air in the Gaseous Phase", *Journal of Physical and Chemical Reference Data,* Article vol. 14, no. 4, pp. 947-970, 1985.

[71] Karaffa, L., Diaz, R., Papp, B., Fekete, E., Sandor, E., and Kubicek, C. P., "A deficiency of manganese ions in the presence of high sugar concentrations is the critical parameter for achieving high yields of itaconic acid by *Aspergillus terreus*", *Applied Microbiology and Biotechnology,* Article vol. 99, no. 19, pp. 7937-7944, Oct 2015.

[72] Kato, Y., Peter, C. P., Akgun, A., and Büchs, J., "Power consumption and heat transfer resistance in large rotary shaking vessels", *Biochemical Engineering Journal,* Article vol. 21, no. 1, pp. 83-91, Sep 2004.

[73] Keegan, D., Kretschmer, B., Elbersen, B., and Panoutsou, C., "Cascading use: a systematic approach to biomass beyond the energy sector", *Biofuels Bioproducts & Biorefining-Biofpr,* Review vol. 7, no. 2, pp. 193-206, Mar-Apr 2013.

[74] Kemp, R., "“Fire burn and cauldron bubble”(W. Shakespeare): what the calorimetric–respirometric (CR) ratio does for our understanding of cells?", *Thermochimica Acta,* vol. 355, no. 1-2, pp. 115-124, 2000.

[75] Kermis, H. R., Kostov, Y., Harms, P., and Rao, G., "Dual excitation ratiometric fluorescent pH sensor for noninvasive bioprocess monitoring: Development and application", *Biotechnology Progress,* Article vol. 18, no. 5, pp. 1047-1053, Sep-Oct 2002.

[76] Kerssemakers, A. A. J., Doménech, P., Cassano, M., Yamakawa, C. K., Dragone, G., and Mussatto, S. I., "Production of Itaconic Acid from Cellulose Pulp: Feedstock Feasibility and Process Strategies for an Efficient Microbial Performance", *Energies,* vol. 13, no. 7, 2020.

[77] Klement, T., Milker, S., Jager, G., Grande, P. M., Dominguez de Maria, P., and Büchs, J., "Biomass pretreatment affects *Ustilago maydis* in producing itaconic acid", *Microb Cell Fact,* vol. 11, pinc. 43, Apr 5 2012.

[78] Klement, T. and Büchs, J., "Itaconic acid - a biotechnological process in change", *Bioresour Technol,* vol. 135, pp. 422-31, May 2013.

[79] Klöckner, W. and Büchs, J., "Shake-Flask Bioreactors," in *Comprehensice Biotechnology (Second Edition)*, vol. 2, Moo-Young, M., Ed.: Elsevier, 2011, pp. 213-226.

[80] Klöckner, W. and Büchs, J., "Advances in Shaking Technologies", *Trends in Biotechnology,* Review vol. 30, no. 6, pp. 307-314, Jun 2012.

[81] Klöckner, W., Tissot, S., Wurm, F., and Büchs, J., "Power input correlation to characterize the hydrodynamics of cylindrical orbitally shaken bioreactors", *Biochemical Engineering Journal,* vol. 65, pp. 63-69, 2012.

[82] Kohli, K., Prajapati, R., and Sharma, B. K., "Bio-Based Chemicals from Renewable Biomass for Integrated Biorefineries", *Energies,* Review vol. 12, no. 2, pinc. 40, Jan 2019, Art. no. 233.

[83] Kollath, I. S. *et al.*, "Manganese Deficiency Is Required for High Itaconic Acid Production From D-Xylose in *Aspergillus terreus*", *Frontiers in Microbiology,* Article vol. 10, pinc. 10, Jul 2019, Art. no. 1589.

[84] Koutinas, A. A. *et al.*, "Valorization of industrial waste and by-product streams via fermentation for the production of chemicals and biopolymers", *Chemical Society Reviews,* Review vol. 43, no. 8, pp. 2587-2627, 2014.

[85] Kreyenschulte, D. *et al.*, "*In situ* reactive extraction of itaconic acid during fermentation of *Aspergillus terreus*", *Biochemical Engineering Journal,* Article vol. 135, pp. 133-141, Jul 2018.

[86] Krull, S., Hevekerl, A., Kuenz, A., and Prüße, U., "Process development of itaconic acid production by a natural wild type strain of *Aspergillus terreus* to reach industrially relevant final titers", *Applied Microbiology and Biotechnology,* vol. 101, no. 10, pp. 4063-4072, May 2017.

[87] Krull, S., Lunsmann, M., Prüße, U., and Kuenz, A., "*Ustilago rabenhorstiana* - An Alternative Natural Itaconic Acid Producer", *Fermentation-Basel,* Article vol. 6, no. 1, pinc. 15, Mar 2020, Art. no. 4.

[88] Kuenz, A. and Krull, S., "Biotechnological production of itaconic acid-things you have to know", *Appl Microbiol Biotechnol,* vol. 102, no. 9, pp. 3901-3914, May 2018.

[89] Kurzrock, T. and Weuster-Botz, D., "New reactive extraction systems for separation of bio-succinic acid", *Bioprocess and Biosystems Engineering,* Article vol. 34, no. 7, pp. 779-787, Sep 2011.

[90] Ladner, T., Held, M., Flitsch, D., Beckers, M., and Büchs, J., "Quasi-continuous parallel online scattered light, fluorescence and dissolved oxygen tension measurement combined with monitoring of the oxygen transfer rate in each well of a shaken microtiter plate", *Microbial Cell Factories,* Article vol. 15, pinc. 15, Dec 2016, Art. no. 206.

[91] Lattermann, C., Funke, M., Hansen, S., Diederichs, S., and Büchs, J., "Cross-section perimeter is a suitable parameter to describe the effects of different baffle geometries in shaken microtiter plates", *Journal of Biological Engineering,* Article vol. 8, pinc. 10, Jul 2014, Art. no. 18.

[92] Liepe, F., Meusel, W., Möckel, H., and Platzer, B., *Verfahrenstechnische Berechnungsmethoden, Teil 4 Stoffvereinigung in fluiden Phasen*. VCH Publishers, Weinheim, 1988.

[93] Lin, P. J., Scholz, A., and Krull, R., "Effect of volumetric power input by aeration and agitation on pellet morphology and product formation of Aspergillus niger", *Biochemical Engineering Journal,* Article vol. 49, no. 2, pp. 213-220, Apr 2010.

[94] Liu, Y. P., Zheng, P., Sun, Z. H., Ni, Y., Dong, J. J., and Zhu, L. L., "Economical succinic acid production from cane molasses by *Actinobacillus succinogenes*", *Bioresource Technology,* vol. 99, no. 6, pp. 1736-1742, Apr 2008.

[95] Lopez-Garzon, C. S. and Straathof, A. J. J., "Recovery of carboxylic acids produced by fermentation", *Biotechnology Advances,* Review vol. 32, no. 5, pp. 873-904, Sep-Oct 2014.

[96] Losen, M., Frolich, B., Pohl, M., and Büchs, J., "Effect of oxygen limitation and medium composition on *Escherichia coli* fermentation in shake-flask cultures", *Biotechnology Progress,* Article vol. 20, no. 4, pp. 1062-1068, Jul-Aug 2004.

[97] Luo, W. J., Lu, H. Q., Lei, F. H., Cheng, L. Y., Li, K., and Li, W., "Structural elucidation of high-molecular-weight alkaline degradation products of hexoses", *Food Science & Nutrition,* Article vol. 8, no. 6, pp. 2848-2853, Jun 2020.

[98] Magalhaes, A. I., de Carvalho, J. C., Medina, J. D. C., and Soccol, C. R., "Downstream process development in biotechnological itaconic acid manufacturing", *Applied Microbiology and Biotechnology,* Review vol. 101, no. 1, pp. 1-12, Jan 2017.

[99] Maier, U., Losen, M., and Büchs, J., "Advances in understanding and modeling the gas–liquid mass transfer in shake flasks", *Biochemical Engineering Journal,* vol. 17, no. 3, pp. 155-167, 2004.

[100] Marques, M. P. C., Cabral, J. M. S., and Fernandes, P., "Bioprocess scale-up: quest for the parameters to be used as criterion to move from microreactors to lab-scale", *Journal of Chemical Technology and Biotechnology,* Review vol. 85, no. 9, pp. 1184-1198, Sep 2010.

[101] Marvel, C. S. and Shepherd, T. H., "Polymerization Reactions of Itaconic Acid and Some of Its Derivatives", *Journal of Organic Chemistry,* Article vol. 24, no. 5, pp. 599-605, 1959.

[102] Matuz-Mares, D. *et al.*, "Expression of alternative NADH dehydrogenases (NDH-2) in the phytopathogenic fungus *Ustilago maydis*", *Febs Open Bio,* Article vol. 8, no. 8, pp. 1267-1279, Aug 2018.

[103] Mehmood, N. *et al.*, "Oxygen Supply Controls the Onset of Pristinamycins Production by *Streptomyces pristinaespiralis* in Shaking Flasks", *Biotechnology and Bioengineering,* Article vol. 108, no. 9, pp. 2151-2161, Sep 2011.

[104] Meier, K., Klöckner, W., Bonhage, B., Antonov, E., Regestein, L., and Büchs, J., "Correlation for the maximum oxygen transfer capacity in shake flasks for a wide range of operating conditions and for different culture media", *Biochemical Engineering Journal,* vol. 109, pp. 228-235, 2016.

[105] Micheletti, M., Barrett, T., Doig, S. D., Baganz, F., Levy, M. S., Woodley, J. M., and Lye, G. J., "Fluid Mixing in Shaken Bioreactors: Implications for Scale-Up Predictions From Microlitre-Scale Microbial and Mammalian Cell Cultures", *Chemical Engineering Science,* Article; Proceedings Paper vol. 61, no. 9, pp. 2939-2949, May 2006.

[106] Morita, T., Konishi, M., Fukuoka, T., Imura, T., and Kitamoto, D., "Identification of *Ustilago cynodontis* as a New Producer of Glycolipid Biosurfactants, Mannosylerythritol Lipids, Based on Ribosomal DNA Sequences", *Journal of Oleo Science,* Article vol. 57, no. 10, pp. 549-556, Oct 2008.

[107] Mrotzek, C., Anderlei, T., Henzler, H.-J., and Büchs, J., "Mass transfer resistance of sterile plugs in shaking bioreactors", *Biochemical Engineering Journal,* vol. 7, pp. 107-112, 2001.

[108] Müller, M. J., Stachurski, S., Stoffels, P., Schipper, K., Feldbrügge, M., and Büchs, J., "Online evaluation of the metabolic activity of *Ustilago maydis* on (poly)galacturonic acid", *J Biol Eng,* vol. 12, pinc. 34, 2018.

[109] Müller, W., "Optimierung und Scale-Up der Itaconsäureproduktion aus regionalen Reststoffströmen mit *Ustilago cynodontis* im 2 L bis 150 L Fermenter", *RWTH Aachen University,* Master Thesis 2021.

[110] Nagai, K., "New developments in the production of methyl methacrylate", *Applied Catalysis a-General,* Article vol. 221, no. 1-2, pp. 367-377, Nov 2001.

[111] Nascimento, M. F., Marques, N., Correia, J., Faria, N. T., Mira, N. P., and Ferreira, F. C., "Integrated perspective on microbe-based production of itaconic acid: From metabolic and strain engineering to upstream and downstream strategies", *Process Biochemistry,* Review vol. 117, pp. 53-67, Jun 2022.

[112] Okabe, M., Lies, D., Kanamasa, S., and Park, E. Y., "Biotechnological production of itaconic acid and its biosynthesis in *Aspergillus terreus*", *Appl Microbiol Biotechnol,* vol. 84, no. 4, pp. 597-606, Sep 2009.

[113] Otten, A., Brocker, M., and Bott, M., "Metabolic engineering of *Corynebacterium glutamicum* for the production of itaconate", *Metabolic Engineering,* Article vol. 30, pp. 156-165, Jul 2015.

[114] Palmonari, A. *et al.*, "Characterization of molasses chemical composition", *Journal of Dairy Science,* Article vol. 103, no. 7, pp. 6244-6249, Jul 2020.

[115] Panchaksharam, Y. *et al.*, "Roadmap for the Chemical Industry in Europe towards a Bioeconomy", *Action Plan RoadtoBio,* 2019.

[116] Panic, V. V., Seslija, S. I., Popovic, I. G., Spasojevic, V. D., Popovic, A. R., Nikolic, V. B., and Spasojevic, P. M., "Simple One-Pot Synthesis of Fully Biobased Unsaturated Polyester Resins Based on Itaconic Acid", *Biomacromolecules,* Article vol. 18, no. 12, pp. 3881-3891, Dec 2017.

[117] Pastoors, J. *et al.*, "Respiration-based investigation of adsorbent-bioprocess compatibility", *Biotechnology for Biofuels and Bioproducts,* Article vol. 16, no. 1, pinc. 12, Mar 2023, Art. no. 49.

[118] Pena, C., Galindo, E., and Buchs, J., "The viscosifying power, degree of acetylation and molecular mass of the alginate produced by Azotobacter vinelandii in shake flasks are determined by the oxygen transfer rate", *Process Biochemistry,* Article vol. 46, no. 1, pp. 290-297, Jan 2011.

[119] Peter, C. P., Lotter, S., Maier, U., and Büchs, J., "Impact of out-of-phase conditions on screening results in shaking flask experiments", *Biochemical Engineering Journal,* Article vol. 17, no. 3, pp. 205-215, Mar 2004.

[120] Peter, C. P., Suzuki, Y., and Buchs, J., "Hydromechanical stress in shake flasks: correlation for the maximum local energy dissipation rate", *Biotechnol Bioeng,* vol. 93, no. 6, pp. 1164-76, Apr 20 2006.

[121] Philip, P., Meier, K., Kern, D., Goldmanns, J., Stockmeier, F., Bahr, C., and Buchs, J., "Systematic evaluation of characteristics of the membrane-based fed-batch shake flask", *Microbial Cell Factories,* Article vol. 16, pinc. 17, Jul 2017, Art. no. 122.

[122] Purkus, A., Hagemann, N., Bedtke, N., and Gawel, E., "Towards a sustainable innovation system for the German wood-based bioeconomy: Implications for policy design", *Journal of Cleaner Production,* Article vol. 172, pp. 3955-3968, Jan 2018.

[123] Raval, K., Kato, Y., and Büchs, J., "Comparison of torque method and temperature method for determination of power consumption in disposable shaken bioreactors", *Biochemical Engineering Journal,* vol. 34, no. 3, pp. 224-227, 2007.

[124] Raval, K. and Büchs, J., "Extended Method to Evaluate Power Consumption in Large Disposable Shaking Bioreactors", *Journal of Chemical Engineering of Japan,* Article vol. 41, no. 11, pp. 1075-1082, Nov 2008.

[125] Raval, K., Kato, Y., and Büchs, J., "Characterization of heat transfer of large orbitally shaken cylindrical bioreactors", *Biochemical Engineering Journal,* vol. 86, pp. 1-7, 2014.

[126] Regestein, L., Giese, H., Zavrel, M., and Buchs, J., "Comparison of two methods for designing calorimeters using stirred tank reactors", *Biotechnol Bioeng,* vol. 110, no. 1, pp. 180-90, Jan 2013.

[127] Regestein, L. *et al.*, "From beech wood to itaconic acid: case study on biorefinery process integration", *Biotechnol Biofuels,* vol. 11, pinc. 279, 2018.

[128] Robert, C., de Montigny, F., and Thomas, C. M., "Tandem synthesis of alternating polyesters from renewable resources", *Nature Communications,* Article vol. 2, pinc. 6, Dec 2011, Art. no. 586.

[129] Rocha-Valadez, J. A., Hassan, M., Corkidi, G., Flores, C., Galindo, E., and Serrano-Carreon, L., "6-Pentyl-alpha-pyrone production by Trichoderma harzianum: The influence of energy dissipation rate and its implications on fungal physiology", *Biotechnology and Bioengineering,* Article vol. 91, no. 1, pp. 54-61, Jul 2005.

[130] Russell, A. D., "Lethal Effects of Heat on Bacterial Physiology and Structure", *Science Progress,* vol. 86, no. 1-2, pp. 115-137, 2003.

[131] Sandor, E. *et al.*, "Carbon-Source Dependent Interplay of Copper and Manganese Ions Modulates the Morphology and Itaconic Acid Production in *Aspergillus terreus*", *Frontiers in Microbiology,* Article vol. 12, pinc. 14, May 2021, Art. no. 680420.

[132] Saur, K. M. *et al.*, "Holistic Approach to Process Design and Scale-Up for Itaconic Acid Production from Crude Substrates", *Bioengineering,* vol. 10, no. 6, pinc. 723, 2023.

[133] Schlembach, I., Hosseinpour Tehrani, H., Blank, L. M., Büchs, J., Wierckx, N., Regestein, L., and Rosenbaum, M. A., "Consolidated bioprocessing of cellulose to itaconic acid by a co-culture of *Trichoderma reesei* and *Ustilago maydis*", *Biotechnol Biofuels,* vol. 13, no. 1, pinc. 207, Dec 14 2020.

[134] Shi, D. J., Gao, Y., Sun, L., and Chen, M. Q., "Superabsorbent poly(acrylamide-co-itaconic acid) hydrogel microspheres: Preparation, characterization and absorbency", *Polymer Science Series A,* Article vol. 56, no. 3, pp. 275-282, May 2014.

[135] Sieben, M., Hanke, R., and Buchs, J., "Contact-free determination of viscosity in multiple parallel samples", *Sci Rep,* vol. 9, no. 1, pinc. 8335, Jun 6 2019.
[136] Stephan, K. and Laesecke, A., "The Thermal Conductivity of Fluid Air", *Journal of Physical and Chemical Reference Data,* Article vol. 14, no. 1, pp. 227-234, 1985.
[137] Sugiyama, M., Sasano, Y., and Harashima, S., "Mechanism of yeast adaptation to weak organic acid stress," in *Stress Biology of Yeasts and Fungi*: Springer, 2015, pp. 107-121.
[138] Sumino, Y. and Akiyama, S.-I., "Measurement of the overall volumetric coefficient of heat transfer of a shaking flask", *Journal of Fermentation Technology,* vol. 65, no. 3, pp. 285-289, 1987.
[139] Suresh, S., Srivastava, V. C., and Mishra, I. M., "Critical analysis of engineering aspects of shaken flask bioreactors", *Critical Reviews in Biotechnology,* vol. 29, no. 4, pp. 255-278, Dec 2009.
[140] Tabuchi, T., Sugisawa, T., Ishidori, T., Nakahara, T., and Sugiyama, J., "Itaconic Aaicd Fermentation by a Yeast Belonging to the Genus *Candida*", *Agricultural and Biological Chemistry,* Article vol. 45, no. 2, pp. 475-479, 1981.
[141] Tan, L., Sun, Z. Y., Okamoto, S., Takaki, M., Tang, Y. Q., Morimura, S., and Kida, K., "Production of ethanol from raw juice and thick juice of sugar beet by continuous ethanol fermentation with flocculating yeast strain KF-7", *Biomass & Bioenergy,* Article vol. 81, pp. 265-272, Oct 2015.
[142] Thuy, N. T. H., Kongkaew, A., Flood, A., and Boontawan, A., "Fermentation and crystallization of succinic acid from *Actinobacillus succinogenes* ATCC55618 using fresh cassava root as the main substrate", *Bioresource Technology,* Article vol. 233, pp. 342-352, Jun 2017.
[143] VerifiedMarketResearch. (2020, 14.07.2023). *Global Itaconic Acid Market Size By Derivative, By Application, By Georgraphic Scope And Forecast*. Available: https://www.verifiedmarketresearch.com/product/itaconic-acid-market/
[144] Wagner, W. and Pruss, A., "The IAPWS formulation 1995 for the thermodynamic properties of ordinary water substance for general and scientific use", *Journal of Physical and Chemical Reference Data,* Review vol. 31, no. 2, pp. 387-535, Jun 2002.
[145] Wang, J. Q., Cui, Z. F., Li, Y. Y., Cao, L. P., and Lu, Z. M., "Techno-economic analysis and environmental impact assessment of citric acid production through different recovery methods", *Journal of Cleaner Production,* Article vol. 249, pinc. 11, Mar 2020, Art. no. 119315.
[146] Wang, S.-J. and Zhong, J.-J., "Chapter 6 - Bioreactor Engineering," in *Bioprocessing for Value-Added Products from Renewable Resources*, Yang, S.-T., Ed. Amsterdam: Elsevier, 2007, pp. 131-161.
[147] Waxman, M. and Davis, H., "Density of Ultra-Pure Air at 298.15 K for Mass Transfer Buoyancy Corrections", *Journal of Research of the National Bureau of Standards (USA),* vol. 83, no. 5, pinc. 415, 1978.
[148] Weiermueller, J., Akermann, A., Laudensack, W., Chodorski, J., Blank, L. M., and Ulber, R., "Brewers' spent grain as carbon source for itaconate production with engineered *Ustilago maydis*", *Bioresource Technology,* Article vol. 336, pinc. 9, Sep 2021, Art. no. 125262.
[149] Wierckx, N., Miebach, K., Ihling, N., Hussnaetter, K. P., Büchs, J., and Schipper, K., "Perspectives for the application of Ustilaginaceae as biotech cell factories", *Essays Biochem,* Apr 16 2021.

[150] Wucherpfennig, T., Hestler, T., and Krull, R., "Morphology engineering - Osmolality and its effect on *Aspergillus niger* morphology and productivity", *Microbial Cell Factories,* Article vol. 10, pinc. 15, Jul 2011, Art. no. 58.
[151] Zambanini, T. *et al.*, "Promoters from the itaconate cluster of Ustilago maydis are induced by nitrogen depletion", *Fungal Biol Biotechnol,* vol. 4, pinc. 11, 2017.
[152] Zambanini, T. *et al.*, "Efficient itaconic acid production from glycerol with *Ustilago vetiveriae* TZ1", *Biotechnol Biofuels,* vol. 10, pinc. 131, 2017.
[153] Zhang, B., Wu, L., Liu, X. C., and Bao, J., "Plant Proteins as an Alternative Nitrogen Source for Chiral Purity L-Lactic Acid Fermentation from Lignocellulose Feedstock", *Fermentation-Basel,* Article vol. 8, no. 10, pinc. 13, Oct 2022, Art. no. 546.
[154] Zhu, P., Luo, R., Li, Y. Z., and Chen, X. L., "Metabolic Engineering and Adaptive Evolution for Efficient Production of L-Lactic Acid in *Saccharomyces cerevisiae*", *Microbiology Spectrum,* Article vol. 10, no. 6, pinc. 11, Dec 2022.

# 7. Appendix

## Appendices for Chapter 2

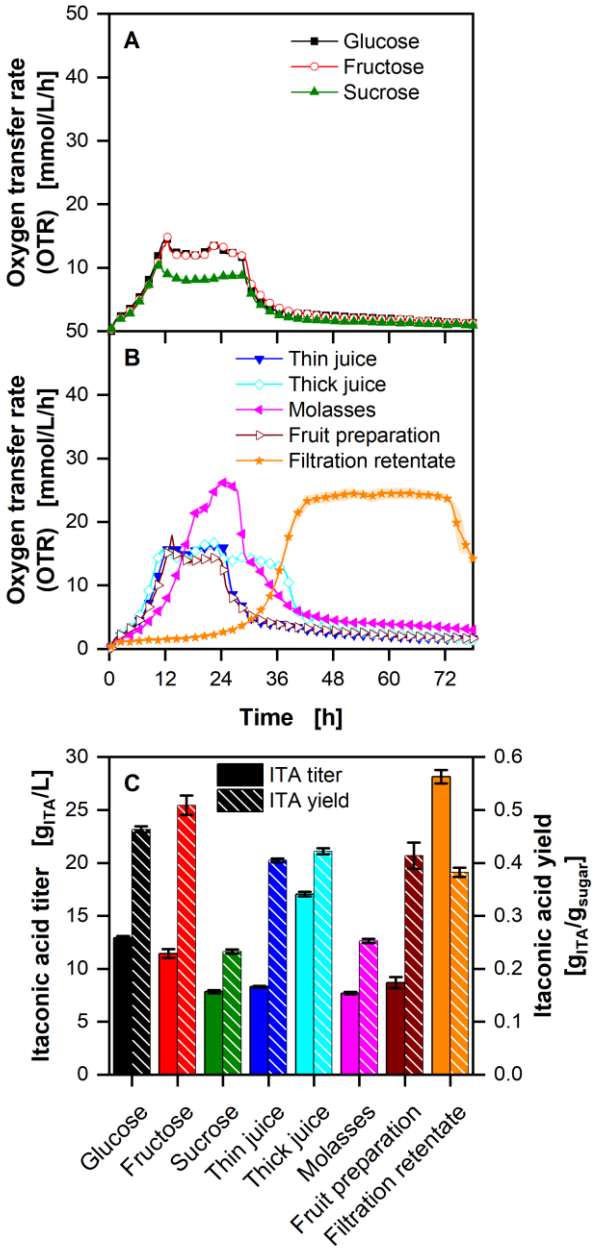


**Appendix 1: Cultivation of *U. maydis* Mutterschiff with different carbon sources with limiting ammonium chloride concentrations (1 g/L).**

(A) Oxygen transfer rates of the pure sugars (glucose, fructose, and sucrose). (B) Oxygen transfer rates of complex substrates. (C) Itaconic acid titers and yields of the cultivations after 78 hours of cultivation. Cultivations were performed in a 96 round deep-well MTP, filled with 300 µL modified Verduyn medium at 30 °C, 350 rpm shaking frequency and a shaking diameter of 50 mm. 100 mM MES were added to the cultivations. The initial pH was set to 6.5 for all cultivations. The different carbon sources are specified in Appendix 2. Graphs show the mean of three replicates, with standard deviation as shaded area. Due to high

reproducibility of the measurements, the standard deviation might not be visible for every data point. For clarity, only every fourth data point is shown.

**Appendix 2: Feedstocks used for Figure 2.2 and Appendix 1.**

| Feedstock | Sugar concentration [g/L] | Availability | Handling | Cost | Manufacturer |
|---|---|---|---|---|---|
| Glucose | 27.9 | High | Easy | High | Sigma-Aldrich |
| Fructose | 22.5 | High | Easy | High | Sigma-Aldrich |
| Sucrose | 33.7 | High | Easy | High | Sigma-Aldrich |
| Thin juice | 20.5 | High | Difficult (solids) | Low | Pfeifer & Langen Industrie- und Handel-KG |
| Thick juice | 40.4 | High | Easy | Low | Pfeifer & Langen Industrie- und Handel-KG |
| Molasses | 32.0 | High | Difficult (viscosity) | Low | Pfeifer & Langen Industrie- und Handel-KG |
| Fruit preparation | 21.0 | High | Difficult (solids) | Low | Zentis GmbH & Co. KG |
| Filtration retentate | 93.6 | Low | Easy | High | GNT Europe GmbH |
| Filtration permeate | 65.8 | Low | Easy | High | GNT Europe GmbH |

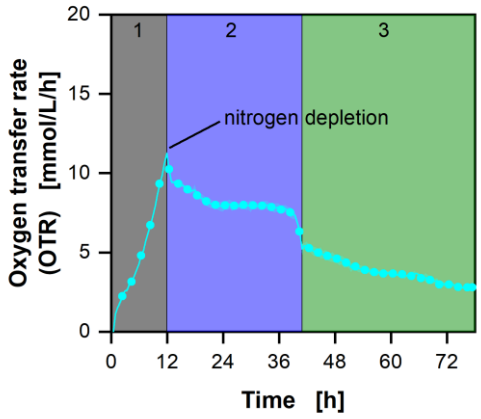


**Appendix 3: Typical phases of itaconic acid production by Ustilaginacea grown on glucose with limiting ammonium chloride concentration (1 g/L).**

Due to the similarity of these phases, only *U. cynodontis* ITA Max pH is shown as an example. Cultivation phases are indicated by number. 1: Exponential growth phase. 2: Nitrogen-limited production phase. 3: Carbon depletion and starvation. Cultivations were performed in a 96 round deep-well MTP, filled with 300 µL modified Verduyn medium with 25 g/L glucose at 30 °C, 350 rpm shaking frequency and a shaking diameter of 50 mm. 30 mM MES were added to the cultivations. The initial pH was set to 6.5 for all cultivations. The graph shows the mean of three replicates, with the standard deviation as shaded area. Due to high reproducibility of the measurements, the standard deviation might not be visible for every data point. For clarity, only every fourth data point is shown.

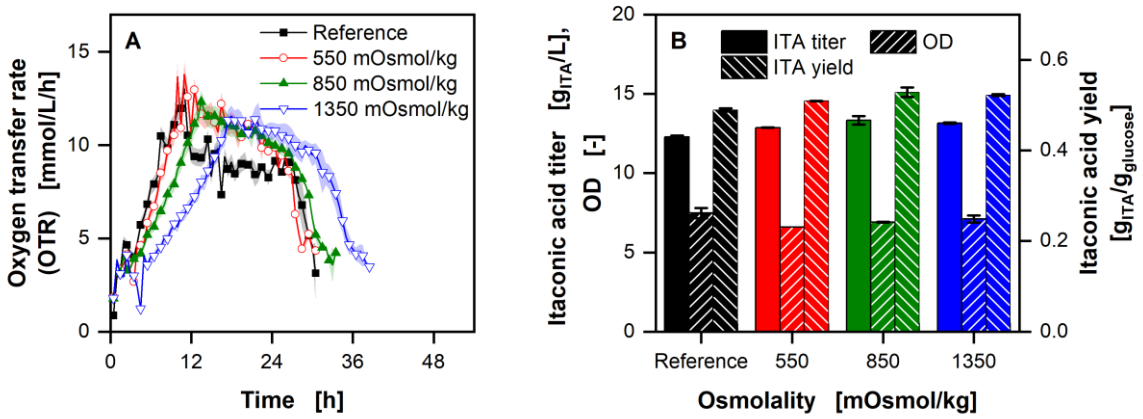


**Appendix 4: Influence of osmolality on growth and productivity of *U. maydis* Mutterschiff with limiting ammonium chloride concentration (1 g/L $NH_4Cl$).**

(A) Course of the oxygen transfer rates with increasing osmolality. (B) Itaconic acid titer, OD, and yield at the end of the respective fermentations. Osmolality was increased by addition of 0.1, 0.25, and 0.5 M NaCl. The reference medium has an osmolality of 350 mOsmol/kg. Cultivations were performed in 250 mL RAMOS flasks filled with 10 mL modified Verduyn medium with 25 g/L glucose at 30 °C, 350 rpm shaking frequency and a shaking diameter of 50 mm. 100 mM MES were added to the cultivations. The initial pH was at 6.5 for all cultivations. The final pH reaches 3.71 ± 0.01, 3.57 ± 0.00, 3.57 ± 0.01, and 3.45 ± 0.01 for the reference, 550, 850 and 1350 mOsmol/kg cultivations, respectively. Graphs show the mean of duplicates. Shadows and error bars show the minimum and maximum values. For clarity, only every second data point is shown.

# Appendices for Chapter 3

**Appendix 5: Composition of thick juice.**

| Analyte | Measurement | Unit | Method |
|---|---|---|---|
| Sucrose | 842 ± 8 | g/L | HPLC |
| Glucose | > 1 | g/L | HPLC |
| Fructose | > 1 | g/L | HPLC |
| Lactic acid | 1.17 ± 0.13 | g/L | HPLC |
| $Cl^-$ | 0.048 ± 0.000 | wt% | IC |
| $NO_3^-$ | 0.0524 ± 0.01 | wt% | IC |
| $SO_4^{2-}$ | 0.0833 ± 0.01 | wt% | IC |
| Ca | 72.93 ± 1.00 | mg/kg | ICP-OES |
| Fe | < 2 | mg/kg | ICP-OES |
| K | 6660 ± 20 | mg/kg | ICP-OES |
| Mg | 12.11 ± 0.16 | mg/kg | ICP-OES |
| Na | 547 ± 3 | mg/kg | ICP-OES |
| P | 53 ± 3 | mg/kg | ICP-OES |
| $NH_4^+$ | 0.0122 | wt% | CFA |
| $PO_4^{3-}$ | > 0.0008 | wt% | CFA |

Substrate analysis was performed by the group of Stephan Noack (IGB-1, Forschungszentrum Jülich GmbH) and is thankfully acknowledged. The analysis was performed using gas chromatography time-of-flight mass spectrometry (GC-ToF-MS) as published in de Wit et al. (2023) [28] for qualitative analysis of impurities. For quantitative analysis, inductively coupled plasma optical emission spectroscopy (ICP-OES) is used for cations, while anions are quantified via ion exchange chromatography (IC). Additionally, $NH_4^+$ and $PO_4^{3-}$ concentrations are determined by confirmatory factor analysis (CFA). HPLC, according to Section 3.2.3. Offline Analytics is used with a column of 30 cm in length and 8 mm in diameter at a flow rate of 0.6 mL/min to quantify sugar and lactic acid

content. The resulting data is depicted in Appendix 5. Density is determined to 1.3310 ± 0.0023 g/cm³ with a DMA48 density meter (Anton Paar, Graz, Austria) at 20 °C. Even though pigments are not detected using GC-ToF-MS, ICP-OES, IC, CFA, or HPLC, thick juice shows a light to medium brown color. As it can be found in the literature, colorization of thick juice occurs during sugar production from the alkaline degradation of hexose sugars and Maillard reactions forming melanoidins [24]. Both compound groups have a large molecule size of over 2 kDa and contain a variety of active groups, such as carboxyl and aldehyde groups [24, 97]. Furthermore, colorants unrelated to sucrose, e.g., phenols, flavonoids, and melanin, are present in crude substrates [14]. In both cases, due to their size and active groups, most of these molecules are expected to be more hydrophobic at low pH values.

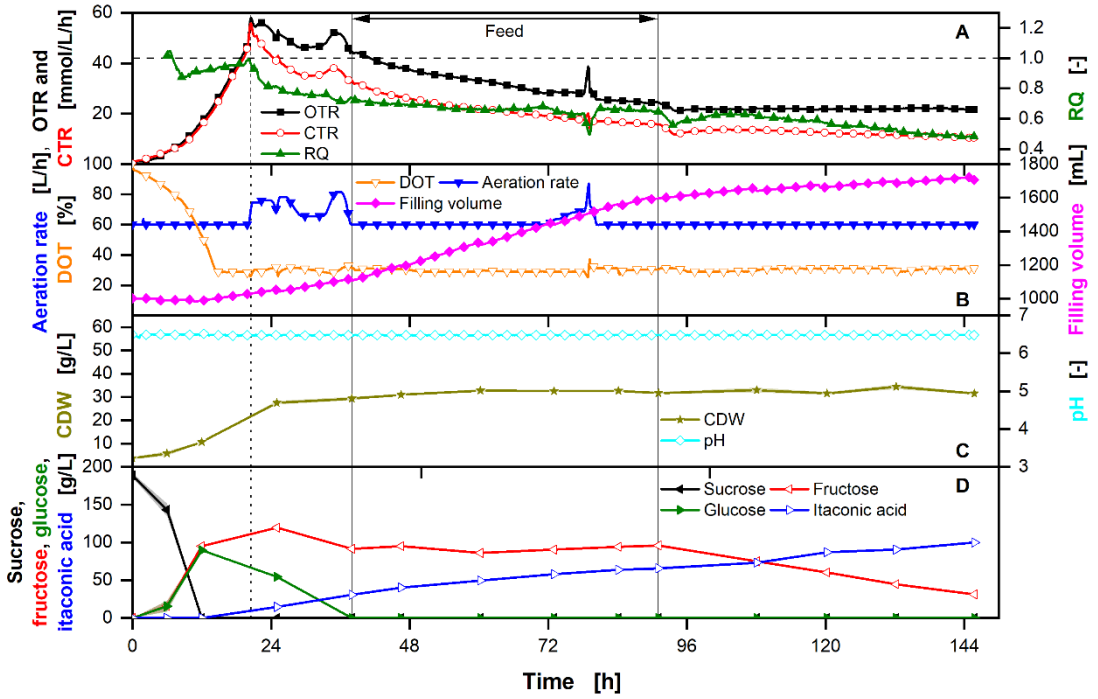


**Appendix 6: Extended-batch fermentation of *U. maydis* Mutterschiff grown with thick juice as sole carbon source with limiting ammonium chloride concentration (4 g/L $NH_4Cl$).**

(A) Oxygen and carbon dioxide transfer rates and respiratory quotient. The black dotted line indicates the start of the nitrogen limitation. The black horizontal dashed line indicates an RQ = 1. (B) Dissolved oxygen tension, absolute aeration rate, and filling volume. (C) Cell dry weight concentration and pH. (D) Sugar (sucrose, glucose, fructose) and itaconic acid concentrations. For the batch phase, 200 g/L sucrose from thick juice were initially added to the medium. During the feed phase (between the vertical solid lines) 200 g of additional sucrose in form of thick juice were added to the fermentation vessel. Vertical dotted lines show the addition of antifoam. Cultivation was performed in a 2 L Sartorius BIOSTAT® stirred tank reactor (Sartorius AG, Göttingen, Germany) with an initial filling volume of 1 L at 30 °C. Dissolved oxygen tension was kept > 30 % by first increasing stirring frequency from 800 to 1200 rpm and second the gas flow rate from 60 to 180 L/h. pH was kept constant at 6.5 by addition of 1 M HCl and 5 M NaOH. RQ values are only shown for OTR values > 5 mmol/L/h. Samples were taken regularly and analyzed via HPLC. Concentrations are shown as mean values of three replicates and standard deviation as shaded area. Due to high reproducibility of the measurements, the standard deviation might not be visible for every data point. For clarity, only every 15$^{th}$ data point is shown for the online data.

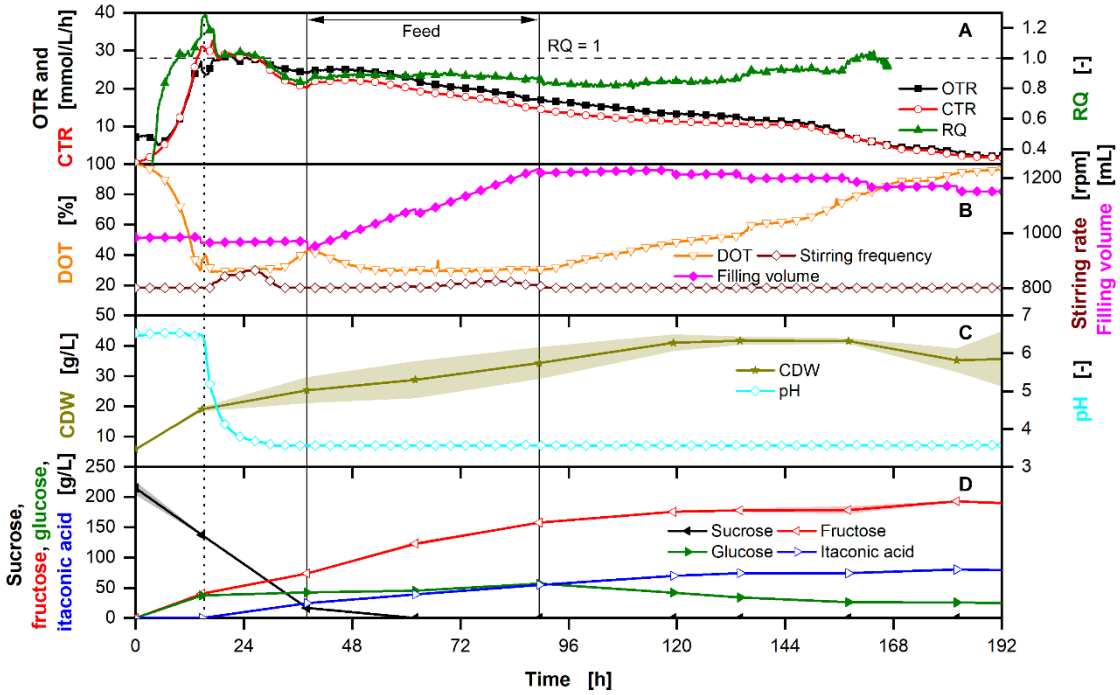


**Appendix 7: Overfed extended-batch fermentation of *U. cynodontis* ITA Max pH with pH shift and thick juice as carbon source.**

(A) Oxygen and carbon dioxide transfer rates and respiratory quotient. The black dotted line indicates the start of the nitrogen limitation. The black horizontal dashed line indicates an RQ = 1. (B) Dissolved oxygen tension, stirring rate and filling volume. (C) Cell dry weight concentration and pH. (D) Sugar (sucrose, glucose, fructose) and itaconic acid concentrations. For the batch phase, 215 g/L sucrose from thick juice are initially added to the medium. During the feed phase (between the vertical solid lines), 215 g of additional sucrose from juice is added to the fermentation vessel. Cultivation is performed in a 2 L stirred tank reactor with an initial filling volume of 1 L at 30 °C with a constant aeration and stirring rate of 1 L/min and 1200 rpm, respectively. For clarity, only every 20$^{th}$ measured online data point is shown.

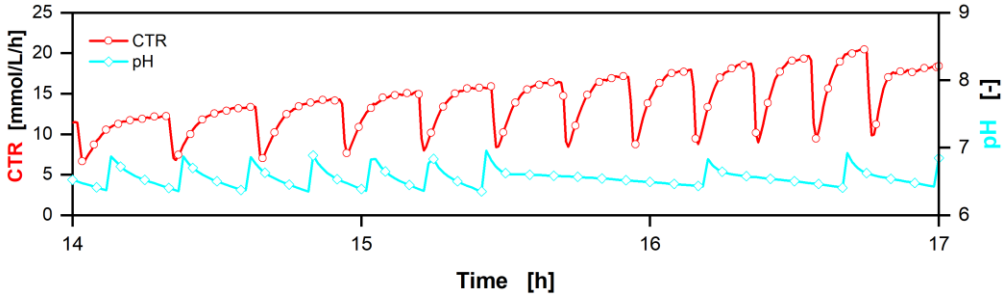


**Appendix 8: Close-up view of pH and CTR in the 150 L batch fermentation, shown in Figure 3.4, between 14 and 17 h of cultivation before the pH shift.**

Cultivation is performed in a 150 L stirred tank pressure reactor with an initial filling volume of 105 L at 30 °C with a constant stirring rate of 285 rpm. For clarity, only every fifth measured online data point is shown.

Appendix 8 displays a close-up view of pH and CTR between 14 and 17 h of cultivation in the 100 L fermentation. During the first hours of cultivation, the pH fluctuates slightly. In every control step, it is regulated to 6.5 by addition of NaOH. This is coupled with a change in $CO_2$ solubility, resulting in an oscillating CTR. The pH is constant, and the CTR stabilized after the drop in OTR, indicating the beginning of nitrogen limitation.

# Appendices for Chapter 4

**Appendix 9: Geometry of each flask size in addition to the weight and number of flasks per tray.**

| Nominal flask volume ($V_F$) [mL] | Maximum diameter (d) [mm] | Height of flask [mm] | Wall thickness [mm] | Inner neck diameter ($d_N$) [mm] | Neck height ($H_{pl}$) [mm] | Weight [g] | Number of flasks per tray [-] |
|---|---|---|---|---|---|---|---|
| 50 | 49.6 | 90 | 0.8 | 2.09 | 3.07 | 39.9 | 100 |
| 100 | 60.0 | 105 | 0.8 | 2.09 | 3.05 | 60.1 | 74 |
| 250 | 81.3 | 145 | 0.9 | 3.22 | 4.27 | 130.0 | 40 |
| 500 | 101.0 | 180 | 0.9 | 3.28 | 4.16 | 16.1 | 26 |
| 1000 | 126.7 | 220 | 1.3 | 3.96 | 5.19 | 279.8 | 16 |
| 2000 | 163.0 | 280 | 1.5 | 4.76 | 4.98 | 521.1 | 9 |
| 5000 | 216.4 | 365 | 1.8 | 4.76 | 5.52 | 1182.0 | 5 |

The neck geometry and weight of the flask were determined by measuring ten flasks of each size and calculating the mean. The other values are based on the DIN 12380/ISO 1773 norm for narrow-neck shake flasks. The number of flasks per tray was given by Kuhner Shaker GmbH (Birsfelden, Germany) for a standard F tray (800 x 420 mm).

**Appendix 10: Maximal liquid height, liquid-to-flask height ratio, and heat transfer area for each case flask size and case.**

The liquid height was calculated according to the liquid distribution model from Büchs et al. (2007) [20]. The heat transfer area (A) includes the whole area up to the maximum liquid height for the entire flask, not only the bulk liquid, due to film formation.

| Nominal flask volume ($V_F$) [mL] | Constant $V_L/V_F$ | | | Constant $k_La$ | | | Constant $OTR_{max,plug}$ | | |
|---|---|---|---|---|---|---|---|---|---|
| | Max. liquid height [cm] | Liquid to flask height ratio [%] | Heat transfer area [$cm^2$] | Max. liquid height [cm] | Liquid to flask height ratio [%] | Heat transfer area (A) | Max. liquid height [cm] | Liquid to flask height ratio [%] | Heat transfer area (A) |
| 50 | 1.93 | 21.4 | 34.5 | 2.22 | 24.6 | 38.4 | 2.24 | 24.9 | 38.7 |
| 100 | 2.31 | 22.0 | 53.9 | 2.47 | 23.5 | 56.4 | 2.48 | 23.6 | 56.5 |
| 250 | 3.25 | 22.4 | 101.6 | 3.25 | 22.4 | 101.6 | 3.25 | 22.4 | 101.6 |
| 500 | 4.16 | 23.1 | 156.7 | 3.77 | 20.9 | 146.3 | 3.90 | 21.6 | 149.4 |
| 1000 | 4.92 | 22.4 | 249.4 | 4.39 | 20.0 | 231.8 | 4.29 | 19.5 | 227.4 |
| 2000 | 6.19 | 22.1 | 409.2 | 5.30 | 18.9 | 369.2 | 5.13 | 18.3 | 362.8 |
| 5000 | 8.46 | 23.2 | 718.2 | 6.81 | 18.6 | 618.5 | 6.36 | 17.4 | 588.7 |

**Appendix 11: Estimating the gas side heat transfer coefficient by comparing 1/U to l/k and $1/h_L$.** Calculations are based on Equations 4.31 – 4.33. Values are given in $10^{-4}$ $m^2 \cdot K/W$.

| Nominal flask volume ($V_F$) [mL] | Constant $V_L/V_F$ | | | Constant $k_La$ | | | Constant $OTR_{max,plug}$ | | |
|---|---|---|---|---|---|---|---|---|---|
| | 1/U | l/k | $1/h_L$ | 1/U | l/k | $1/h_L$ | 1/U | l/k | $1/h_L$ |
| 50 | 52.8 | 6.7 | 1.5 | 51.7 | 6.7 | 1.7 | 51.7 | 6.7 | 1.6 |
| 100 | 69.6 | 6.7 | 1.6 | 68.7 | 6.7 | 1.6 | 68.6 | 6.7 | 1.6 |
| 250 | 105.2 | 7.5 | 1.6 | 105.2 | 7.5 | 1.6 | 105.2 | 7.5 | 1.6 |
| 500 | 137.1 | 7.5 | 1.6 | 134.9 | 7.5 | 1.5 | 139.1 | 7.5 | 1.5 |
| 1000 | 184.6 | 10.8 | 1.6 | 189.3 | 10.8 | 1.5 | 189.8 | 10.8 | 1.4 |
| 2000 | 256.3 | 12.5 | 1.5 | 263.7 | 12.5 | 1.4 | 266.3 | 12.5 | 1.4 |
| 5000 | 307.5 | 15.0 | 1.5 | 307.5 | 15.0 | 1.3 | 307.5 | 15.0 | 1.3 |

The estimation of the gas side heat transfer is based on Equations 4.31 – 4.33 with $\rho = 1000$ kg/m$^3$, $\eta = 0.001$ Pa s, $P/V_L$ according to Equation 4.15, $c_p = 4.184$ kJ/kg/K [144] and $k_L = 0.5562$ W/m/K [65] $1/h_L$ can be estimated for the different flask sizes and cases. In addition, with the thickness of the flask wall given in Appendix 9 and the thermal conductivity of borosilicate (1.2 W/m/K (flask specifications, Schott AG, Mainz, Germany)) l/k can also be determined (see Table above). $h_g$ cannot easily be calculated. However, 1/U can be compared to l/k and $1/h_g$. For easy readability, not all 1/U values are shown, but only the ones calculated with the maximal U for each flask size (see Table above).

It is obvious, that l/k and $1/h_L$ are at least one order of magnitude smaller than 1/U. Therefore, based on Equation 4.31, the gas side heat transfer coefficient is the limiting step in heat transfer for shake flasks. This results Equation A.1:

$$\frac{1}{U} = \frac{1}{h_L} + \frac{l}{k} + \frac{1}{h_g} \approx \frac{1}{h_g} \tag{A.1}$$

with

$$h_g \gg \frac{l}{k} > h_L \tag{A.2}$$